

Model-based Feedforward Control for Inkjet Printheads

Amol Ashok KHALATE

Ph.D. Thesis

Cover design: Aditya Pawar

MODEL-BASED FEEDFORWARD CONTROL FOR INKJET PRINTHEADS

PROEFSCHRIFT

ter verkrijging van de graad van doctor
aan de Technische Universiteit Delft,
op gezag van de Rector Magnificus Prof. ir. K.C.A.M. Luyben,
voorzitter van het College voor Promoties,
in het openbaar te verdedigen op
vrijdag 17 December 2013 om 12:30 uur

door

Amol Ashok KHALATE

Master of Technology in Control System Engineering,
Indian Institute of Technology (I.I.T.), Kharagpur, India
geboren te Phaltan, India

Dit proefschrift is goedgekeurd door de promotor:

Prof. dr. R. Babuška

Copromotor: Dr. ir. X. Bombois

Samenstelling promotiecommissie:

Rector Magnificus,

Prof. dr. R. Babuška,

Dr. ir. X. Bombois,

Prof. dr. ir. J. Geraedts,

Prof. dr. ir. F. van Keulen,

Prof. dr. G. Scorletti,

Prof. dr. ir. M. Steinbuch,

Prof. dr. ir. P.P.J. van den Bosch,

Prof. dr. ir. J. Hellendoorn,

voorzitter

Technische Universiteit Delft, promotor

Technische Universiteit Delft, copromotor

Technische Universiteit Delft

Technische Universiteit Delft

Ecole Centrale de Lyon, Ecully Cedex, France

Technische Universiteit Eindhoven

Technische Universiteit Eindhoven

Technische Universiteit Delft, reservelid



Canon
CANON GROUP

Embedded Systems
INSTITUTE

This work has been carried out as part of the Octopus project with Océ Technologies B.V. under the responsibility of the Embedded Systems Institute.

ISBN: 978-94-6186-245-7

Copyright © 2013 by Amol A. Khalate.

All rights reserved. No part of the material protected by this copyright notice may be reproduced or utilized in any form or by any means, electronic or mechanical, including photocopying, recording or by any information storage and retrieval system, without written permission from the copyright owner.

Printed in the Netherlands by CPI Wöhrmann Print Service

To my family

Acknowledgments

Finally, the day has dawned to thank the contributors who made my PhD voyage possible and memorable. I must thank a large number of people, not only those who helped me during the last five and a half years of my PhD research but also those who encouraged and enabled me to pursue PhD in the first place.

Foremost, I would like to express my sincere gratitude to my supervisors prof.dr. Robert Babuška and dr.ir. Xavier Bombois for showing faith in me and giving me an opportunity to carry out this doctoral research. Special thanks to Xavier for his continuous supervision, technical discussions, critical feedbacks, support and motivating words which helped me to establish and enhance my research skills. He has, through these times, encouraged me to achieve higher goals and have given me the freedom to perform innovative research. He has always been a great support not only on professional level but also on personal level. Both Xavier and Robert have patiently helped me in writing research papers and, finally, this thesis. I would like to thank them, specially, for their faith and the inspiration they have provided in the final phase of PhD, without which it would not have been possible for me to realize this thesis. It is a great honor to work with both of you and I hope that we shall continue our collaborations in the future.

I would like to express my special gratitude to prof.dr. Gérard Scorletti, at Ecole Centrale de Lyon, for hosting me a couple of times. His immense knowledge coupled with guided discussions helped me to gain valuable insights that were crucial for the theoretical contribution of this thesis. Thank you Gérard for the warm hospitality and for introducing me to French cuisine and countryside. I would also like to thank Benoît Bayon who not only provided valuable inputs to the research but also has always been there to extend any help I needed. It has been a pleasure working with both of you and I am looking forward to continue our close cooperation in the years to come.

I was very fortunate to receive guidance from late prof.ir. Okko Bosgra. Discussions with him provided new insights and opened further research possibilities. His enthusiasm to perceive new advancements, which I had observed during our discussions, inspired me to continue my research with a new zest.

It would not have been possible for me to pursue this research without the help of my colleagues from Océ. I would like to thank Sjirk Koekebakker for showing great interest in my research and providing valuable inputs to improve its quality. I would like to express my sincere indebtedness to Wim de Zeeuw, Herman Wijshoff,

Piere Klerken, René Waarsing, Jan Simons and Paul Gronen, for sharing their experiences and extending their support. Exchange of ideas with all of you was crucial for understanding the inkjet systems and your critical feedback helped me to improve the applicability of my research.

I would like to extend my acknowledgment to my project colleague Mohamed Ezzeldin for the collaboration during PhD. We had thoroughly enjoyed the time spent together during the experiments, evening shopping in Venlo and the train journeys. I would also like to thank my colleagues from Embedded Systems Institute, Frans Reckers, Twan Basten, and Jacques Verriet, from whom I have learned quite essential things in planning and managing the research activities.

During my PhD, I have been greatly benefited from the discussions I had with my DCSC colleagues Ilhan Polat, Stefan Kuiper, Navin Balini, Alexander Haber, Ivo Houtzager, Dang Doan, Arturo Tejada Ruiz, Roland Tó th and Yasher Zeinaly. I thank them for their cooperation. I would like to thank Kitty, Ellen, Saskia, Esther, Linda and Olaf for their administrative support without whom my conference travels, DISC activities and purchases from external vendors would not have been possible.

I would like to thank the members of my PhD committee for providing me with constructive remarks, which helped me improve this thesis.

Finalizing the thesis was a daunting task and it would not have been possible without some special efforts. Thank you Arend van Buul and Xavier Bombois for Dutch translation, and Max Potters, Leo Hendriks and Arne Dankers for proof-reading the propositions and summary of my PhD thesis. Thanks to Ilhan Polat who ensured my Latex is running. The print version of my thesis was not possible without his great efforts. I would like to express my heartfelt appreciation to Kaushal Butala for offering succor and cooperation during the final phase, when I needed it quite immensely. He has been there beside me, credible and helpful, like a younger brother. I am grateful to Aditya Pawar for preparing nice cover page and Nithin for providing support to bring out the first print version.

The days at DCSC would have felt very long if I would have not been surrounded by wonderful people. Thank you Alfredo, Bart, Eric, Ismini, Lakshmi, Max, Nicolas, and Samira for wonderful time while sharing the same office. I will always adore the frequent talks, discussions and lunches with you, Aleksandar, Alfredo, Ali, Aleksander, Andrea, Arne, Bart, Dieky, Eric, Hans, Ilya, Ivo H., Ivo G., Jacopo, Marco, Max, Mohammad, Noor, Pawel, Patricio, Ruxandra, Sadegh, Samira, Skander, Solomon, Stefan, Subramanya, Yasher, Zhe, Zulkiffi. I had learned many things about research and education while being a teaching assistant along with Ali. Thank you Ali for the professional advices and support during writing of the thesis. Be it technical or non-technical, Samira has always provided prompt solutions to my queries, thank you Samira for the support during PhD and during finale of the thesis. Marco, Subramanya, and Yasher have extended genuine helping hands during PhD and especially, when I was away from DCSC.

The story would not be complete without my three musketeers, Dang Doan, Ilhan Polat and Navin Balini.

Dang, with whom I had shared office in DCSC, is the most humble, modest and accommodative person I have met. His immense curiosity for learning new things, his discipline, and his commitment to improve education and research environments in his home country, Vietnam fascinates me. The discussions we had on science, social responsibilities and philosophy have enlightened me. Thank you Dang, it has been a pleasure to have a friend and colleague like you.

Ilhan has been one of the most reliable ally and friend. It did not matter whether the issue was related to mathematics, software or even professional advice, he has been the one on whom I can always count on. It is very rare to see someone going out of their ways to help others. I have no words to express my deepest gratitude for the support you have provided. A genuine person with a great sense of humor, I thank you Ilhan for everything.

Navin has been an exceptional and a trustworthy friend I have been blessed with during my PhD. He has whole heartedly provided support when I needed it the most. He is the one who has observed me carefully and has provided critical inputs for my improvement. Both on personal and professional fronts, Navin has given me valuable advices, which I respect a lot. I thank you, Navin, for such a warm friendship.

Pursuing PhD would have been a distant dream for me without a few good men who inspired me to achieve higher feat. I owe my professional career to prof.dr. Goshaidas Ray, who provided me the optimism that despite my limitations, I can contribute to research. I would like to thank my friend Girish Galgali for encouraging me to seek higher studies. I would like to express my sincere gratitude dr. Paresh Date for providing valuable guidance regarding doctoral research and for inculcating the attitude to strive for the best. Thanks to my mentors M.V. Dhekane and M.M. Patil who have imparted me strength and have supported me to achieve my dreams. I am grateful to my friend Vikrant Hiwarkar who have provided valuable insights about the PhD life.

I would like to express my sincere gratitude to educational and technological institutes for shaping me. Thank you Zilla Parishad Primary School, Takali Sikan-dar, for teaching the 'never give up' attitude, Sakharwadi Vidyalaya, Sakharwadi for nurturing curiosity required for a researcher, YCJC, Phaltan and GCOE, Jalgaon for laying the foundation of engineering, IIT Kharagpur for providing an opportunity to discover the researcher in me and TUDelft for providing vibrant international research environment.

My stay during the PhD has been enjoyable and exciting, thanks to my friends, Amit, Sameer, Somnath, Sudam and my family friends Navin and Rajitha, Xavier and Thiya, Murugeyan and Thenmozhi, Pradyumna and Indu, Sushil and Jayu, Amit and Swati, and Shahzad and Shazia. My friends from school, college and ISRO, Kiran, Nitin, Prashant, Rahul, Sachin, Sheetal, and Suresh have provided me enormous support.

I would like to extend my indebtedness to my parents, Shri. Ashok Khalate and Smt. Surekha Khalate, for their endless love, support and encouragement to achieve higher triumph. Their constant faith in me is the reason which kept me going. I would like to thank my brother, Atul and sister, Ashwini for their support.

For their constant encouragement to finish my PhD, I express my sincere gratitude to my in-laws, Shri. Shivajirao Ghatge and Smt. Shubhada Ghatge.

Finally, I would like to thank my wife, Roopali, for her love, support and patience through out these years. Without you, it would have been difficult to handle the ups and downs during the PhD. Thank you for the strength and the courage you have extended me to finish the thesis.

Amol Ashok KHALATE,
Eindhoven, December 2013.

Contents

Acknowledgements	vii
1 Introduction	1
1.1 Inkjet Technology	1
1.1.1 Classification of Inkjet Technologies	2
1.1.2 Micro-manufacturing using Inkjet Technology	4
1.2 System description	7
1.2.1 Working principle of a DoD inkjet printhead	9
1.2.2 Performance of a DoD Inkjet Printhead	10
1.2.3 Performance Limiting Issues	11
1.3 State of the art in inkjet printhead control	13
1.4 Problem formulation	16
1.4.1 The research objective	16
1.4.2 Approach	18
1.5 Outline of the thesis	19
2 Inkjet Printhead Modeling	21
2.1 Introduction	21
2.2 Physical Modeling	23
2.2.1 Narrow Gap Model	24
2.3 Data-based Modeling	27
2.3.1 Measurement of the piezo sensor signal	28
2.3.2 Overview of Prediction Error Identification Method (PEM)	30
2.3.3 Experimental modeling a single ink channel dynamics	32
2.3.4 DoD dependence of a single ink channel dynamics	36
2.3.5 Identification of the cross-talk model	37
2.4 Uncertainty Ink channel dynamics	40

2.4.1	Uncertainty on the physical model	40
2.4.2	Uncertainty on the data-based model	44
2.5	Summary	45
3	Feedforward Control of an inkjet channel: Theory	47
3.1	Introduction	47
3.2	Limitations of the control system	49
3.3	Control Objective	50
3.4	Constrained Feedforward Control	53
3.4.1	Optimal Constrained Feedforward Control	53
3.4.2	Robust Constrained Feedforward Control	54
3.5	Unconstrained Feedforward Control	56
3.5.1	Optimal Unconstrained Feedforward Control	56
3.5.2	Robust Unconstrained Feedforward Control	57
3.6	Summary	66
4	Feedforward Control of an inkjet channel: Results	69
4.1	Introduction	69
4.2	Simulation Results	70
4.2.1	Constrained Feedforward Control	70
4.2.2	Unconstrained Feedforward Control	77
4.3	Experimental Results	83
4.3.1	Optimal Constrained Feedforward Control	83
4.3.2	Robust Constrained Feedforward Control	88
4.4	Summary	91
5	MIMO Feedforward Control of a DoD Inkjet Printhead	93
5.1	Introduction	93
5.2	Robust Constrained MIMO Feedforward Control	94
5.3	Unconstrained MIMO Feedforward Control	98
5.3.1	Optimal Unconstrained MIMO Feedforward Control	98
5.4	Simulation results	99
5.5	Experimental results	102
5.6	Summary	109

6	Conclusions and Recommendations	111
6.1	Conclusions	111
6.1.1	Data-based modeling of Inkjet printhead	111
6.1.2	Robust feedforward control inkjet printhead	113
6.2	Recommendations	114
6.2.1	Inkjet printhead design	115
6.2.2	Data-based modeling	116
6.2.3	Control and performance monitoring of inkjet printhead . . .	117
A	Performance measures of a DoD Inkjet Printhead	121
B	Experimental Setup	123
C	Robust Unconstrained Feedforward Control using FIR Filters	127
	Bibliography	131
	Summary	139
	Curriculum Vitae	141

Introduction

In this chapter, we provide a brief overview of inkjet technology and its recent popular application as a micro-manufacturing tool. This will justify the increasing interest for research in inkjet systems and, in particular, the Drop-on-Demand inkjet systems. The construction of a piezo-based DoD inkjet printhead and its working is discussed. Further, the performance of a DoD inkjet printhead is characterized by droplet properties. The operational issues of the DoD inkjet systems, limiting the printhead performance, are summarized and an overview of the literature tackling these issues is presented to investigate the research question and the problem formulation. We conclude this chapter by giving an overview of this thesis.

1.1 Inkjet Technology

Inkjet technology has been a hidden player in accelerating development in science and technology by providing easy and cheap solutions to printing and sharing information at offices and homes. The basic principle of inkjet technology is to jet ink droplets through a nozzle in a controlled manner onto the print media or substrate. In the late 19th century, Plateau and Lord Rayleigh established the founding principles for inkjet (Groot Wassink 2007) while William Thompson, in 1858, first proposed to use electrostatic forces to control the position of ink drops on the paper (The Siphon recorder, UK Patent 2147/1867). However, lack of computing power delayed the translation of these inventions into commercial products until 1951, when Siemens introduced the first inkjet-based printer. Since then a substantial research has been pursued in this domain which has helped in making the printers smaller, faster and affordable. In the last couple of decades, inkjet has proven its edge over the conventional document printing techniques (e.g. offset, gravure, or screen-printing). It has become an even more important printing technology in today's world of variable data printing. Recently, inkjet technology has emerged as a promising tool for micro-manufacturing. This is mainly due to

the facts that it can handle diverse materials and it is a non-contact and additive process. Prior to discussing inkjet-based micro-manufacturing, we first present a summary of existing inkjet technologies in the next section.

1.1.1 Classification of Inkjet Technologies

The function of an inkjet printhead is to deliver the ink droplets having specific properties on the substrate. These properties include the drop velocity, its volume and the travel direction deviation. These properties greatly depend on the type of principle used to generate the drops. The inkjet technology can be primarily divided into two classes depending on whether the ink drops are generated when they are needed on the substrate or they are continuously jetted and deflected to the substrate when needed. Figure 1.1 shows a broad classification of inkjet technologies. In the next section, we present a brief overview of both inkjet families. For a detailed history and classification of different inkjet technologies, see (Groot Wassink 2007; Wijshoff 2010).

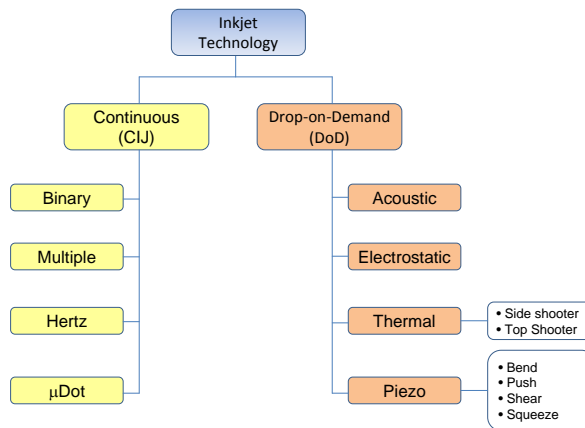


Figure 1.1: Classification of inkjet technologies.

Continuous Inkjet (CIJ) Technology

In continuous inkjet printing, ink under pressure is forced through a nozzle as a continuous stream and uniform droplets are formed by the the action of surface tension, by diameter perturbations or surface tension perturbations (Korvink et al. 2012). These droplets travel through an electric field acquiring an electrostatic charge. Whenever drops are needed on the paper their trajectories are deflected by applying electric pulses on deflector plates. The undeflected drops are recollected

and recycled back to the ink reservoir. Figure 1.2 shows the working principle of CIJ printing.

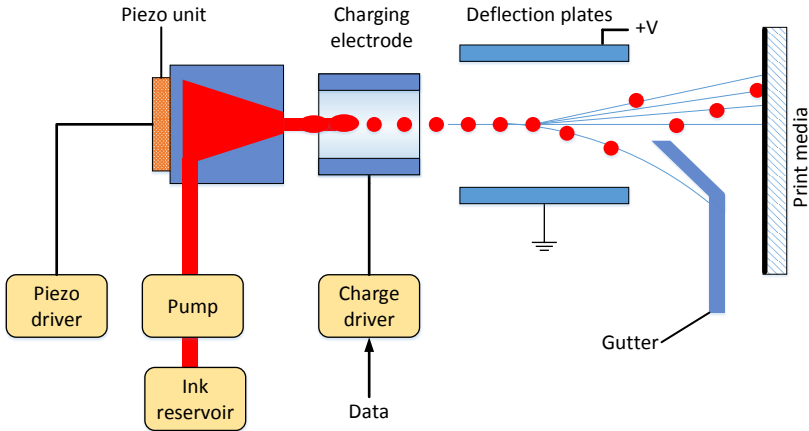


Figure 1.2: Schematic diagram of a continuous inkjet printing.

Depending on the type of deflection pulses that are used, CIJ can be divided into two families: the binary deflection CIJ and the multiple deflection CIJ. The jetting frequency is defined as the number of drops jetted per second and it is one of important measures of inkjet productivity. Typically, CIJ printer jets drops at a jetting frequency of 100 kHz. Some high-end CIJ printers can even reach the jetting frequency of 1 MHz. Even though CIJ is very productive, it can only be cost effective in the continuous production. Therefore, it is commonly used in label printing. The major reason for the unpopularity of CIJ in industrial printing is that it requires a complicated hardware to recirculate the droplets which are not deposited on the substrate and to synchronize the droplet breakup, charging and deflection.

Drop-on-Demand Inkjet Technology

Unlike the CIJ technology, in the Drop-on-Demand (DoD) inkjet technology, the drops are generated whenever required by actuating a transducer that creates pressure waves inside an ink channel. Figure 1.3 shows a schematic diagram of this technology. One can use a heating element to increase the local temperature of the ink and create a small vapor bubble to generate pressure oscillations. The printer using this principle is known as the Thermal Inkjet (TIJ) printer. Most of the desktop inkjet printer used in small offices and homes are based on TIJ technology.

Even though TIJ is cheaper and more compact it is not preferred for industrial applications due to several disadvantages. The major drawback of TIJ is that it can only work with a limited types of ink (generally aqueous) as heating may change chemical and physical properties of the ink. Furthermore, using an heating element to generate droplets limits the jetting frequency and the durability of the printhead.

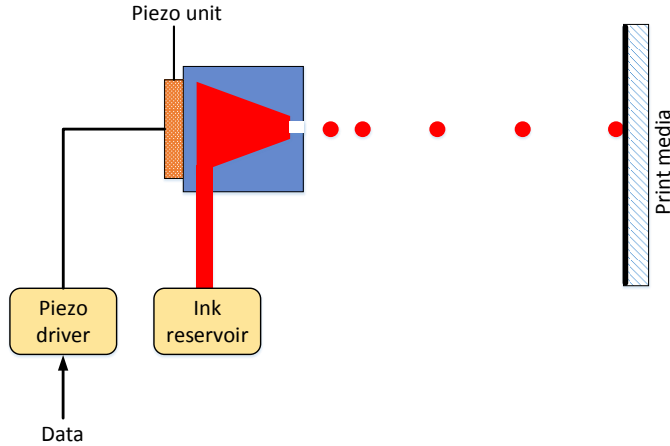


Figure 1.3: Schematic diagram of a drop on demand (DoD) inkjet printing.

The drawbacks of the TIJ can be overcome by using a piezoelectric material to generate pressure oscillations within an ink channel. The piezo-based inkjet technology can handle a wide range of ink material without a need of complicated hardware. Thus, the piezo-based inkjet (PIJ) printheads are more popular for industrial applications offering higher productivity and the possibility to jet fluids with different physical and chemical properties.

Compared to a CIJ, the DoD inkjet printheads do not need ink recirculation mechanism making them more compact and relatively easy to use. Thus, despite the fact that CIJ need less energy to jet droplets, the DoD inkjet technology is preferred in the industry.

1.1.2 Micro-manufacturing using Inkjet Technology

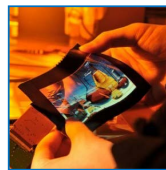
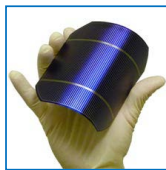
In the early 1980s, the need of high level system integration on a very small space has triggered research and development of microelectromechanical (MEMS) systems (Korvink et al. 2012). It also laid the foundation for micro level manufacturing using the lithography fabrication techniques which are primarily developed only to manufacture electronics integrated circuit. These MEMS devices, e.g. accelerometers, gyroscopes and optical sensors have greatly transformed our life since they can be easily adapted in small devices and are cheap due to high volume production. The photo-lithography-based micro-machining techniques prepares the device

layer-by-layer and are effective for high volume production due to the expensive pre-processing steps. Moreover, photo-lithography can deposit a limited range of materials on the substrate. Thus, it is essential to have a tool which can not only deposit diverse materials but is also cost-effective at low volume production.

In recent years, inkjet technology has emerged as a promising micro-manufacturing tool. The primary reason for this development is the ability of the inkjet technology to deposit materials with diverse chemical, physical and even biological properties on a substrate. Moreover, inkjet printing is an additive process¹. Therefore, it is highly suitable for precise deposition of expensive and rare material so that the wastage of material can be avoided (M.Singh et al. 2010). This avoids several masking steps, otherwise needed, in photo-lithographic fabrications. It also allows to create a complex structure by a layer-by-layer deposition without additional processing costs associated with the lithography (Kawase et al. 2003). Another favorable characteristics of the inkjet technology is that it is a non-contact manufacturing process. Thus, materials can be deposited without having prior interaction with the substrate. This allows the manufacturer a more precise control on the characteristics of the final outcome. Furthermore, as the inkjet technology can be digitally controlled, it provides great flexibility to reduce the development time (unlike in lithography where the masks have to be produced prior to manufacturing). These characteristics make the inkjet technology an unique and versatile micro-manufacturing tool.

Electronics

- Flex Circuits
- RFID
- PCBs
- Solar Cells

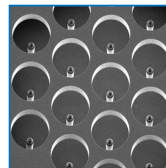


Display

- Flat Panel Displays
- PLED
- LCD
- Flexible Displays

Mechanical

- Rapid Prototyping
- Metal coating
- 3D Modeling

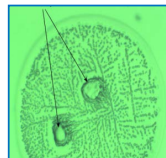
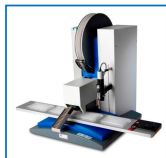


Optics

- Micro Optical Lenses
- Optical waveguide

Chemical

- Material Development
- Substrate Development
- Adhesives



Life Sciences

- DNA printing
- Artificial skin
- Food Science
- patient specific drugs

Figure 1.4: Overview of application of inkjet technology for micro-manufacturing.

¹Additive manufacturing is the process of producing parts by successive depositing of layers of material rather than removing material, as is the case with conventional machining.

We can find several successful applications of the inkjet technology in the field of science and engineering (see Figure 1.4). A detailed review of all these applications is beyond the scope of this chapter. However, we will briefly present those applications of the inkjet technology:

- **Graphics**

After having captured the small office and home market via desktop printers, the new market for document printing is, at the moment, wide-format graphics, variable data printing and industrial marking and coding. Inkjet printers using hot-melt ink, e.g. Colowave 650 by Océ, are popular for advertisement and industrial graphic documentation. The use of ultraviolet (UV) curing ink (Calvert 2001) delivers highly durable prints on almost any print media and also allows inkjet printing for decorative walls, floors and door printing (e.g. Flat-bed printer Arizona by Océ). A recent addition to commercial graphics using inkjet is textile printing (Hitoshi 2006).

- **Electronics**

The use of inkjet have significantly reduced the number of steps to produce PCB (printed circuit boards) (Lee et al. 2005; Pekkanen et al. 2010) and thus, provides an economical solution for small scale production. Its ability to jet different solvents (even molten metal) has enabled us to make flexible printed electronics (Minemawari et al. 2011) and Radio Frequency Identification (RFID) tags (Yang et al. 2007). New organic photosynthesis materials along with inkjet printing also provides a route to cheaper and versatile solar cell production (Krebs 2009). These applications need reliable placement of every droplet of the solvent on the substrate and technologies such as ‘Predict’ by MuTracX ensures this reliability (Starkey 2011).

- **Display Graphics**

The high productivity and the consistency offered by inkjet allows precise jetting of light emitting polymers such as the ones used in Flat Panel Display (FPD) manufacturing (Shimoda 2012). It is indeed an essential tool to make color filters in liquid crystal displays (LCD) and to manufacture Polymer Light Emitting Diode (PLED) (Dijksman et al. 2007) and Flexible displays (Koo et al. 2006).

- **Mechanical prototyping**

Inkjet technology provides an easy way for rapid prototyping which, otherwise, is often a time consuming and an expensive process. Complex fluid can be jetted with inkjet printing enabling small scale production of strong and complex 3D objects close to the customer location (Sanchez et al. 2008).

- **Optics**

It is possible to jet optical polymers and even melted glass providing a cost effective production of micro-lenses (Fakhfour et al. 2008). These lenses are an essential part of medical and fiber optic communication equipments. Inkjet opens new possibilities to miniaturize the optical MEMS (Cox et al. 1995). It is successfully used to make optical waveguides on micro level (Chappell et al. 2008).

- **Chemical Engineering**

Fluid development is crucial for a successful implementation of many new digital micro-production applications. The ability to control mixtures of different solvents at the pico-liter level, allows chemical engineers to tightly control the product characteristics of chemical reactions. Thus, it has found applications in pharmaceutical industry (Scoutaris et al. 2011). Currently, a wide research is going on in the chemical industry for product development using inkjet technology (Williams 2006).

- **Life sciences**

The introduction of inkjet technology in life sciences is opening many new possibilities. The use of expensive material requiring very low wastages make inkjet a crucial tool for this market. Inkjet has been successfully applied for precise jetting of DNA (Goldmann and Gonzalez 2000) and protein substances (Delaney et al. 2009; McWilliam et al. 2011). Scientist are able to produce artificial skins by jetting live animal cells (Boland et al. 2006). In the future, it may become possible for doctors to recommend a precise quantity of drugs needed for a particular patient and subsequently for a pharmacist to print a customized pill (Wu et al. 1996; Williams 2006).

These new applications impose a tremendous demand on inkjet technology (initially developed for document printing) to jet smaller drops at a high jetting frequency with a tighter control on drop properties. In the next section, we discuss the construction of a piezo-based DoD inkjet printhead, its working and the operational issues limiting its performance.

1.2 System description

As discussed in the previous section, a piezo-based DoD inkjet printhead is the most suitable printhead for industrial printing; therefore, we have considered a piezo-based DoD inkjet printhead for this research. The DoD inkjet printhead under investigation is shown in Figure 1.5 and consists of two arrays of 128 ink channels each. Typically, this printhead uses ink which is in the solid-state at room temperature. Therefore, a melting unit (a) is provided to heat solid ink balls and transform the ink in the liquid-state. The ink is then filtered through a primary filtering unit (b) and then transferred to the reservoir unit (c). The channel plate (e), on which 256 ink channels are carved (128 channels on one side), is attached to the bottom of the reservoir. For printing purpose, the printhead is mounted vertically and this will result into draining of the ink due to gravity. To avoid this, the pressure inside the printhead is maintained slightly below the atmospheric pressure using the static pressure hose (d). Flexible electronic cables (f) are used to supply the driving input to all ink channels.

In order to understand the internal construction of a single ink channel, a cross-sectional view of an ink channel is shown in Figure 1.6. A secondary filter is placed before the ink channel to remove any impurities from the liquid ink. A metallic plate with drilled holes, which act as nozzles, is attached at the end of the channel

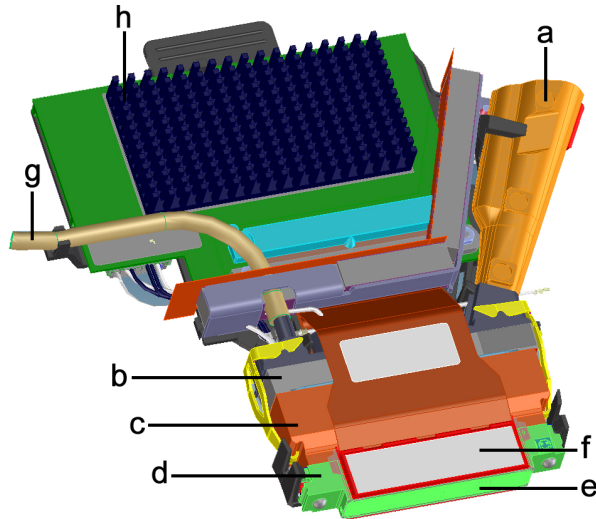


Figure 1.5: 3D CAD drawing of a printhead showing (a) the melting unit, (b) the filter units, (c) the reservoir, (d) the central part, (e) the nozzle plate, (f) the piezo actuator units, (g) the static pressure hose, and (h) the electronic driving supply.

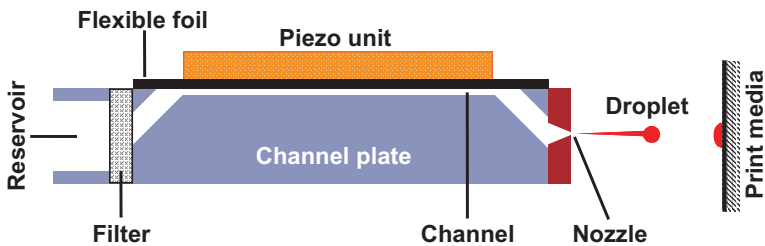


Figure 1.6: A cross-sectional view of an ink channel.

plate. One wall of the ink channel is formed by a flexible foil to which a piezo unit is attached. The piezo unit acts as an actuator. On the application of a voltage, it deforms the wall of the ink channel. The deformation generates a pressure wave inside the ink channel. When specific conditions are met, a droplet is jetted (Groot Wassink 2007).

1.2.1 Working principle of a DoD inkjet printhead

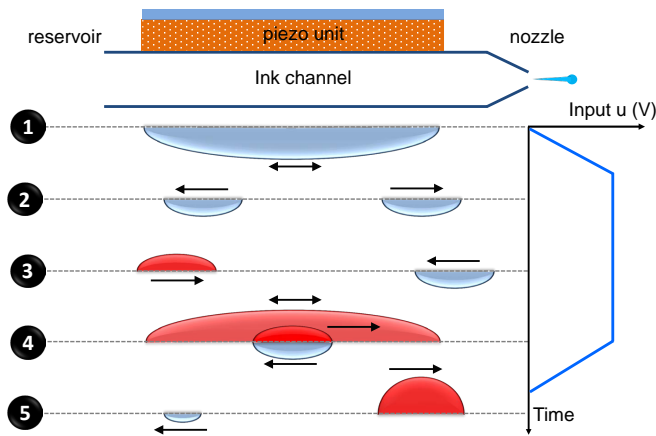


Figure 1.7: Working principle of an ink channel.

Typically, a positive trapezoidal voltage pulse is applied to the piezo unit in order to jet an ink droplet. The process of the drop jetting can be described in the following five steps (see Figure 1.7) (Groot Wassink 2007). To start with, the rising piezo voltage deforms the piezo structure enlarging the channel volume and thereby, generating a negative pressure wave (step 1). With the piezo voltage kept constant, the negative pressure wave splits up and starts propagating in both directions (step 2). The reservoir acts as an open end and thus, the wave reflects back as a positive wave. At the nozzle, the negative pressure wave retracts the meniscus and since the nozzle acts as a closed end, the wave reflects back as a negative pressure (step 3). The meniscus is the interface between the ink and air in the nozzle. Now, when the reflected waves reach the middle of the channel, a positive pressure wave is superimposed on them by restoring the channel volume to its original volume with the reduction in the piezo voltage (step 4). This results in the cancellation of the wave traveling towards the reservoir and in the amplification of the wave traveling towards the nozzle, to such an extent that it is large enough to result in a droplet (step 5). This ensures that an ink droplet is pushed outside

the nozzle once the appropriate conditions² are met (Dijksman 1984). It should also be observed that a trapezoidal actuation pulse (of the appropriate properties) is used to jet a droplet.

Having discussed the construction and the working of an inkjet system, in the next section, we will discuss the performance requirements on a DoD inkjet printhead.

1.2.2 Performance of a DoD Inkjet Printhead

In a printing system, an accurate placement of ink drops on the print media is crucial to achieve a high printing quality. Various factors contribute to ensure a proper drop placement: the drop ejection process, the interaction of ink with the print media, the printhead carriage motion system and the print media feeding system. The improvement in the drop ejection process can, significantly, improve the overall performance of an inkjet print system. Therefore, in this thesis, we focus on increasing the print quality, by improving the drop ejection in a DoD inkjet printhead, i.e. the properties of the jetted drops. These properties are the drop velocity, the drop volume and the jetting direction. To meet the challenging performance requirements posed by new applications (see the section 1.1.2), these drop properties have to be tightly controlled.

A detailed performance measures for a DoD inkjet printhead is presented in Appendix A. Here we will only discuss prime drop quality metrics (Groot Wassink (2007)):

- *Drop volume.*
The required drop volume depends on the application under consideration and the specified resolution. For an application requiring higher resolution, e.g. manufacturing microelectromechanical systems (MEMS), inkjet printhead should jet smaller drops. On the contrary, for applications like display graphics, large drops are desirable to cover larger area. Some applications require a combination of small and large drops (drop-size modulation). Typically, the industrial applications require a drop volume in the range of 0.5 to 40 picoliter.
- *Drop velocity.*
In order to ensure that drops are placed at the prescribed location, the jetted droplets should have a certain velocity, typically from 3 to 10 ms⁻¹ depending on the application and the required accuracy.
- *Drop velocity and volume consistency.* For the print accuracy, it is required that the variations in the drop volume and the drop velocity between successive drops and that between the nozzles should remain within an allowable tolerance, typically ranging from $\pm 2\%$ to $\pm 15\%$ of its nominal value.

²A droplet is formed when the kinetic energy of the fluid pushed out of the nozzle overcomes the surface tension of the fluid (Dijksman 1984).

Apart from these drop quality requirements, a DoD inkjet printhead is expected to deliver higher throughput and yield. The *productivity* of a printhead is mainly determined by the speed with which it can cover the printing area. Naturally, the maximum jetting frequency of an ink channel and the nozzle density (amount of nozzles per inch or NPI ratio) mainly influences the productivity of a DoD inkjet printhead. Generally, for home and small office use, the maximal jetting frequency is low, typically 10kHz, while for industrial applications it is typically 30-70kHz. The nozzle density for home use is around 300 NPI and for industrial use it is typically, 50 – 150 NPI.

In the next section, we will discuss how the operational issues limit the ability of a DoD inkjet printhead to simultaneously deliver both, the specified drop properties and higher productivity.

1.2.3 Performance Limiting Issues

In the previous section, we have discussed that the print accuracy requirement and the throughput requirement can be improved by improving the drop properties and the jetting process. In this section, we present some operational issues which limit the achievable performance of a DoD inkjet printhead. Thus, developing methods to tackle these issues will provide a means to improve the printhead performance.

Residual oscillations

The actuation pulses are designed to provide an ink drop of a specified volume and velocity under the assumption that the ink channel is in a steady state. As discussed in Section 1.2.1 pressure oscillations are generated inside the ink channel on application of the actuation pulse to the piezo actuator and eventually the ink drop is jetted. Figure 1.8 shows the piezo sensor response³ of an inkjet channel to the applied trapezoidal actuation pulse. The ink drop is jetted after around 12 μ s. It can be observed that, after the delivery of an ink drop, the oscillations inside the ink channel take several microseconds to decay. These oscillations are called residual oscillations. In order to ensure consistent drop properties, one has to wait till these oscillations are completely damped before jetting a next drop. If the next ink drop is jetted before the settling of these residual pressure oscillations, the drop properties of this new drop will be different from the properties of the previous drop.

A consequence of the residual oscillations in the ink channel is that the velocity of the drops will only be constant if these drops are jetted at a lower frequency. This limits the highest attainable DoD frequency and thus, the throughput of a DoD inkjet printhead, which is an essential requirement along with the drop property consistency. For this purpose, it is required to be able to jet ink drops with a constant velocity at any rate up to 70 kHz. Given this fact, an important characteristic is the so-called DoD-curve (see Figure 1.9) which represents the ink

³ The piezo sensor signal is proportional to the rate of change of channel pressure (for details see Section 2.3.1).

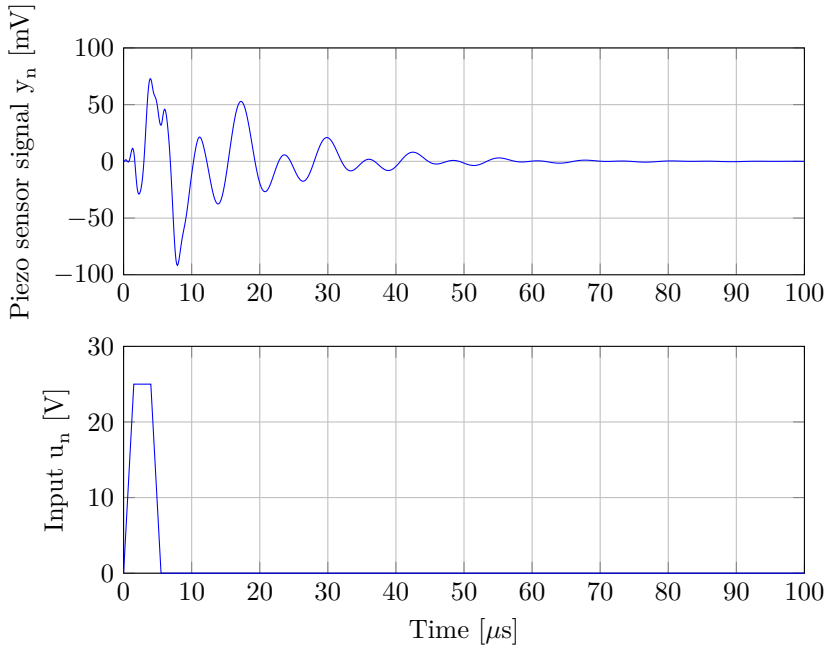


Figure 1.8: Response of the inkjet channel to the actuation pulse.

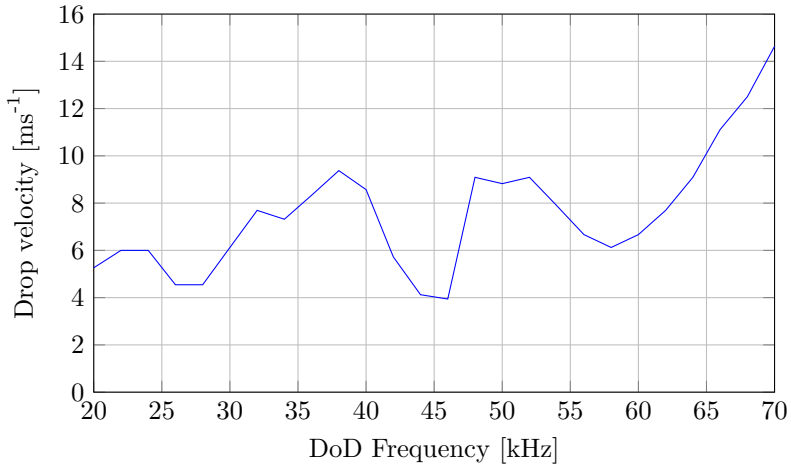


Figure 1.9: DoD-curve: effect of the residual oscillations on the drop velocity.

drop velocity as a function of the jetting frequency (which is also called the DoD frequency). Note that at a given DoD frequency, the drop velocity shown on the DoD-curve is measured for the steady-state drop jetting process, i.e. after jetting several drops. Ideally, the DoD-curve must be flat. However, in practice, for the reasons given above, this DoD-curve is far from flat. Usage of an optimally designed actuation pulse can help to flatten the DoD curve.

Cross-talk

The properties of a drop in a given ink channel are affected when neighboring channels are actuated simultaneously. This phenomenon is called cross-talk. The two major sources of cross-talk are the acoustics, the structural and the electrical interactions. A pressure wave within one channel can propagate to the other channels as they are all connected to the same reservoir (acoustic cross-talk). The ink channel can be deformed due to the actuation of the piezo unit of the neighboring channels and also due to the high pressure inside the ink channel itself. This is known as structural cross-talk. An electrical cross-talk also occurs at the level of electrical circuits that are present in any printhead to operate the channels, e.g., in the form of leakage currents. The structural cross-talk is a major source of disturbance as compared to the acoustic cross-talk. The effect of the electrical cross-talk is usually negligible (Groot Wassink 2007; Wijshoff 2010). As the structural deformation is a local phenomenon, only the simultaneous actuation of few immediate neighbors contribute to the structural cross-talk. Figure 1.10 shows the piezo sensor response of the n -th channel when its immediate right neighboring channel $n + 1$ is actuated. It can be observed that the simultaneous actuation of neighboring channel induces undesired oscillations (through the structural cross-talk) in the n -th channel.

A consequence of these cross-talk induced oscillations is shown in Figure 1.11. The DoD-curve for when the channel ‘ n ’ is actuated alone is shown by the solid line and the dotted line shows the DoD-curve of the same channel measured when the first immediate neighbors on the right and on the left of an ink channel are actuated together. We can see that the cross-talk changes the drop velocities considerably. Ideally, it is required that the drop properties of an ink channel should remain constant irrespective of whether its neighboring channels are actuated or not.

We have seen in this section that the residual oscillations and the cross-talk induced oscillations perturb the drop properties in an ink channel. One can reduce the effect of these operational issues on the drop properties through the design of the actuation pulse. In the next section, we will discuss different approaches used in the literature to design an actuation pulse for a DoD inkjet printhead.

1.3 State of the art in inkjet printhead control

We have seen in Section 1.2.1, that a positive trapezoidal voltage pulse is applied to the piezo actuator to jet an ink droplet of desired properties. The parameters of this positive trapezoidal actuation pulse (or standard pulse) are generally tuned by exhaustive studies on a complex numerical model of an inkjet printhead or on

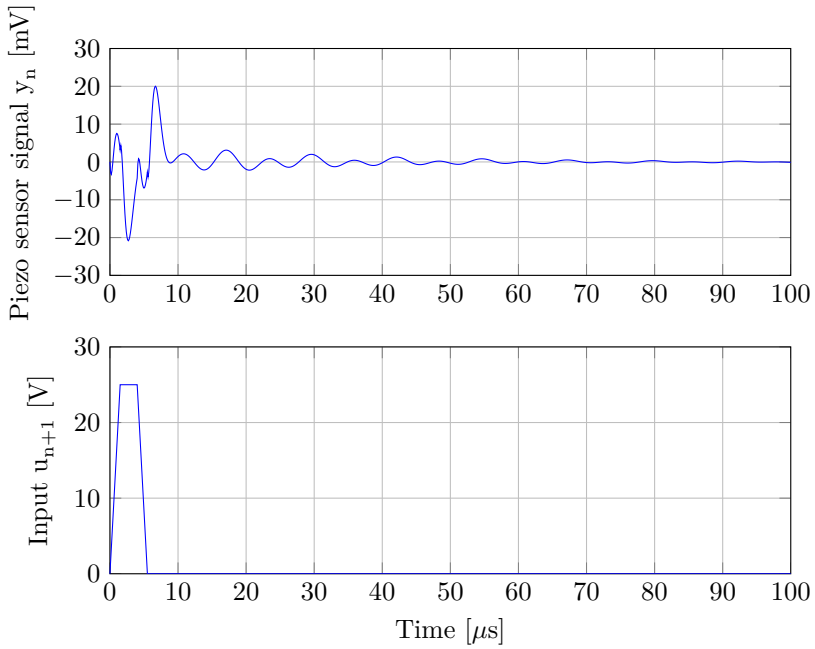


Figure 1.10: Response of the n -th inkjet channel to the actuation immediate right neighboring channel $n + 1$.

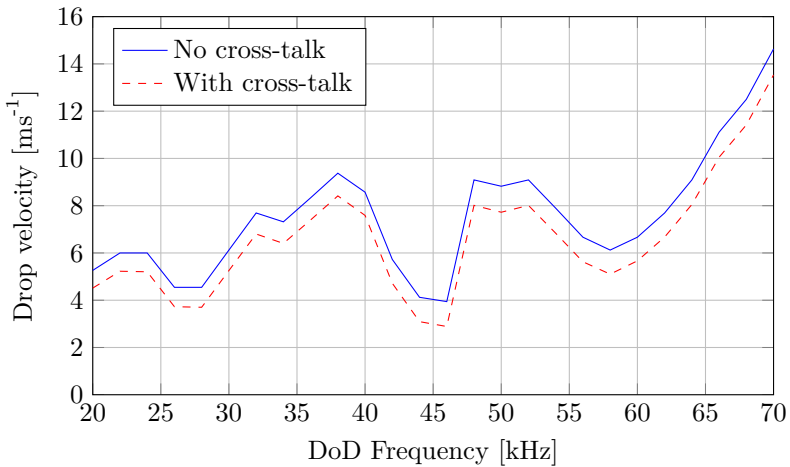


Figure 1.11: DoD-curve: effect of the cross-talk from immediate neighbors on the drop velocity.

an experimental setup (Bogy and Talke 1984; Dong et al. 2006; Jo et al. 2009). Recall that, the main drawback of this standard pulse is that it generates residual oscillations (see Section 1.2.3). In order to damp the residual oscillations, an additional pulse can be applied after applying the standard pulse. Actuation pulses used in the literature to damp the residual oscillations can be broadly classified into two categories based on the polarity of the actuation pulse. The first one is a unipolar actuation pulse (Kwon and Kim 2007; Gan et al. 2009), which consists of the standard pulse to jet an ink droplet and an additional trapezoidal pulse of the same polarity as the standard pulse to damp the residual oscillations. The second category is the bipolar pulse (MicroFab Technologies Inc. 1999; Chung et al. 2005; Kwon 2009a). This pulse consists of the standard pulse to jet an ink droplet and an additional trapezoidal pulse of an opposite polarity, with respect to the standard pulse, to damp the residual oscillations. The advantage of using the bipolar actuation pulse is that the residual oscillations can be damped earlier compared to the unipolar pulse and thus, a higher DoD frequency can be attained. Conventionally, the parameters of the unipolar and the bipolar pulses are obtained by exhaustive experimental studies, see (Gan et al. 2009; MicroFab Technologies Inc. 1999; Chung et al. 2005). The number of experiments needed to design an actuation pulse can be reduced with a wise guess on the parameters of the actuation pulse. It is possible to make an initial guess on the parameters of the actuation pulse as a function of the fundamental period of the channel pressure (Kwon and Kim 2007) or the meniscus position (Kwon 2009a). To determine this period, an experimental approach has been applied in (Groot Wassink 2007; Kwon and Kim 2007; Kwon 2009a,b). The fundamental period of the inkjet printhead can be obtained by measuring the ink-channel pressure using a piezo self-sensing mechanism (Groot Wassink 2007; Kwon and Kim 2007) or by measuring the meniscus position using a CCD camera (Kwon 2009a). Once the fundamental period is measured, the unipolar pulse and the bipolar pulse can be designed by using the parameters recommended in Kwon and Kim (2007) and Kwon (2009a) respectively. However, manual fine tuning of the parameters is needed, since the effect of the refill dynamics⁴ is not considered in the design procedure.

As opposed to the experimental approaches discussed above, a systematic model-based approach to control a DoD inkjet printhead is more effective. Unfortunately, there are a very few applications of systems and control approach available in the open literature. To the best of our knowledge, for the first time, (Groot Wassink 2007) used a systems and control approach to tackle the operational issues in a DoD inkjet printhead. Several numerical models are available in the literature (see (Groot Wassink 2007) for details) to provide inkjet system behavior with higher accuracy. However, these models are highly complex and computationally expensive, making them unsuitable for control purposes. Ideally, for control design, we need a fairly accurate and a simple model. For this purpose, in (Groot Wassink 2007) a physical two-port model has been developed for inkjet printhead. The underlying assumption for this model may not be valid for small droplet printhead considered in this thesis. The primary assumption for experimental modeling approach proposed in (Groot Wassink 2007) is that the inkjet channel dynamics is

⁴Once a droplet is jetted from the nozzle, the ink is pumped inside the ink-channel to refill the volume. This is called the refill dynamics (see Section 2.3 for details).

linear and thus, a model obtained for the non-jetting condition should be valid during the jetting condition at different DoD frequencies. However, it is observed that this is not a valid assumption for the printhead under consideration and thus, the model is not a good representative of the inkjet dynamics at different working conditions. It is proposed in (Groot Wassink 2007) to use this model in iterative learning control (ILC) in order to re-optimize the action pulse. Thus, the actuation pulse obtained provides a better performance for a particular condition. It cannot provide a satisfactory performance if the inkjet dynamics is perturbed by uncertainty which results from the working at different operating points. Moreover, in (Groot Wassink 2007) it is not possible to impose a priori constraints on the shape of the actuation pulse while such constraints are present in practice. Generally, the driving electronics are only able to generate trapezoidal shapes for the piezo actuation input.

In the Octopus project (Basten et al. 2013), wherein the research of this thesis is conducted, (Ezzeldin 2012) has proposed an alternate method to design actuation pulses using an inversion of the inkjet system model. Although, the inverse-based technique has delivered considerable improvement, it has suffered the drawbacks similar to (Groot Wassink 2007) as the model used is not a good representative of different operating points. In order to overcome this deficiency, a model-free approach is presented in (Ezzeldin 2012). The actuation pulse is parameterized to impose the trapezoidal shape constraint. Further, the actuation pulse is optimized by utilizing the measured drop velocities of the jetted drops with the help of a CCD camera and image processing. This approach has delivered significant improvements in the jetted drop properties. It has, further been proposed to use bitmap dependent pulses to improve the print quality.

Based on the available literature, we conclude that the major challenges for inkjet printhead control are to obtain a model which is a good representative of the inkjet system at different operating conditions and to design a constrained robust actuation pulse. In the next section, we will discuss these challenges in more detail to formulate the research objective.

1.4 Problem formulation

In this section, we first formalize the research objective based on state of the art of inkjet printheads and further, we present our approach to meet the objective.

1.4.1 The research objective

In Section 1.2.3, we have seen that the drop properties are mainly influenced by the undesired oscillations within an ink channel generated due to the residual oscillations and the cross-talk. Minimizing these oscillations can substantially improve the performance of a DoD inkjet printhead. Considering a successful use in different engineering disciplines, we chose to explore possibilities with model-based control to improve the inkjet printhead performance. Furthermore, additional benefit of

the model-based control is that the model developed for control purposes may provide useful insight in the system and may be useful for the future development.

In (Groot Wassink 2007; Ezzeldin 2012), we have seen that the performance improvement achieved by using the model-based control is mainly restricted by the ability of the model to describe the inkjet system dynamics. Therefore, it is essential to develop a model representing the printhead dynamics closer to operating conditions. Moreover, this model should be compact enough so that the control techniques available in the literature can be applied with ease.

Furthermore, we have seen that the control techniques (i.e. ILC (Groot Wassink 2007) and inversion-based control (Ezzeldin 2012)) used to design an unconstrained actuation pulse, can provide a satisfactory performance for a particular situation. However, it is difficult to design an actuation pulse which provides a satisfactory performance over the operating range of the printhead, by incorporating information about the inkjet dynamics variation. Moreover, these control techniques do not allow apriori constraints on the pulse shape. Indeed, in practice, the limited computational capacity of the driving electronics of the inkjet printhead restricts us to use only the trapezoidal pulses. Thus, it is essential to develop a method which can utilize the information of the inkjet system at different operating conditions. This method should deliver a robust trapezoidal actuation which will ensure minimum performance over the operating range of the printhead.

Considering the challenges in the modeling of a DoD inkjet printhead and its performance improvement using model-based control, the research question for this thesis is formulated as follows:

Research Question:

Can we represent relevant inkjet system dynamics at different operating regimes in a sufficiently compact way to enable model-based control and can we use that model in a robust feed-forward strategy to improve the performance of the inkjet printhead?

The ‘relevant inkjet system dynamics’ in the model should have an influence on the performance criteria. ‘Different operating regimes’ may not only be restricted to the jetting frequency range but they can also be extended to the allowable deviation in the system parameters (e.g., ink, environment etc.). More importantly, the model will be used for robust control and therefore, it should be able to incorporate system information related to operating conditions in a ‘compact way’. Here, by ‘compact’, we mean to provide description of the inkjet dynamics change over the operating regime in a simpler and concise form, such that the robust control techniques can be easily used. By ‘robust feed-forward strategy’, we mean to provide actuation pulses that obey the limitations of the driving electronics and to ensure minimum performance over the operating regime. ‘To improve the performance of the inkjet printhead’, means to extend the attainable DoD frequency with a tight control on the drop properties.

1.4.2 Approach

In order to achieve the research objective, formulated as the research question in the earlier section, we will primarily focus on developing a model for the inkjet system closer to the operating conditions. For this purpose, we will use data-based modeling approach and will obtain a model $G(q)$ between the actuation input u and the piezo sensor signal y . The measured piezo sensor signal is proportional to the rate of change of the ink-channel pressure. We will use the input signal which is used in practice to jet ink drops, i.e. a series of positive trapezoidal pulses at a given DoD frequency. The amplitude of the trapezoidal pulse is chosen to enable the jetting process and the drop formation. This will facilitate us to get a model $G(q)$ describing the dynamics under working conditions. We will carry out a number of such identification experiments at different DoD frequencies to obtain a set of inkjet models in the operating range of the inkjet printhead. We will represent this set of dynamical models obtained at various operating DoD frequencies by a nominal model $G(q, \Delta)$ with a parametric uncertainty $\Delta \in \mathbf{\Delta}$ on its parameters. We will use a polytopic description to obtain a compact uncertainty set $\mathbf{\Delta}$.

As discussed in Section 1.3, due the limitations of driving electronics, it is not possible to apply feedback control for inkjet printhead. Therefore, we propose to use feedforward control approach to improve the inkjet printhead performance. Note that feedforward controllers are often used to improve the tracking performance (Skogestad and Postlethwaite 2005; Clayton et al. 2009). The design of an optimal feedforward control assumes that the system behavior is accurately captured by the system model. However, in practice the system model is subjected to uncertainties and it is important to take these uncertainties into account during the design of feedforward controller (Devasia 2002). In literature, one can find the design of a robust feedforward controller for uncertain systems using convex optimization involving Linear Matrix Inequality (LMI), e.g. (Giusto and Paganini 1999). Most of the results in literature are available mainly for continuous-time systems which are affected by structured uncertainties. For such systems, in (Scorletti and Fromion 2006; Kose and Scherer 2009), more advanced results are presented to design robust feedforward controller using finite dimensional convex optimization with the help of multipliers (Desoer and Vidyasagar 1975) and Integral Quadratic Constraints (IQC) (Megretski and Rantzer 1997). However, there are very few results available for robust feedforward control design for uncertain discrete-time system (Ohrn et al. 1995; Fujimoto et al. 2001). In this thesis, we have designed robust feedforward control for uncertain discrete-time systems based on the solution of robust filtering problem (Geromel et al. 2000, 2002; Xie et al. 2004). Furthermore, we have extended the results of (Geromel et al. 2000, 2002) and thus, one of the contribution of this thesis is a less conservative feedforward control design for discrete-time systems affected by polytopic uncertainties. Our approach of utilizing robust feedforward control to design actuation pulses for inkjet printhead is described further.

The uncertain system $G(q, \Delta)$, $\Delta \in \mathbf{\Delta}$, obtained in the first step will be further used to design the actuation pulse. We will parameterize the set of actuation pulses $u(k, \theta)$ that the driving electronics can generate with the pulse parameter vector θ (k is the discrete-time index). Then a template $y_{\text{ref}}(k)$ will be designed for the

desired output, i.e., an output profile with fast decaying oscillations. Further, we will design a robust actuation pulse which will ensure a minimum performance for all the models in the uncertainty set. The parameters of this robust actuation pulse θ_{rob} will be obtained by minimizing the worst-case norm of the tracking error $e(k)$ with an uncertain inkjet system $G(q, \Delta)$.

In order to validate the proposed approach, we will use an experimental setup with a small droplet printhead developed at Océ Technologies. This feature of the thesis is a step towards bridging the gap between the control theory development and the control practice. In general, research conducted in this thesis is applicable to a wide range of DoD inkjet printheads including recently introduced MEMS inkjet printheads (Bos et al. 2011; Kima et al. 2012).

1.5 Outline of the thesis

This thesis comprises of three main parts: inkjet modeling, single input single output (SISO) inkjet control and multi input multi output (MIMO) inkjet control. Chapter 2 discusses the available modeling methods and presents an approach of data-based modeling for the inkjet printhead. The dynamic variations observed due to the changes in the operating conditions is incorporated using the polytopic uncertainties on the nominal model of ink channel. In chapter 3, we first tackle the residual oscillations problem for a single ink channel. A robust feedforward control is proposed to design constrained and unconstrained actuation pulses, providing improvements in the performance. Chapter 4 presents simulation and experimental results to show the efficacy of the proposed methods to control the ink channel. Chapter 5 considers the MIMO inkjet printhead control problem and extends the frame work laid in Chapter 3 to tackle the cross-talk problem. Finally, conclusions and recommendations are given in Chapter 6.

Inkjet Printhead Modeling

In this chapter a physical model is reviewed which can describe the dynamics of an ink channel. In order to obtain the inkjet model quickly a data-based model development procedure is presented. The experimental investigation suggests that the system dynamics is influenced by the DoD frequency. Therefore, the set inkjet models obtained at various DoD frequencies is represented by a nominal model with parametric uncertainty. Based on these observations a gray-box model is obtained by introducing uncertainty on the parameters of the physical model.

2.1 Introduction

In the previous chapter we have seen that the performance of a DoD inkjet printhead can be improved by effectively minimizing the residual oscillations and the cross-talk effect. This additional passive damping can be provided by the re-design of the actuation pulses. Model-based control techniques, one of most popular control approach, can be employed for the actuation pulse re-design. Most essential requirement of the model-based control techniques is that they need a fairly accurate model of the system. Therefore, in this section we will discuss the modeling approach for a DoD inkjet printhead. As discussed in Section 1.2 the printhead under investigation consists of two arrays each containing 128 ink channels. In general, developing a MIMO model for such a large number of ink-channels is a complex and daunting task. Given the geometrical arrangement in the printhead, it is well known that a particular ink-channel is affected only by those ink-channels which lie in its close proximity. For the printhead considered in this thesis, experimental investigation had shown that the n -th ink-channel is dominantly influenced by its immediate neighbors, that is the $(n - 1)$ -th and $(n + 1)$ -th ink-channels. Exploiting this structure, we describe the printhead dynamics by a simplified MIMO model which consists of a series of Multi-Input-Single-Output models, as shown in Figure 2.1.

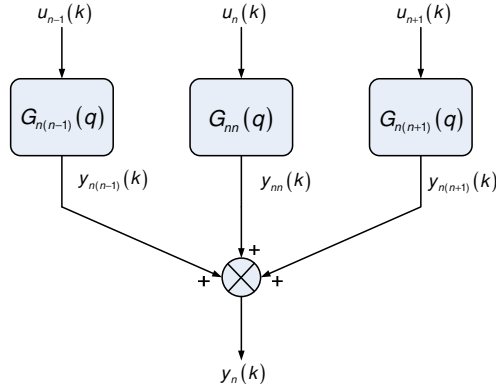


Figure 2.1: Schematic diagram of the inkjet channel with the cross-talk.

The goal of this thesis is to improve the drop consistency of a DoD inkjet printhead. A droplet jetting through an ink channel is a discrete-event. Modeling of the inkjet printhead as a discrete-event system is a complex and time consuming task. Moreover, controller design using such a discrete-event model will prohibit use of well developed linear time-invariant (LTI) control theory. Hence, we will use internal signal y of an ink channel to predict the drop consistency. There are two internal signals¹ which could be used to predict the jetting process; the first one is the meniscus velocity and the second one is the piezo sensor signal (which is proportional to the ink channel pressure) (Dijksman 1984; Groot Wassink 2007). In the next section we will investigate modeling of the dynamics from the piezo input to these internal signals.

Let y_n be the output internal signal of the n -th channel. Observe that in Figure 2.1, this output y_n is the sum of contributions from the n -th channel and its immediate neighbors:

$$\begin{aligned} y_n(k) &= y_{nn}(k) + y_{n(n-1)}(k) + y_{n(n+1)}(k) \\ &= G_{nn}(q)u_n(k) + G_{n(n-1)}(q)u_{n-1}(k) + G_{n(n+1)}(q)u_{n+1}(k), \end{aligned} \quad (2.1)$$

where u_j is the input from the j -th ink-channel, $G_{ij}(q)$ is the transfer function from the j -th ink channel to the output of the i -th ink channel and q is the forward shift operator, k is the discrete time index such that kT_s gives the time and T_s is the sampling time.

Additional observations that help us in further simplifying the model structure

¹The meniscus position provides better information regarding the jetting process compared to the piezo sensor signal or the meniscus velocity. However, for the printhead under investigation we do not have a good model for the meniscus position and it is not also possible to measure the meniscus position during the jetting. Therefore, we have restricted the choice of the internal variables to the meniscus velocity (for which a physical model is available) and the piezo sensor signal (which can be measured experimentally to construct a data-based model).

are:

1. The geometry of all the ink-channels is identical leading to very similar input-output relations.
2. The cross-talk effects due to the left and right neighboring ink-channels are similar due to symmetrical structural arrangement.

These two observations lead to:

$$\begin{aligned} G_{nn}(q) &= G_d(q) \\ G_{n(n-1)}(q) &= G_{n(n+1)}(q) = G_c(q), \quad \forall n. \end{aligned} \quad (2.2)$$

where $G_d(q)$ is a transfer function for the direct ink channel dynamics and $G_c(q)$ a transfer function for the cross-talk.

Using (2.2), the response of the piezo sensor signal y_n of the n th channel (2.1) can be simplified as follows:

$$y_n(k) = G_d(q)u_n(k) + G_c(q)u_{n-1}(k) + G_c(q)u_{n+1}(k). \quad (2.3)$$

In other words, the MIMO inkjet printhead modeling now reduced to modeling of two single input single output (SISO) models $G_d(q)$ and $G_c(q)$.

In the next section we will discuss the physical modeling of the ink channel dynamics and subsequently the data-based modeling of an inkjet printhead.

2.2 Physical Modeling

In the previous section we have discussed with some assumption we can reduce the MIMO modeling of an inkjet printhead to the modeling of two SISO dynamical systems, i.e. the direct ink-channel dynamics and the cross-talk dynamics. In this section we will discuss physical modeling approach to describe the direct ink channel dynamics. In the literature, several analytic and numerical models are available for the inkjet channel dynamics in the literature (for details see (Groot Wassink 2007)). Analytical models are obtained by introducing several assumptions and simplifications. Due to this, the accuracy of analytical models is low compared to numerical models. On the other hand, numerical models are very complex and therefore computationally expensive. If the intended use of the model is to design model-based control then it is one preferred to have a simpler model with a sufficient accuracy. Hence, often a lumped-parameter modeling approach is adopted which uses an equivalent electric circuit to describe the dynamics of the ink channel (Berger and Recktenwald 2003; Park et al. 2006). This modeling technique is a useful and commonly applied analysis approach for designing piezoelectric inkjet systems. In this modeling framework, resonances are modeled using capacitors, resistors and inductors in series. However, these models lack accuracy. A two-port model is proposed in (Groot Wassink 2007) to describe the ink channel dynamics

utilizing the concept of bilaterally coupled systems. The ink channel is divided into subsystems, namely, reservoirs, piezoelectric actuators, channels, connections, and nozzles. Each subsystem is modeled as a two-port system based on first principle modeling. The two-port model of an ink channel is obtained by connecting the subsystems and applying the boundary conditions. This model has less complexity and requires little computational time. However, due to modeling discrepancies, this model could not accurately capture the first resonance frequency of the channel dynamics, which is the most important resonance frequency to predict the drop properties. Therefore, we selected the ‘narrow-gap model’ (Wijshoff 2010) for control synthesis purposes as it offers the best compromise between the model accuracy and the computational time. We discuss this model in the next section.

2.2.1 Narrow Gap Model

The narrow-gap model is an analytical model, which describes the dynamic system from the piezo input voltage u to the meniscus velocity y . A detailed derivation of the narrow-gap model (NGM) for the considered DoD inkjet printhead using the narrow channel theory (Beltman 1998) is given in (Wijshoff 2010). In this model, a narrow channel wave equation is used to describe the acoustics inside the ink channel. In this model, a narrow channel wave equation is used to describe the acoustics inside the ink channel. This wave equation is a simplified form of the Navier-Stokes equation (conservation law for fluids). The properties of the ink considered in the model are as follows: the viscosity is $10 \cdot 10^{-3}$ Pa·s, the surface tension is $28 \cdot 10^{-3}$ Nm⁻¹ and the speed of sound in the ink is 1250 ms⁻¹.

In the narrow-gap model, the frequency response $\mathcal{H}(\omega)$ of the system is computed using the sine sweep method. Note that to avoid confusion of different outputs, we will purposely use different notation for the meniscus velocity dynamics than G_d used in (2.3). This method consists of solving the wave equation for a sinusoidal input signal $u(t) = |u| \sin(\omega_1 t + \phi_1)$ at some frequency ω_1 . Supposing that the corresponding meniscus velocity is given by $y(t) = |y| \sin(\omega_1 t + \phi_2)$, the frequency response of the system at ω_1 is given by:

$$|\mathcal{H}(\omega)| \Big|_{\omega=\omega_1} = \frac{|y|}{|u|} \quad (2.4a)$$

$$\angle \mathcal{H}(\omega) \Big|_{\omega=\omega_1} = \phi_2 - \phi_1 \quad (2.4b)$$

By repeating this procedure over a fine frequency grid, we obtain the frequency response given in solid line in Figure 2.2. It can be seen that the system is non-minimum phase. The narrow-gap model is experimentally validated in (Wijshoff 2008) by measuring the meniscus velocity on an experimental setup with the help of a laser vibrometer. The empirical frequency function $\mathcal{H}(\omega)$ cannot be used for the feedforward control leading to the optimal piezo actuation. A transfer function model of the inkjet system is indeed needed for the optimization. Hence, we fit a discrete-time model $H(q)$ to the frequency response obtained from the narrow-gap model. We first used the system identification toolbox of MATLAB to approximate

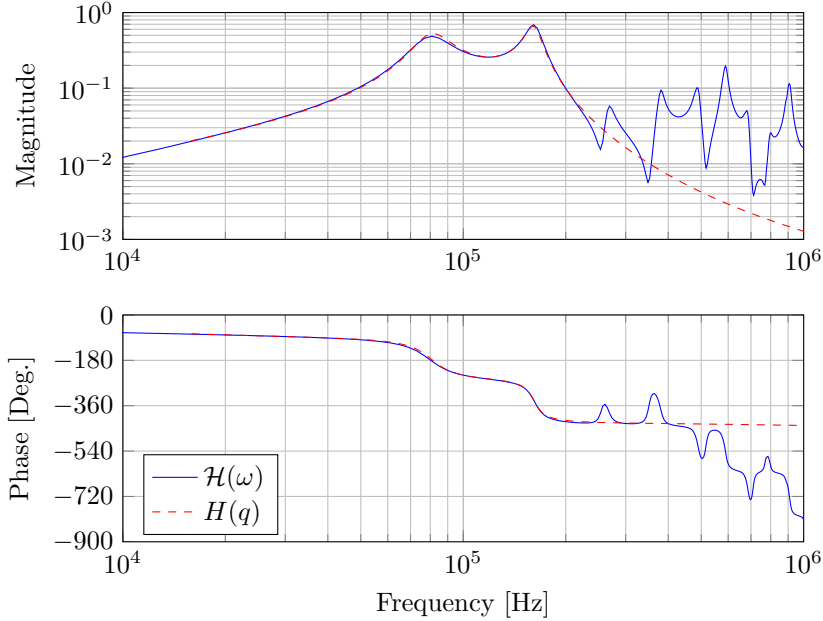


Figure 2.2: Frequency response of the narrow-gap model $\mathcal{H}(\omega)$ (solid) and frequency response $H(e^{i\omega})$ of the approximated transfer function $H(q)$ (dashed).

the empirical frequency function $\mathcal{H}(\omega)$ by a 16th order transfer function (Khalate et al. 2010, 2011). We further discarded the higher order resonant modes to obtain a simplified fourth order transfer function $H(q)$. Since it is well known that the influence of the higher order resonant modes on the drop properties is negligible compared to the first resonant mode (Dijksman 1984). The non-minimum phase behavior present in the frequency response is also captured by the fitted model $H(q)$ shown by the dashed line in Figure 2.2.

The approximated discrete time model $H(q)$ between the piezo voltage u to the meniscus velocity y for a sampling time T_s chosen equal to $0.25\mu\text{s}$ is given as follows:

$$H(q) = g \left(\frac{q^2 + b_1q + b_2}{q^2 + a_1q + a_2} \right) \left(\frac{q + b_3}{q^2 + a_3q + a_4} \right) \quad (2.5)$$

where q is the forward shift operator and the nominal values of the coefficients are

$$\begin{aligned} b_1 &= -3.4465, b_2 = 2.4575, b_3 = -0.5746, g = 1.1820 \times 10^{-3} \\ a_1 &= -1.9538, a_2 = 0.9696, a_3 = -1.9102, a_4 = 0.9732. \end{aligned}$$

This inkjet channel dynamics can be represented in the state-space form as follows:

$$x_S(k+1) = A_S x_S(k) + B_S u(k)$$

$$y(k) = C_S x_S(k) \quad (2.6)$$

where

$$A_S = \begin{bmatrix} 0 & -a_2 & 0 & 0 \\ 1 & -a_1 & 0 & 0 \\ 0 & b_3 & 0 & -a_4 \\ 0 & 1 & 1 & -a_3 \end{bmatrix}, \quad B_S = \begin{bmatrix} g(b_2 - a_2) \\ g(b_1 - a_1) \\ gb_3 \\ g \end{bmatrix}, \quad C_S = [0 \ 0 \ 0 \ 1]. \quad (2.7)$$

This approximated model $H(q)$ will be used in the next chapter for further analysis and for the actuation pulse design.

Remark 2.1 *The narrow-gap model $\mathcal{H}(\omega)$ depends on the printhead geometry and the properties of the ink material. Hence, the discrete-time transfer function $H(q)$ approximating the frequency response of the narrow-gap model will not be the same for different ink materials and printhead geometries. However, in such situation, we can repeat the procedure above to obtain the discrete-time transfer function $H(q)$ corresponding to the considered situation.*

Remark 2.2 *The narrow-gap model presented in (Wijshoff 2010) is obtained under the assumption that the acoustic behavior inside the ink-channel is linear. This assumption is valid for the inkjet printheads used in the graphical printing industry. This is thanks to the fact that the meniscus movement with a wide variety of ink materials used in this industry is linear, as these ink materials behave as Newtonian fluids. For several emerging new industrial applications (Williams 2006), this will not be the case anymore. However, we will see in Section 3.4.1 that the proposed method for the constrained actuation pulse design is not limited to linear models. If a nonlinear inkjet system model is available for a non-Newtonian fluid, one can still use the proposed approach to design the actuation pulse in order to damp the residual oscillations.*

Remark 2.3 *The narrow-gap model, almost perfectly, describes the relation between $u(k)$ and $y(k)$ when one single ink drop is jetted from an ink channel which was at rest. Also, this describes only the SISO dynamics from the piezo input of n -th channel to the meniscus velocity of n -th channel. The cross-talk effect can not be predicted accurately for the considered printhead.*

It is not always easy or economical to obtain a good physical model of an ink channel. Furthermore, the modeling of a MIMO model is much complex task. In such scenarios, experimental measurements of the system can be used to obtain a black-box model relating the the input and the output. Hence, in the next section we will discuss the data-based modeling approach for inkjet system.

2.3 Data-based Modeling

The printhead designers often use simple physical models discussed in the earlier section to predict the system behavior and to optimize the printhead performance. However, it is not always possible to obtain a good physical model for a single ink channel. Especially, physical modeling of a multi-input multi-output (MIMO) inkjet printhead, i.e. a model with the cross-talk effect, is a difficult and a time consuming task. In practice, inkjet application users rely extensively on experimental data (see (Bogy and Talke 1984; Chung et al. 2005; MicroFab Technologies Inc. 1999; Gan et al. 2009; Dong et al. 2006; Kwon and Kim 2007; Kwon 2009a)) to fine tune the printhead performance. This is due to insufficient knowledge of the various complex interactions taking place inside an inkjet printhead. In such situations, it is convenient to obtain a model by utilizing the measured experimental input output data. Moreover, it will also be useful for printhead designers to validate their physical model and to quickly design the actuation pulse.

In this section we utilize system identification to obtain a MIMO model for an inkjet printhead dynamics using experimental measurement. The physical model obtained in Section 2.2.1 describes the dynamics between the piezo input and the meniscus velocity. However, it is difficult to experimentally measure the meniscus velocity when an ink channel is jetting. Therefore, we exploit the self-sensing mechanism of the piezo-unit and use it simultaneously as an actuator and a sensor. We obtain a model G_d from the piezo input to the piezo sensor output (which is proportional to the derivative of the channel pressure). This gives us sufficient insight about the jetting process.

A similar identification approach is used in (Groot Wassink 2007) wherein, experimental data are obtained when the ink channel is in the non-jetting condition. A low amplitude (non-jetting) multi-sine is used as an excitation signal and the piezo sensor response is measured. A frequency response of the inkjet system is estimated using the measured input-output data. The underlying assumption in this approach is that the dynamics between the piezo input and the piezo sensor output do not change whether or not the channel is in the jetting condition. Such an assumption is very restrictive because the *refill dynamics* and the nonlinearities in drop formation have a significant influence on the input-output relation. Once a droplet is jetted from the nozzle the ink is pumped inside the ink-channel to refill the volume. This is called the refill dynamics. The meniscus position and the meniscus velocity is influenced by this slow refill dynamics.

Therefore, for identification we use the input signal which is used in practice to jet ink drops, i.e. a series of positive trapezoidal pulses at a given DoD frequency. The amplitude of the trapezoidal pulse is chosen to enable the jetting process and the drop formation. In this way, we get a model describing the dynamics under working condition. Further, as the influence of the refill dynamics on the jetted drop will change with the change in the jetting frequency, the inkjet model obtained at different DoD frequencies will not be the same. Therefore, we carry out a number of identification experiments at different DoD frequencies.

Using the assumptions (2.2) discussed in Section 2.1 and (2.3) the MIMO system identification problem for a printhead has now been reduced to identifying two

single input single output (SISO) models $G_d(q)$ and $G_c(q)$. $G_d(q)$ will be identified by exciting only at the n -th channel ($u_{n-1} = u_{n+1} = 0$) and $G_c(q)$ will be identified by exciting only at the $(n + 1)$ -th channel ($u_n = u_{n-1} = 0$).

In the sequel we will first present the experimental measurement of the piezo sensor signal and then formal identification of a single ink channel G_d and the cross-talk dynamics G_c . We here adopt the prediction-error identification method (time-domain identification).

Remark 2.4 *In Section 1.4.2, it is described that the problem of improving the drop consistency will be formulated as a control problem pertaining to regulate the internal variables of the inkjet printhead. In Section 3.3, it will be discussed that in order to formulate this control problem for a general setting, we will use the well-known fact that the meniscus velocity mainly governs the drop properties (Dijksman 1984). Therefore, ideally, one should have constructed a data-based model for the meniscus dynamics $H(q)$. Unfortunately, in the current experimental setup it is not possible to measure the meniscus behavior. Therefore, we propose to use the only available sensor in the inkjet printhead, i.e. the piezo sensor signal, to obtain a data-based model from the piezo input to the piezo sensor signal $G(q)$.*

According to (Dijksman 1984; Groot Wassink 2007), the piezo sensor signal also gives sufficient information about the drop jetting process in an inkjet system. Based on this, using G instead of H for control purpose will have little impact. Another advantage of measuring the piezo sensor signal is that it may enable the adaptability of the printhead. Indeed, the change in the printhead dynamics over the lifespan of the printhead could be modeled using the proposed data-based modeling technique and the feedforward control approach presented in the next chapter can be used to re-tune the actuation (and, by doing so, extends the life of the printhead).

Since the possibility of identifying a model for the meniscus dynamics could nevertheless be useful to designers during the printhead design phase, it is recommended to explore other measurement methods to monitor the meniscus behavior during the jetting.

2.3.1 Measurement of the piezo sensor signal

In this section we will discuss the piezo sensor functionality available in the experimental setup (see in Appendix B). Self-sensing of a piezo unit has been employed in various applications for simultaneous actuation and sensing. Generally, the self-sensing unit uses a bridge circuit with a piezo actuator in one arm and a passive capacitor of equivalent capacitance in the other arm. This ensures that one can measure the dynamic behavior of the piezo structure. However, in case of an inkjet channel, the measured signal p from this bridge circuit consists of two contributions (see Figure 2.3). The first contribution p_1 is the generated charge which is proportional to the piezo deformation due to the applied actuation voltage and is referred to as the direct-path. The second contribution p_2 originates from the force exerted by the ink in the channel and is referred to as the indirect-path. As the second contribution has information about the jetting process, it is the required

sensor signal and has to be extracted from the measured signal p . Typically, the contribution of the indirect-path (i.e. the sensor signal p_2) is very small compared to the direct-path. Consequently, it is difficult to measure the sensor signal (indirect-path) while simultaneously using the piezo as an actuator.

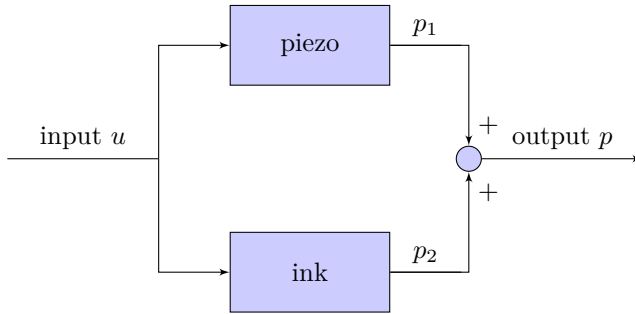


Figure 2.3: The basic principle to measure the acoustic sensor signal

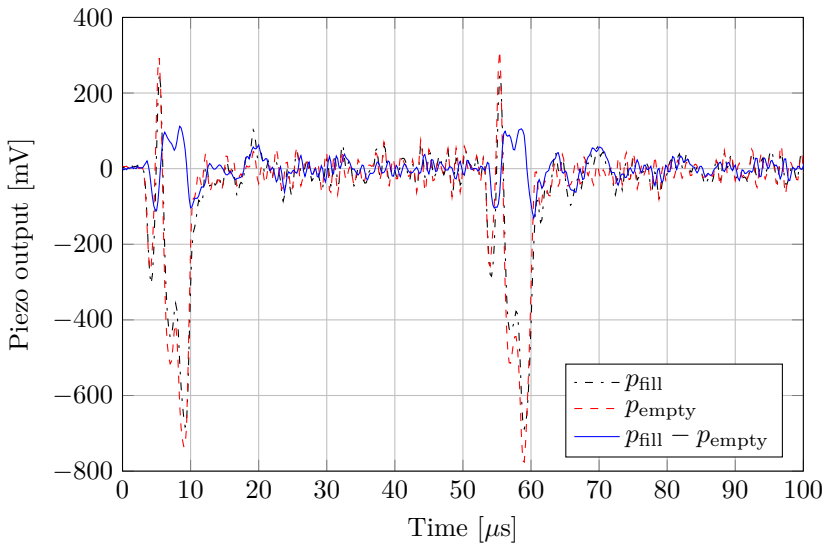


Figure 2.4: Experimental data obtained while jetting at a DoD frequency of 20kHz: the response of the filled ink channel p_{fill} , response of the empty ink channel p_{empty} , and the reconstructed piezo sensor signal $p_{\text{fill}} - p_{\text{empty}}$.

In (Groot Wassink 2007), a hardware compensation method is proposed to extract the sensor signal p_2 . In this method, two ink channels with a similar piezo capacitance are connected in the bridge circuit. Out of these two ink channel one ink channel is filled with the ink and the other ink channel is empty. Thus, the sensor signal p_2 is obtained by subtracting the measured signals of the two ink

channels. However, there are several drawbacks of this method. A major difficulty is to make the hardware changes in the ink printhead to create an empty ink channel. Another drawback is that even though the ink channel is empty, a small contribution due to the deformation of the structure is present in the indirect-path. Also, there will be always a small difference in the piezo capacitance. In order to overcome these drawbacks, we use the off-line approach to reconstruct the sensor signal p_2 . We have carried out two experiments and measure the piezo output signal p from the ink channel by applying the same actuation pulse at a fixed DoD frequency. The first experiment is carried out with the ink inside the channel and the measured piezo output signal $p_{\text{fill}} = p_1 + p_2$ is stored. During the second experiment the channel is kept empty and the measured piezo output signal $p_{\text{empty}} = p_1$ is stored. Thus, the sensor signal p_2 is obtained by offline subtraction of the signal p_{empty} from the signal p_{fill} . Fig. 2.4 shows the signals p_{fill} , p_{empty} and the reconstructed piezo sensor signal $p_2 = p_{\text{fill}} - p_{\text{empty}}$ at a DoD frequency of 20kHz.

2.3.2 Overview of Prediction Error Identification Method (PEM)

Prior to discussing the identification results, in this section we first provide an overview of the identification procedure which we will use for the identification of G_d and G_c .

Framework

Consider the identification a SISO system, e.g. identifying the direct dynamics G_d in (2.3) by applying excitation signal u only at the n -th channel ($u_{n-1} = u_{n+1} = 0$). The measured output signal $y(k)$ of the true system \mathcal{S} is assumed to be generated as follows:

$$y(k) = G_0(q)u(k) + v(k), \quad (2.8)$$

where $G_0(q)$ is a linear time-invariant dynamical system, $u(k)$ is an input sequence, and $v(k)$ denotes the measurement noise. Note that the measurement noise is not correlated to the input $u(k)$. Further, the measurement noise $v(k)$ is modeled as $v(k) = S_0(q)e(k)$ with $S_0(q)$ a linear time-invariant monic stable filter, and $e(k)$ a stationary stochastic zero-mean white noise process with variance σ_e^2 .

The objective of PEM is to find the best parametric models $G(q, \psi)$ and $S(q, \psi)$ for the unknown transfer functions $G_0(q)$ and $S_0(q)$ using a set of measured data $u(k)$ and $y(k)$ ($k = 1, \dots, N$) generated by the true system $\mathcal{S} = \{G_0, S_0\}$. The set of models $\{G(q, \psi), S(q, \psi)\}$ is denoted by \mathcal{M} . If we choose the parametrization \mathcal{M} rich enough to describe the true system \mathcal{S} then there will exist a parameter ψ_0 such that $G(q, \psi_0) = G_0(q)$ and $S(q, \psi_0) = S_0(q)$, i.e. $\mathcal{S} \in \mathcal{M}$. Note that the input signal used in the identification experiment should be persistently exciting².

²The input excitation signal is called persistently exciting if the number of parameters to be identified in G are smaller than the order of excitation of the input signal. The order of excitation of the input signal is n if the power spectrum of the input signal is unequal to 0 at n number of

Parameter Estimation

For the given measurement data $Z^N := \{y(k), u(k) | k = 1, \dots, N\}$ and a model $\{G(q, \psi), S(q, \psi)\} \in \mathcal{M}$ we define the prediction error (or the residuals) $\epsilon(k, \psi)$ as follows (Ljung 1999):

$$\epsilon(k, \psi) = S(q, \psi)^{-1}(y(k) - G(q, \psi)u(k)). \quad (2.9)$$

The parameter vector $\hat{\psi}_N$ of the identified model $G(\hat{\psi}_N)$ and $S(\hat{\psi}_N)$ of G_0 and S_0 is determined as follows:

$$\hat{\psi}_N = \arg \min_{\psi} V_N(\psi, Z^N) = \arg \min_{\psi} \frac{1}{N} \sum_{k=1}^N \epsilon^2(k, \psi). \quad (2.10)$$

It is important to note that, when $\mathcal{S} \in \mathcal{M}$, the identified parameter vector $\hat{\psi}_N$ is a consistent estimate of ψ_0 , i.e. $\hat{\psi}_N \rightarrow \psi_0$ with probability 1 when $N \rightarrow \infty$ (Ljung 1999).

Model Structure Validation

With the parameter estimation procedure, the optimal model within the chosen model structure can be obtained. However, if the model structure \mathcal{M} is not able to describe the true system \mathcal{S} , this optimal model will be a poor estimate of G_0 and H_0 . It is thus crucial to know whether the model structure is rich enough to represent the true system, i.e. $\mathcal{S} \in \mathcal{M}$. The residuals are the differences between the model output and the measured output and hence, they represent the portion of the data which are not explained by the model. Thus, statistical analysis of $\epsilon(k) = \epsilon(k, \hat{\psi}_N)$, such as the auto-correlation function R_ϵ and the cross-correlation function $R_{\epsilon u}$ defined as follows are useful for model structure validation:

$$\begin{aligned} \hat{R}_\epsilon^N(\tau) &= \frac{1}{N} \sum_{k=1}^N \epsilon(k)\epsilon(k-\tau) \\ \hat{R}_{\epsilon u}^N(\tau) &= \frac{1}{N} \sum_{k=1}^N \epsilon(k)u(k-\tau). \end{aligned} \quad (2.11)$$

When $\mathcal{S} \in \mathcal{M}$, $\epsilon(k, \hat{\psi}_N) \rightarrow \epsilon(k, \psi_0) = \epsilon(k)$ when $N \rightarrow \infty$. Consequently, \hat{R}_ϵ and $\hat{R}_{\epsilon u}$ could be considered as estimate of $R_\epsilon = \sigma_e^2 \delta(\tau)$ (where $\delta(\tau)$ is the unit pulse) and $R_{\epsilon u}(\tau) = 0, \forall \tau$. Using the variance of these estimates confidence bounds could be built in which \hat{R}_ϵ and $\hat{R}_{\epsilon u}$ should lie to validate the hypothesis $\mathcal{S} \in \mathcal{M}$ (Ljung

points in the normalized frequency interval $(-\pi, \pi)$ (for details, see (Ljung 1999)).

1999).

Model Validation

To further validate the model, another dataset $Z_{\text{val}} = \{y, u\}$ can be used to verify the ability of the model to predict $y(k)$ from $u(k)$. For this purpose, $y(k)$ can be compared to $\hat{y}(k) = \hat{G}(q, \hat{\psi}_N)u(k)$. A good measure of the fit between y and \hat{y} is :

$$\text{Best Fit} = \left(1 - \frac{|y - \hat{y}|}{|y - \bar{y}|} \right) \times 100\% \quad (2.12)$$

where \bar{y} is the mean of y .

The Best Fit is a measure on how good the model \hat{G} is able to reproduce the data.

2.3.3 Experimental modeling a single ink channel dynamics

In this section we will discuss identification of a single ink channel dynamics G_d using the PEM. As discussed in the previous section, the excitation signal for identification should be chosen which is used in practice to jet ink drops. Hence, the input signal should be a series of positive trapezoidal pulses which enable the jetting process and the drop formation. In this way, we get a model describing the dynamics under working condition. Therefore, we will first present the design of the excitation signal for the identification experiment.

Remark 2.5 *In practice, random bitmap patterns are jetted with an inkjet print-head. Therefore, in order to obtain a model of inkjet printhead close to the operating point, one should ideally conduct experiments with all possible bitmap patterns. This is of course virtually impossible. Hence, we choose to operate the inkjet print-head under continuous jetting at different DoD frequencies in order to demonstrate the data-based modeling approach (with a limited number of experiments). Even though the selected set of operating conditions is not complete, this approach allows to cover many possible operating conditions and fairly reflects the main non-linear phenomenon i.e. the refill mechanism. Note that our approach also considers few possibilities where 0's are present in a bitmap³. Indeed, the pattern 1111 at a DOD frequency of 20kHz is equivalent with 10101010 at a DoD frequency 40kHz and with 100100100100 at 60kHz etc. As will be evidenced by the experimental results in Chapter 5, this choice turns out to be justified. However, our approach does not consider all different bitmaps containing 0's, e.g. 111101010100100100.*

Note that the data-based model could be further refined by considering in addition bitmap patterns containing 0's . In (Ezzeldin 2012), it is shown that, while jetting

³In a bitmap pattern, 1's represent the request to jet a droplet and 0's represent the request not to jet a droplet during the time period associated with the chosen DoD frequency.

a bitmap pattern, the pre-history of only a few number of droplets jetted before the current droplet has influence on the drop properties of the current droplet. Using these results, one could design a limited number of representative bitmap patterns. The data-based model obtained using this set of operating conditions could even more closely represent the inkjet printhead behavior in real life printing.

Remark 2.6 *Similar to the physical model $H(q)$, as discussed in Remark 2.1, the model obtained with the experimental modeling approach depends on the printhead geometry and the properties of the ink material. Thus, for different printhead geometries or ink materials one can repeat the same identification procedure to obtain the ink channel model for the new situation. Note that for the same printhead geometry and the same type of ink material, the change in the ink toner color (i.e. cyan, magenta, black and yellow) has negligible effect on the ink channel dynamics. For the ink used in the printhead under investigation, the change in the first resonant frequency is less than 1 kHz. In such a scenario, one can use the same data-based model for all ink colors rather than identifying different models for each color.*

Design of the standard resonating pulse

It is easy to determine the standard resonating pulse if we know the ink channel dynamics. Indeed, it is well known that the jetting pulse should be a positive trapezoidal pulse with the pulse duration equal to the half of the time period of the first resonant mode of the ink channel (Kwon 2009a). For the printhead considered in this thesis, we know the standard pulse for the physical model. In general, the inkjet practitioners do not have this information as G_d is not known at this stage. In order to circumvent this chicken and egg problem we have identified, using the procedure presented in the next section, an initial model of G_d using trapezoidal input (with a duration $3 \mu\text{s}$ and an amplitude 25 V) which is not guaranteed to jet a drop. This allowed us to determine that the first resonant frequency is around 80 kHz. We have therefore designed our input for the identification as a trapezoidal pulse of duration $6 \mu\text{s}$ (i.e. $\frac{1}{2}(\frac{1}{80 \times 10^3})$) and the amplitude 25 V. The rise time and the fall time⁴ of the trapezoidal pulse is chosen equal to $1.5 \mu\text{s}$. It is important to note that if this pulse allows to jet a drop, it is certainly not a pulse which leads to a flat DoD curve since it has not been designed to reduce the residual oscillations. As mentioned earlier, the input signal for the identification will be a series of this standard pulse at a given DoD frequency.

Identification of a single ink channel dynamics

As discussed in the introduction of Section 2.3, due to various effects which occur only when the ink channel is jetting and influencing the drop properties, it is

⁴The rise time and the fall time of the standard pulse mainly influence the satellite drops. For the ink (viscosity equal to $10 \cdot 10^{-3}$ Pa·s) used in the printhead under consideration, the influence of the rise time and the fall time is almost negligible (for more details on print-ability of ink see (Derby 2010)). For the higher ink viscosity practitioners may have to do some additional experiment to fine tune the rise time and the fall time of the standard pulse.

important to obtain the ink channel model in the jetting condition. The narrow-gap model $H(q)$ describes the ink channel dynamics once a single droplet is jetted (i.e. very low DoD frequency). Therefore, in order to have a model describing the other internal (piezo sensor) signal at similar conditions we will obtain G_d at low DoD frequency. Hence, at a lower DoD frequency, say 15 kHz, we collect the piezo input and the piezo sensor output after jetting several ink drops. The standard pulse, $u_{\text{std}}(k)$, designed in the previous section is used for jetting the drops from the channel number 65, see Figure 2.5. We thus apply the input only to one channel and set the inputs of other ink channels to zero. Note that in the actual experiment, the number of pulses applied are equal to 360. In Figure 2.5 we show only the first three pulses. This input signal meets the persistence of excitation condition (see (Ljung 1999)). The sampling frequency is 2.5 MHz and the length of the measured data is 60×10^3 . The response of the piezo sensor, $y_{nn}(k)$, to this excitation is also given in Figure 2.5.

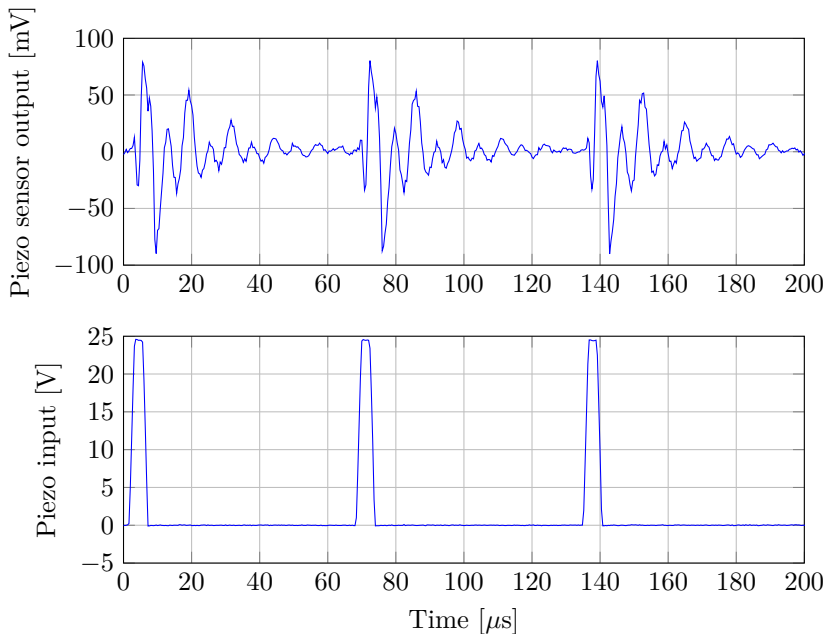


Figure 2.5: Experimental data for identifying the direct dynamics, obtained while jetting at a DoD frequency of 15kHz.

Note that the Prediction-Error identification encounters numerical problem when the sampling frequency is too high compared to the dynamics of the interest. Therefore, the experimental data is down-sampled by a factor four using the MATLAB command `decimate`. The Prediction-Error identification algorithm (available in the MATLAB Identification Toolbox) is employed on the down-sampled experimental data of length 2000. This gives us a discrete time transfer function. Its frequency response is shown in Figure 2.7 (solid-line). The chosen model structure \mathcal{M} uses different parameters for the model G and S (i.e. Box-Jenkins model

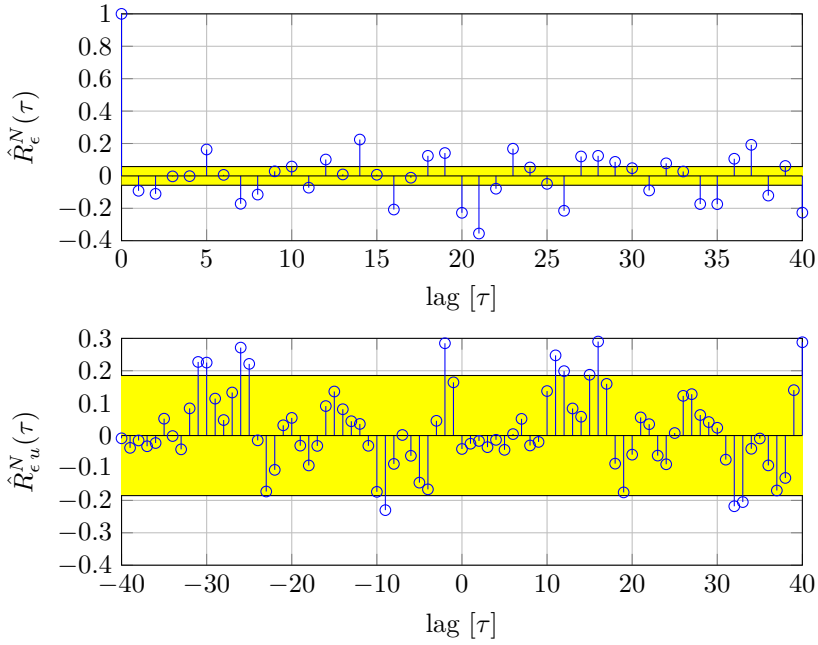


Figure 2.6: Residual tests for the direct-channel.

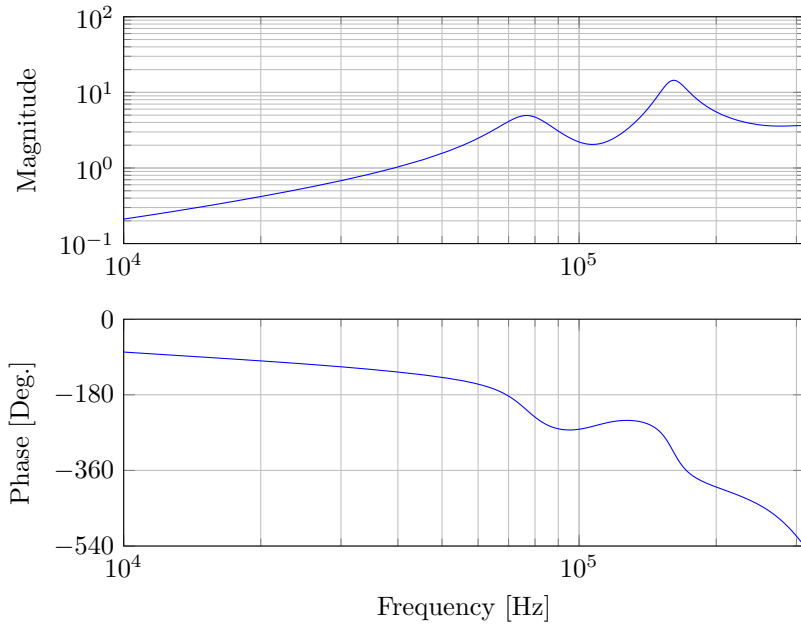


Figure 2.7: Frequency responses of the identified direct dynamics G_d

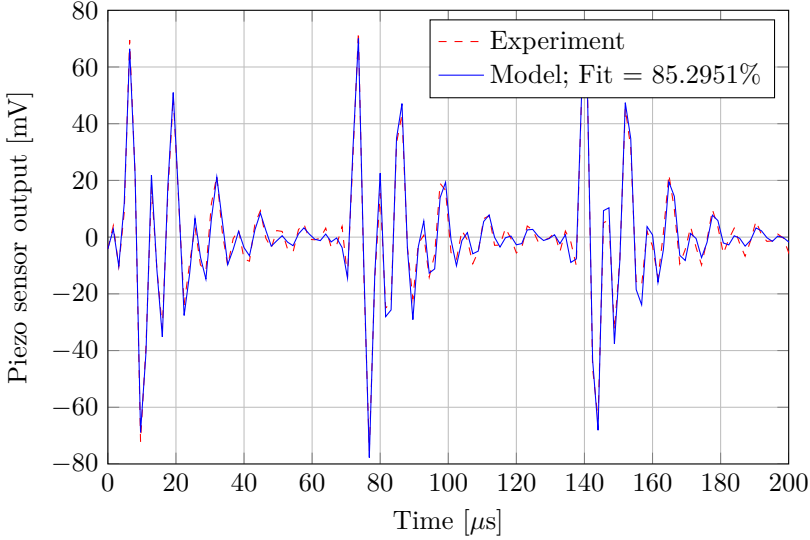


Figure 2.8: Best Fit between the measured and the simulated outputs for the direct dynamics G_d .

structure) and the order of G is 6 and the one of S is 2. Due to the inherent nonlinearities of the system, this model structure is not completely validated as \hat{R}_ϵ and $\hat{R}_{\epsilon,u}$ do not completely in their confidence bounds (see Figure 2.6). However, since increasing the model orders does not improve the results of the model structure validation test, we have opted for this model structure.

To validate further our model we used a set of down-sampled data of length 2000 which is different from the data set used for identification. In Figure 2.8, we compare the actual measured output y of this data set with the simulated output $\hat{y}(k) = \hat{G}(q)u(k)$. We do not see major difference and this is confirmed by the value of the Best Fit equal to 85.29%. Note that the data presented in Figure 2.8 is down-sampled and hence, there is a change in the peak to peak amplitude due to removed samples with respect to Figure 2.5. In the sequel we will refer to the model identified in this section and represented in Figure 2.7 as the nominal direct dynamics G_d .

2.3.4 DoD dependence of a single ink channel dynamics

In the previous section we identified the model G_d for a particular DoD frequency of 15 kHz. As discussed earlier, the slow refill dynamics could influence the ink channel dynamics G_d differently at different DoD frequencies. Hence, the model obtained at different DoD frequencies may be different from G_d . In order to verify this hypothesis, we carry out a number of experiments to obtain input-output data at various DoD frequencies (ranging from 20kHz to 70kHz). By repeating the Prediction Error identification algorithm on all these data sets we obtain a set

of models. The Bode magnitude plots for several DoD frequencies are shown in Figure 2.9.

In Figure 2.9, observe that at all considered DoD frequencies, the model contains two resonant modes. The frequency at which the first resonant mode occurs varies significantly i.e. in the interval [76.5 93.18] kHz. Also the amplitude varies considerably in i.e. the interval [4.94 7.77] (i.e. [13.87 17.80]dB). For the second resonant mode, the variations in frequency and amplitude are [155.20 166.5] kHz and [14.40 20.78] ([23.17 26.35]dB) respectively. The variation in the second peak will be neglected since higher order peaks are known to be of very less influence for the ink drop properties when compared to the first resonant mode (Dijksman 1984).

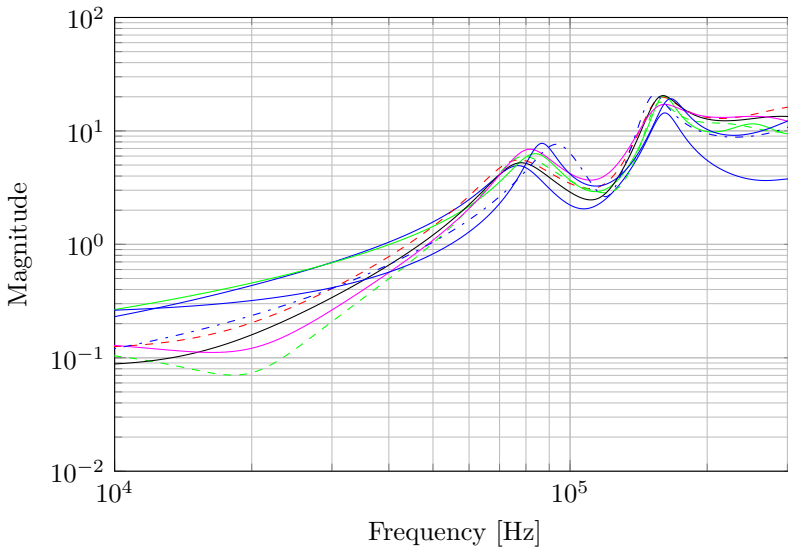


Figure 2.9: Magnitude plot of the transfer function from the piezo input to the piezo sensor signal.

2.3.5 Identification of the cross-talk model

In order to obtain the cross-talk dynamics G_c , we actuated the first neighbor of the n -th ink channel (i.e. the input signal $u_{n+1}(k)$ corresponding to the $(n+1)$ th channel) with the standard pulse. Figure 2.10 shows measurement of the piezo input $u_{n+1}(k)$ and the piezo sensor $y_{n(n+1)}(k)$ on the experimental setup. We again use Prediction Error identification algorithm with the same Box-Jenkins model structure and the same orders for the model and noise as used previously. The frequency response of the identified transfer function is shown with a solid line in Figure 2.12. Similar to Section 2.3.3, we have done the model structure validation (see Figure 2.11) and we have compared the simulated output and the actual output using validation data. The Best Fit is here 82.87% (see Figure 2.13).

We have seen that the direct dynamics depend on the DoD frequency due to the refill effect. However, the cross-talk does not depend on the DoD frequency. This is mainly due to the fact that cross-talk occurs due to structural deformation which is entirely independent of the DoD frequency. Also, the contribution of the acoustic influence (which may depend on the DoD frequency) in the cross-talk is negligible compared to the structural deformation (Wijshoff 2008).

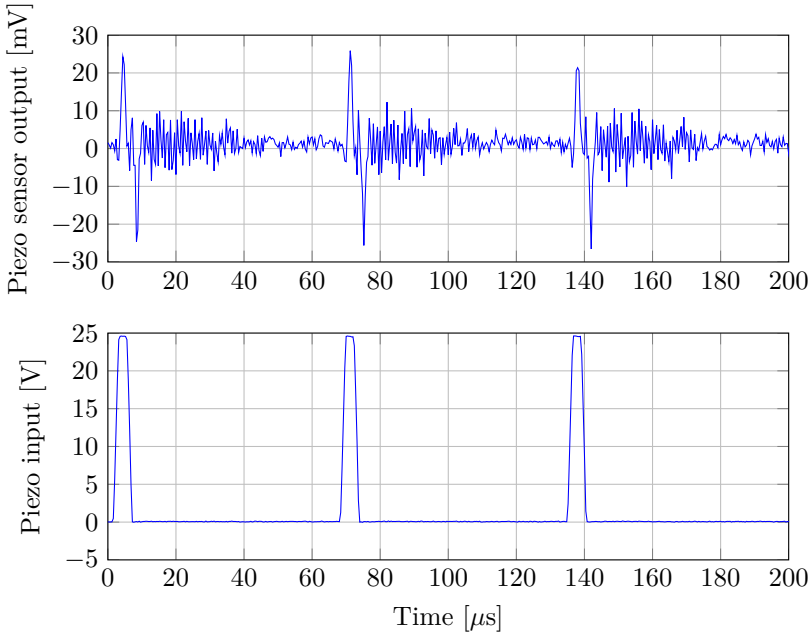


Figure 2.10: Experimental data with the cross-talk obtained while jetting at a DoD frequency of 15kHz.

One can think of using the set of identified linear models to describe the inkjet channel as a linear parameter varying (LPV) system (Tóth 2010) with the jetting frequency as a scheduling variable (and further optimizing the operating points for identification (Khalate et al. 2009)). However, as the images are printed in bitmap format and thus it is difficult to define the jetting frequency. In such scenario, one can use the history of the number of drop jetted prior to jetting the current drop as a scheduling variable. Another approach to tackle this situation is to design a pulse which is working well for all the identified models. In order to compute such pulse it is useful to represent this set of identified model by the nominal models with parametric uncertainty. Therefore, in the next section we will discuss construction of such uncertainty on the nominal model.

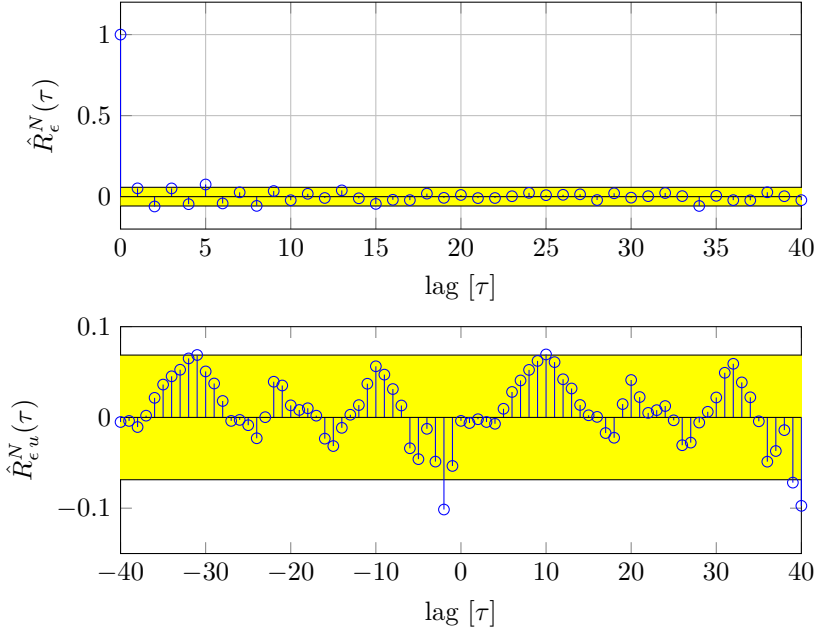


Figure 2.11: Residual tests for the cross-talk dynamics.

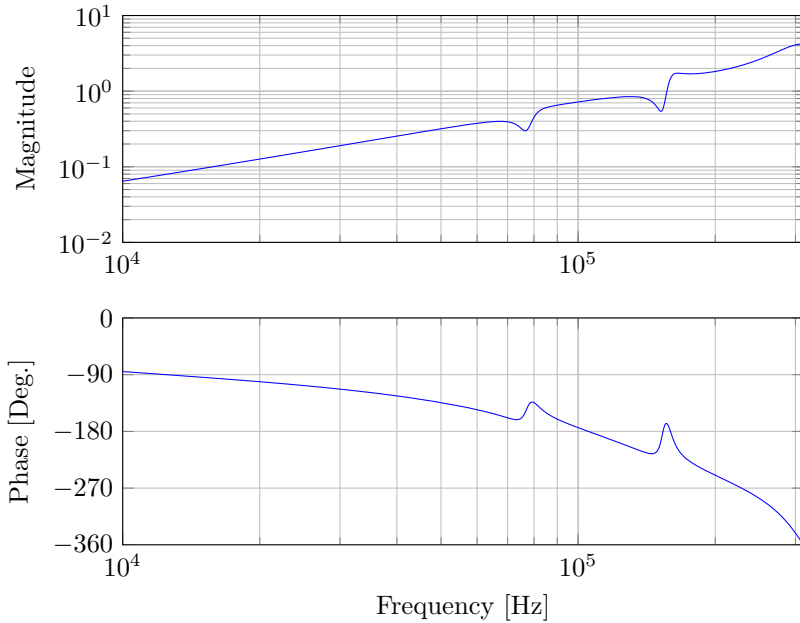


Figure 2.12: Frequency responses of the identified cross-talk dynamics G_c .

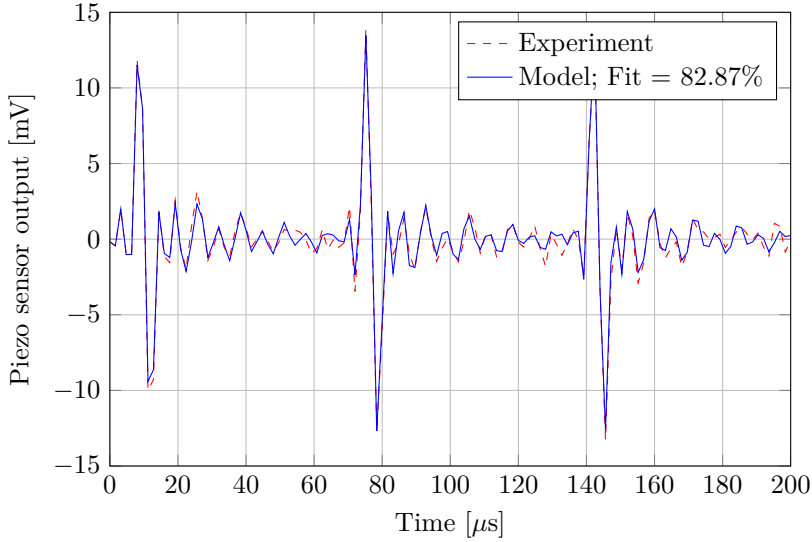


Figure 2.13: Best Fit between the measured and the simulated outputs for the cross-talk dynamics G_c .

2.4 Uncertainty Ink channel dynamics

For design of printhead control, it is essential to represent this set of dynamical models obtained at various operating DoD frequencies. In this section, we present an approach to construct an uncertainty Δ on the parameter of the nominal model, e.g. $H(q)$, such that the uncertain system $H(q, \Delta)$ encompasses the set of dynamical models at various DoD frequencies (Khalate et al. 2012). We will also consider uncertainty on the model $G_d(q)$. It is important to obtain a compact formulation of the uncertainty as it will greatly simplify the control design procedure (which will be discussed in the next chapter).

2.4.1 Uncertainty on the physical model

In Section 2.3.4, we considered that the main variation of the dynamics of the system (characterized by two resonance peaks) is a variation of the first resonance peak. The variation observed in the second peak is neglected since it has a smaller amplitude and since higher frequency dynamics are known to be of less influence on the ink drop properties compared to the first resonant mode (Dijksman 1984). Figure 2.14 shows the relation of the identified piezo sensor model $G(q)$ and the physical meniscus model $H(q)$. Here, the transfer function $G_{p2mv}(q)$ from the piezo sensor signal to the meniscus velocity is unknown. Moreover, since we can not measure the meniscus velocity experimentally, it is not possible to translate the variations observed in $G(q)$ on the parameters of $H(q)$.

Hence, the size of uncertainty on the transfer function $H(q)$ between the piezo

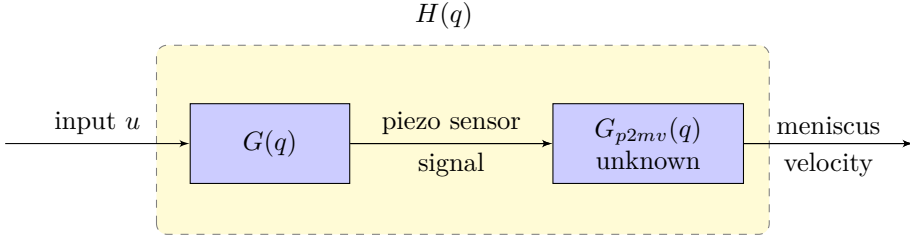


Figure 2.14: Relation between the piezo sensor dynamics $G(q)$ and the meniscus velocity dynamics $H(q)$.

input and the meniscus velocity cannot only be based on the system identification results, but also on physical insights and some trials. In the sequel, the uncertain meniscus velocity model will be described by systems where the frequency of the first resonance peak varies from 75kHz to 86kHz and its damping ratio varies from 0.0366 to 0.1585. Note that the damping ratio of the resonant mode is considered instead of the amplitude. This will help to describe compact uncertainty on the resonant mode properties. With respect to the frequency and the damping ratio of the first peak of the nominal model $H(q)$ used in Section 2.2.1, the uncertainty set corresponds to a variation in an interval of $[-7\% + 7\%]$ for the frequency and $[-70\% + 30\%]$ for the damping ratio. The nominal model is thus not in the center of our uncertainty region.

As mentioned earlier we need a compact description of the uncertainty. Hence, the variation of the first resonance peak has now to be parameterized. For this purpose, let us first consider the following continuous-time version of $H(q)$ (see (2.5)):

$$H(s) = \left(\frac{g_1(s + \alpha)}{s^2 + 2\zeta_{n1}\omega_{n1}s + \omega_{n1}^2} \right) \left(\frac{s^2 + 2\zeta_{n3}\omega_{n3}s + \omega_{n3}^2}{s^2 + 2\zeta_{n2}\omega_{n2}s + \omega_{n2}^2} \right). \quad (2.13)$$

The variation in the frequency ω_{n1} and the damping ratio ζ_{n1} of the first mode is represented in Figure 2.15.A.

The parametric uncertainty in the coefficients ω_{n1} and ζ_{n1} of the continuous-time transfer function is translated into the uncertainty Δ on the coefficients a_1 and a_2 of the discrete-time transfer function $H(q)$ using standard results (Rabbath 1995):

$$a_1 = -2r \cos \theta, \quad a_2 = r^2 \quad (2.14)$$

where $r = e^{-\zeta_{n1}\omega_{n1}T_s}$, $\theta = T_s\omega_{n1}\sqrt{1 - \zeta_{n1}^2}$ and T_s is the sampling time.

Using these relations, the box-type uncertainty in the parameters ω_{n1} and ζ_{n1} is mapped onto a set Δ in the parameter space of the coefficients a_1 and a_2 as shown in Figure 2.15.B. In particular, the four vertices of the uncertainty on a_1 and a_2 , when expressed relative to the nominal values $a_{1,\text{nom}} = -1.9538$ and $a_{2,\text{nom}} = 0.9696$, are as follows

$$\Delta_1 = [0.8103/100 \quad 1.3928/100]^T, \quad \Delta_2 = [0.4031/100 \quad 1.0927/100]^T,$$

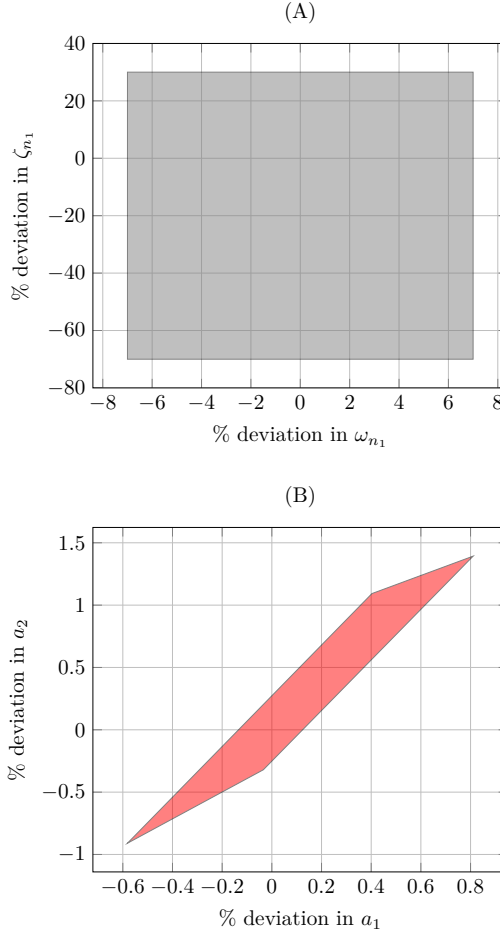


Figure 2.15: Parametric uncertainty relative to the nominal value.

$$\Delta_3 = [-0.0342/100 \quad -0.3206/100]^T, \quad \Delta_4 = [-0.5813/100 \quad -0.9097/100]^T.$$

The convex combination of these four vertices forms the set $\mathbf{\Delta} = \text{conv}(\Delta_1, \Delta_2, \Delta_3, \Delta_4)$. In other words, any perturbation in the parameters ω_{n1} and ζ_{n1} will be mapped in perturbation/uncertainty $\Delta = [\Delta^{(1)} \quad \Delta^{(2)}]^T = \sum_{i=1}^4 \alpha_i \Delta_i$ with $\sum_{i=1}^4 \alpha_i = 1$ (i.e. $\Delta \in \mathbf{\Delta}$) on the coefficients a_1 and a_2 . These perturbation on the coefficients a_1 and a_2 can be represented in the following manner

$$a_1(\Delta) = a_{1,\text{nom}}(1 + \Delta^{(1)}) \quad (2.15)$$

$$a_2(\Delta) = a_{2,\text{nom}}(1 + \Delta^{(2)}), \quad (2.16)$$

with $a_{1,\text{nom}}$ and $a_{2,\text{nom}}$ defined just above.

Now, the set of dynamical models obtained at various DoD frequencies can thus

be represented by the uncertain inkjet system $H(q, \Delta), \Delta \in \mathbf{\Delta}$. The frequency response of the uncertain inkjet system, which is represented by $H(q, \Delta)$, is shown by shaded area in Figure 2.16.

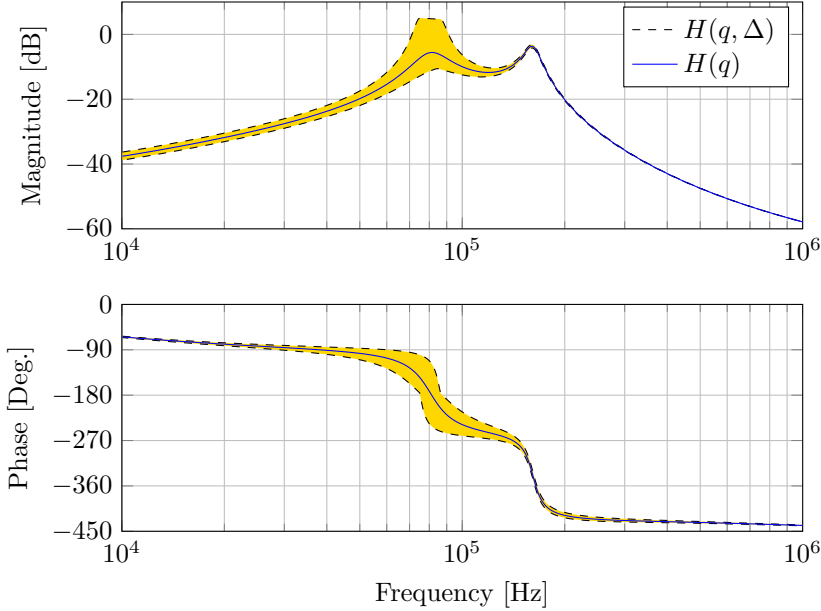


Figure 2.16: Frequency response of uncertain ink channel dynamics $H(q, \Delta)$.

In the next chapter, we will design a robust pulse to tackle the uncertainty in the inkjet system. As a state-space description of the systems is useful to design this robust control, it is important to obtain the state-space description of uncertain inkjet system $H(q, \Delta), \Delta \in \mathbf{\Delta}$. It can be seen that the uncertainty Δ enters affinely in the state-space matrices A_S and B_S (2.6) of the inkjet system. Thus, the state-space matrices of the inkjet system $H(q, \Delta)$ for the admissible uncertainty $\Delta \in \mathbf{\Delta}$ belong to the polytope

$$\left[A_S(\Delta), B_S(\Delta), C_S \right] = \sum_{i=1}^4 \alpha_i \left[A_{S_i}, B_{S_i}, C_S \right] \quad (2.17)$$

where the matrices $A_{S_i} = A_S(\Delta_i)$, $B_{S_i} = B_S(\Delta_i)$, $i = 1, \dots, 4$, are the system matrices of a fixed inkjet system at the i -th vertex of the polytope and α_i are positive scalars such that $\sum_{i=1}^4 \alpha_i = 1$. The matrix C_S is independent of Δ . We will see in the next chapter that the robustness of the actuation pulse can be improved if we consider this set of multiple dynamical models $H(q, \Delta)$ with $\Delta \in \mathbf{\Delta}$ for the actuation pulse design.

2.4.2 Uncertainty on the data-based model

In previous section we have seen that it is possible to represent the set of linear models obtained different DoD frequencies by perturbing the nominal parameters of the model $H(q)$ in an uncertainty set Δ . Using similar approach we can encompass the set of identified models, given in Section 2.3.4, by perturbing the nominal parameters of the model $G_d(q)$ in an uncertainty set Δ . Thus, every identified model can be represented by an uncertain inkjet system $G_d(q, \Delta)$, $\Delta \in \Delta$, where Δ is a perturbation on the nominal parameters of $G_d(q)$. Note that the uncertainty set Δ for $G(q)$ will be different than Δ obtained for $H(q)$ in the previous section. However, for simplicity we will use the same notation to describe uncertainty on both the models.

As discussed in the previous section, we only consider perturbation on the first resonance peak. We neglect the variation in the second peak since higher order peaks are known to be of less influence for the ink drop properties (Dijksman 1984). Recall that for the first resonant mode the variations in frequency and amplitude is [76.19 90.77] kHz and [12.67 17.47] dB, respectively. Using this variations in the mode properties we design the uncertainty set Δ . The procedure for to design Δ is similar to the one discussed in the previous section. We consider perturbation on only two parameters related to the frequency and the amplitude of the first resonant mode, thus, the dimension of Δ is 2 (i.e. $\Delta \in \mathbb{R}^2$). The frequency response of this uncertain system $G_d(q, \Delta)$, $\Delta \in \Delta$ is shown by the shaded area in Figure 2.17. This shaded area corresponds to the variations of the first resonant mode observed in Figure 2.9.

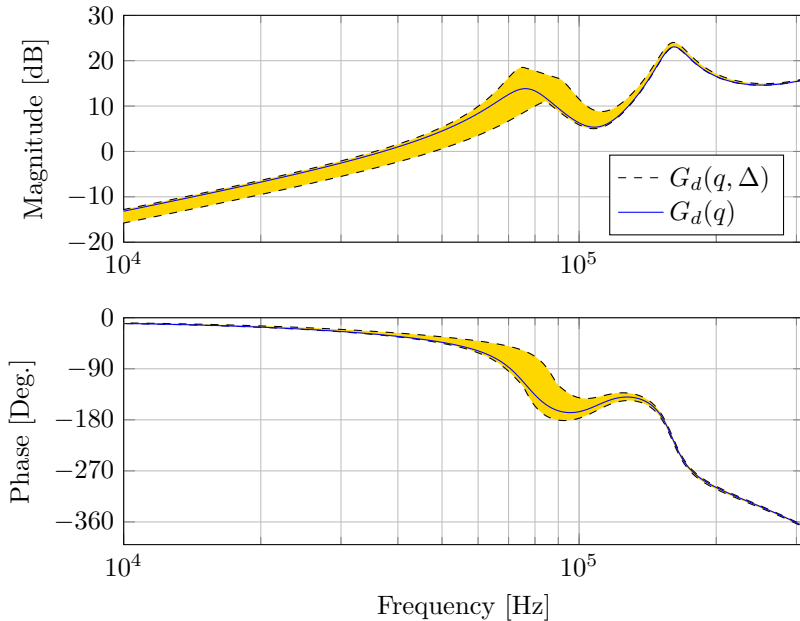


Figure 2.17: Frequency response of uncertain ink channel dynamics $G_d(q, \Delta)$.

2.5 Summary

In this chapter, in order to predict the performance of printhead we have reviewed available physical models from the literature and discussed the narrow-gap model in detail. However, it is not always possible to obtain a reasonably accurate physical model for an ink channel. Hence, we have presented a data-based modeling approach (based on prediction-error identification) to obtain a model of a single ink channel dynamics. To start with, the experimental setup itself has been introduced and various sensor functionalities have been discussed, especially the piezo sensor which utilizes the self-sensing mechanism. After taking an overview of the prediction-error identification method we have applied it on the measured experimental data to obtain a model between the piezo input and the piezo sensor output. The novelty of the identification approach presented in this chapter compared the methods in the literature is that it uses an excitation signal which can jet the ink droplet so as to get a model closer to the operating point. On further experimental exploration we found that the nonlinear effects in the drop formation has greater influence on the linear model obtained at any given DoD frequency and we identified a set of models at various DoD frequencies. Using this information of dynamics variation we have designed a compact uncertainty set Δ on the parameters of the nominal model to represent the set of models obtained at different DoD frequencies. The nominal model and the uncertain inkjet system model (grey-box) will be used in the next chapter to design optimal and robust actuation pulses.

Feedforward Control of an inkjet channel: Theory

As discussed in the previous chapter, the performance of an inkjet system is mainly limited due to the residual oscillations inside the ink channel. In this chapter we present various methods to (re-)design actuation pulses in order to damp the residual oscillations and thus to improve the performance. First, we discuss the limitations of the control system which enforce the use of feedforward control (FFC) and also restrict the shape of actuation pulses. Further, physical insight is used to formulate the drop consistency problem as a feedforward control problem. Using the nominal inkjet system model, developed in the previous chapter, an optimal actuation pulse is designed as the solution of an optimization problem. However, we have seen in the previous chapter that the nominal model is not sufficient to represent the inkjet system dynamics at all DoD frequencies. The set of the inkjet system models obtained at various DoD frequencies can be represented by a parametric uncertainty on the nominal model. A constrained robust pulse is designed to provide improved performance in presence of this uncertainty by minimizing the worst-case squared error compared to the constrained optimal pulse. Moreover, the design of optimal and robust unconstrained actuation pulses is investigated in order to improve the performance by relaxing the shape constraints on the pulse design.

3.1 Introduction

We have seen in the previous chapter that a positive trapezoidal voltage pulse is applied to the piezo actuator to jet an ink droplet of desired properties. The parameters of this positive trapezoidal actuation pulse (or standard pulse) are generally tuned by exhaustive studies on a complex numerical model of the inkjet printhead or on an experimental setup (Bogy and Talke 1984; Dong et al. 2006;

Jo et al. 2009). Recall that the main drawback of this standard pulse is that it generates residual oscillations. In order to damp the residual oscillations, an additional pulse can be applied after the standard pulse. The actuation pulses used in the literature to damp the residual oscillations can be broadly classified into two categories based on the polarity of the actuation pulse. The first one is a unipolar actuation pulse (Kwon and Kim 2007; Gan et al. 2009), which consists of the standard pulse to jet an ink droplet and an additional trapezoidal pulse of the same polarity as the standard pulse to damp the residual oscillations. The second category is the bipolar pulse (MicroFab Technologies Inc. 1999; Chung et al. 2005; Kwon 2009a), which consists of the standard pulse to jet an ink droplet and the residual oscillations are damped by an additional trapezoidal pulse of opposite polarity. The advantage of using the bipolar actuation pulse is that the residual oscillations can be damped earlier compared to the unipolar pulse and thus, higher DoD frequency can be attained. Conventionally, the parameters of the unipolar and the bipolar pulse are obtained by exhaustive experimental studies, see (Gan et al. 2009; MicroFab Technologies Inc. 1999; Chung et al. 2005). The number of experiments needed to design an actuation pulse can be reduced with a wise guess on the parameters of the actuation pulse. As discussed in Section 2.3.3, it is possible to make an initial guess on the parameters of the actuation pulse as a function of the fundamental period of the channel pressure (Kwon and Kim 2007) or the meniscus position (Kwon 2009a). To determine this period, the authors of (Groot Wassink 2007; Kwon and Kim 2007; Kwon 2009a) use an experimental approach. The fundamental period of the inkjet printhead can be obtained by measuring the ink-channel pressure using a self-sensing mechanism (Groot Wassink 2007; Kwon and Kim 2007) or by measuring the meniscus position using a CCD camera (Kwon 2009a). The meniscus is the ink and air interface in the nozzle. Once the fundamental period is measured, the unipolar pulse and the bipolar pulse can be designed using the parameters recommended in Kwon and Kim (2007) and Kwon (2009a) respectively.

As opposed to the approaches in (Kwon and Kim 2007; Kwon 2009a), we will design the actuation pulse for the DoD inkjet printhead with a systematic model-based approach. For this purpose, we require a model of the system that we want to control. Here, we consider the discrete-time models $H(q)$ (relating the piezo input to the meniscus velocity) and $G_d(q)$ (relating the piezo input to the piezo sensor signal) developed in the previous chapter. Both models give the information about the jetting behavior inside an ink channel. Consequently, using these models we can compute the piezo actuation input which will damp the residual oscillations. Mainly due to the limitations of the driving electronics (see Section 3.2), the optimal input cannot be computed using a feedback controller, but must be computed off-line based on the model (feedforward control).

In the literature, we can find other applications of systems and control theory to design, off-line, the optimal piezo actuation. In (Ezzeldin 2012), the actuation pulses are obtained by inverting $H(q)$ and it is discussed that it is far from trivial as the system $H(q)$ is non-minimum phase. In (Groot Wassink 2007), an iterative learning approach is used to design the optimal pulse off-line. The main drawback of the approach in (Groot Wassink 2007) is that it is not possible to put a priori

constraints on the shape of the optimal pulse while such constraints are generally present in practice. Indeed, the driving electronics are generally only able to generate trapezoidal shapes for the piezo actuation input. The approach presented in this chapter allows us to deal with such shape constraints. We propose to parameterize a class of piezo input satisfying these shape constraints and to determine the optimal input within this class using an optimization-based approach.

For simplicity and to avoid repetition, in this chapter, we will present the control method using the meniscus velocity model $H(q)$. One can easily apply the developed methods to the piezo sensor signal model $G_d(q)$. Now, we assume that the possible piezo inputs can be parameterized as $u(k, \theta)$ with θ a parameter vector and k the discrete time index. We then design a template $y_{\text{ref}}(k)$ for the desired meniscus velocity¹, i.e., a meniscus velocity profile with fast decaying residual oscillations. Based on this template $y_{\text{ref}}(k)$ and the transfer function $H(q)$, an optimal actuation pulse $u(k, \theta_{\text{opt}})$ will be determined as the one minimizing the norm of the tracking error.

We have seen in Section 2.4 that inkjet system models $H(q)$ and $G_d(q)$ only represent the dynamics of the system when a single drop is jetted. These models are therefore not representative of the dynamics of the system when jetting a series of drops at a certain DoD frequency. In order to take into account this model variation, we can encompass the set of dynamical models obtained at various operating DoD frequencies in a compact uncertainty set $H(q, \Delta)$ ($\Delta \in \mathbf{\Delta}$) (and $G(q, \Delta)$). In this chapter, we design a robust actuation pulse which will ensure a minimum performance for all models in the uncertainty set. The robust actuation pulse is obtained by minimizing the worst-case norm of the tracking error $e(k)$ over the uncertain inkjet system $H(q, \Delta)$. Recent developments in electronics may circumvent the pulse shape constraints in the near future. Therefore, we also investigate the possibilities to design unconstrained actuation pulses to improve the inkjet system performance.

In the next section we discuss the control system limitations which restrict us to use feedforward control.

3.2 Limitations of the control system

The printhead under investigation has very limited control capabilities. The possibility to use feedback control is ruled out due to the following limitations of the actuation system

- No sensor is provided for real-time measurement of the channel pressure or of the meniscus velocity.

¹Note that here the desired inkjet system behavior is described using the meniscus velocity as we will use the meniscus velocity model $H(q)$. However, if one would like to use the piezo sensor signal model $G_d(q)$ then the desired inkjet system behavior can be described by the piezo sensor signal $y_{\text{ref}}(k)$ with fast decaying residual oscillations.

- The driving electronics limit the range of the actuation pulses that can be generated in practice. The only possible choice for the actuation pulse is the trapezoidal waveform (Figure 3.1).
- The sample time required for control computation must be very short due to high drop jetting (DoD) frequency.

In this scenario, the ink channel dynamics can be controlled using a feedforward strategy. The goal is to generate a trapezoidal actuation pulse for the piezo actuator such that the control objectives are met. Recall that the standard pulse does not provide satisfactory performance as it is not capable of damping the residual oscillations generated after jetting the ink drop. Therefore, we add a negative trapezoidal pulse in addition to the standard positive trapezoidal pulse in order to damp the residual oscillations, see Figure 3.1. The actuation signal then consists of a positive trapezoidal pulse (called resonating pulse), which is responsible for jetting the ink drop, followed by the negative trapezoidal pulse which damps the residual oscillations. This negative pulse is called the quenching pulse. We will see in the sequel that the optimal starting time for this additional negative pulse is approximately equal to the period of the first resonant frequency. This enables the proposed actuation pulse to jet ink drops at faster DoD frequencies compared to the method proposed in (Gan et al. 2009; Kwon and Kim 2007). Now, the actuation pulse can be characterized by the rise time (t_r), the dwell time (t_w), the fall time (t_f) and the amplitude (V) of both the resonating and the quenching pulse. The time interval between the resonating pulse and the quenching pulse is t_{dQ} . Thus, an actuation pulse $u(k, \theta)$ is defined by the parameter vector θ as follows:

$$\theta = [t_{rR} \ t_{wR} \ t_{fR} \ V_R \ t_{dQ} \ t_{rQ} \ t_{wQ} \ t_{fQ} \ V_Q]^T. \quad (3.1)$$

Note that in Figure 3.1, the time parameters (t_r, t_w, t_f, t_{dQ}) of the actuation pulse are restricted to be equal to an integer multiple of the sampling period T_s . As opposed to the approaches in (MicroFab Technologies Inc. 1999; Chung et al. 2005; Kwon 2009a), the optimal parameter vector of the bipolar pulse will be determined using a systematic (optimization-based) approach as shown in the sequel.

3.3 Control Objective

The goal of this thesis is to improve the drop consistency of a DoD inkjet print-head. A droplet jetting through an ink channel is a discrete event. Therefore, for controlling drop properties directly we need to formulate the control problem in a discrete event setting which is difficult to deal with. Hence, in order to formulate the control problem in general setting we use the well known property i.e. the fact that the meniscus velocity mainly governs the drop properties (Dijksman 1984). We further make the following assumptions:

- The meniscus velocity is sufficient to predict inkjet system dynamics (Dijksman 1984; Groot Wassink 2007).

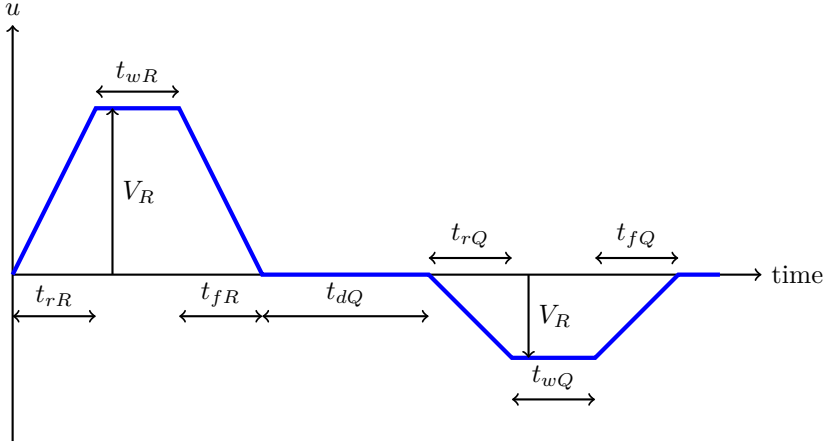


Figure 3.1: Proposed piezo actuation pulse.

- The piezo sensor signal gives sufficient information about the drop jetting process in an inkjet system (Dijksman 1984; Groot Wassink 2007).

These assumptions are verified later using experimental results.

Note that the above assumptions are valid for small droplet (around 20 – 50 pL) inkjet printheads. The meniscus position may also play an important role in predicting the drop properties once the droplet volume becomes very small (around 5 – 10 pL). In such a scenario one has to consider both the meniscus position and the meniscus velocity for the pulse design problem as proposed in (Brandt 2010). However, since we do not have a good model to describe the meniscus position we restrict ourself to regulating the meniscus velocity and the piezo sensor signal to improve the drop consistency.

Note that for simplicity and to avoid repetition we will present the control method using the meniscus velocity model $H(q)$. One can easily apply the developed methods to the piezo sensor signal model $G_d(q)$.

In order to define the optimization problem leading to the optimal parameter vector θ_{opt} , we need a template $y_{\text{ref}}(k)$ for the desired meniscus velocity. In this section we describe the procedure to construct the desired meniscus velocity trajectory $y_{\text{ref}}(k)$ using the transfer function model $H(q)$ and the standard pulse.

For the considered inkjet printhead, the standard pulse is represented in Figure 3.1 and corresponds to a parameter vector $\theta_{\text{std}} = [1.5 \ 2.5 \ 1.5 \ 25 \ 0 \ 0 \ 0 \ 0]^T$ when using the parametrization of Section 3.2. Note that parameters of this standard pulse are optimized by Océ using trial and error method. These parameters are slightly different than the ones obtained in Section 2.3.3, i.e. when one does not have any information about the printhead architecture. This standard pulse allows to jet one drop at the desired velocity, but the residual oscillation generated by this standard pulse perturbs the subsequent drops. Such a behavior can be observed in Figure 3.2 (dashed line) where we represent the response of the model $H(q)$ to the

standard pulse. As shown in Figure 3.2, we can characterize the meniscus velocity response $y(k)$ in two parts. Part A of the response $y(k)$ allows the drop to be jetted at the desired drop velocity. A procedure is described in (Dijksman 1984) to predict the properties of the jetted drop using Part A of the meniscus velocity profile. Since we want to jet the ink drop at the desired ink-drop velocity, the desired meniscus velocity $y_{\text{ref}}(k)$ should be the same as $y(k)$ in Part A. Note that the meniscus velocity peak is an important feature and that a changed velocity-peak will result in drop having different velocity.

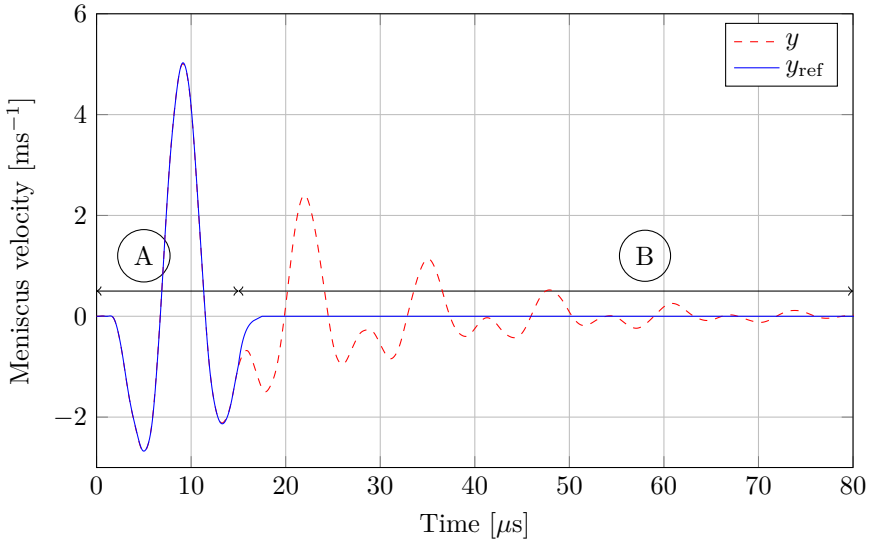


Figure 3.2: Reference meniscus velocity trajectory y_{ref} (solid) and the meniscus velocity response y to the standard pulse (dashed).

Part B of the response $y(k)$ represents the residual oscillations. This is an undesired behavior, since, the residual oscillations perturb the subsequent drops. Therefore, in Part B, we force the desired meniscus velocity $y_{\text{ref}}(k)$ to zero. This means fast decaying residual oscillations. This template $y_{\text{ref}}(k)$ is represented by the solid line in Figure 3.2.

Thus, the desired meniscus velocity $y_{\text{ref}}(k)$ is a meniscus velocity profile to jet an ink drop with the desired drop-velocity and fast decaying residual oscillations. If the actuation pulse is designed in such a way that the meniscus velocity $y(k)$ follows the reference trajectory $y_{\text{ref}}(k)$, then the channel will come to rest very quickly after jetting the ink drop. This will create the condition to jet the ink drops at higher jetting frequencies. Note that the velocity-peak is a major feature and that a changed velocity-peak will result in drops having different velocities.

In the next section we discuss an optimization based method to obtain the actuation pulse which can follow effectively the desired trajectory designed above.

3.4 Constrained Feedforward Control

In the previous section we have translated the drop consistency problem into a trajectory tracking problem. In this section we will design the actuation pulse with the constraints discussed in Section 3.2 to follow the desired trajectory y_{ref} . We will first obtain the optimal actuation pulse considering the nominal model $H(q)$ of the system. Subsequently, we extend this method to obtain a robust pulse which can handle the parametric uncertainty $\Delta \in \mathbf{\Delta}$ in the model $H(q, \Delta)$.

3.4.1 Optimal Constrained Feedforward Control

We are now ready to formulate the optimization problem which will lead to the optimal piezo input. The optimal input is the trapezoidal input $u(k, \theta)$ which minimizes the difference between the reference trajectory y_{ref} and the meniscus velocity $y(k)$. More precisely, we can define the objective function as the following sum of weighted square errors

$$\begin{aligned} \mathcal{J}_{\text{nom}}(\theta) &= \sum_{k=0}^N w(k) \left(y_{\text{ref}}(k) - y(k, u(k, \theta)) \right)^2 \\ &= \sum_{k=0}^N w(k) \left(y_{\text{ref}}(k) - H(q)u(k, \theta) \right)^2 \end{aligned} \quad (3.2)$$

where $N = \frac{T}{T_s}$, T_s is sampling time chosen equal to $0.1 \mu\text{s}$, T is chosen equal to $100 \mu\text{s}$, $w(k)$ is a user-defined time-domain weighting, $H(q)$ is the discrete-time model from piezo input to the meniscus velocity, q is here the forward shift operator and $u(k, \theta)$ is the proposed actuation pulse parameterized by the parameter vector θ (see Section 3.2).

Thus, the optimal actuation pulse parameter θ_{opt} is the parameter vector θ obtained by solving the following optimization problem

$$\theta_{\text{opt}} = \arg \min_{\theta} \mathcal{J}_{\text{nom}}(\theta), \quad \text{subject to } \theta_{LB} \leq \theta \leq \theta_{UB}, \quad (3.3)$$

where, θ_{LB} and θ_{UB} are the vectors containing the lower and the upper bounds on each element of the parameter vector θ .

This is a constrained nonlinear optimization problem which can be solved off-line using standard algorithms. We use the MATLAB function `fmincon`. This function implements a range of optimization techniques. In our experiments we used the default option which is sequential quadratic programming (Powell 1978; Pshenichnyj 1994).

Remark 3.1 *The proposed framework is very general and it is not restricted to the meniscus velocity. It is possible to construct the objective function using several other system variables such as the piezo sensor signal, the meniscus position, the*

DoD curve, the flight profile of jetted drops and the velocities of the jetted drops. Moreover, the linear model $H(q)$ for the inkjet system can also be replaced by a nonlinear model if this model allows the computation of the meniscus velocity for all possible piezo inputs. Use of nonlinear models will be more accurate when non-Newtonian fluids are jetted.

Remark 3.2 *Instead of using a model $H(q)$ to generate $y(k, u(k, \theta))$ in (3.2), an actual experimental setup could be used for this purpose. By computing the gradient numerically, we could then perform the optimization of θ . This would be of use when an accurate model is not available. A possible application of this can be the jetting of a non-Newtonian fluid with the inkjet printhead. In this case, a linear model could lead to inaccurate results and obtaining a nonlinear model of the inkjet system may also not be always possible. In such a scenario, one can still obtain the actuation pulse with the proposed method by using the ink channel pressure instead of the meniscus velocity. Indeed, this pressure can be measured by using the piezo unit as an ink-channel pressure sensor (i.e. the self-sensing mechanism (Groot Wassink 2007), (Kwon and Kim 2007), (de Jong 2007)), see Section 2.3.1.*

3.4.2 Robust Constrained Feedforward Control

In the previous section, we have obtained the optimal pulse using the nominal model $H(q)$ in order to effectively damp residual oscillations inside an ink channel. However, in Section 2.4, we have seen that the set of models obtained at different DoD frequencies are not the same as the nominal model and this set of models can be represented by uncertain inkjet system $H(q, \Delta)$, $\Delta \in \mathbf{\Delta}$ (Khalate et al. 2011; Koekebakker et al. 2013). This uncertain set will be used to design a robust actuation pulse, which will ensure a minimum performance for all systems in the polytopic uncertainty rather than obtaining an optimal actuation pulse whose performance is only good for one single element of this set (as we did in the previous section). For this purpose, we define the robust performance index $\mathcal{J}_{\text{rob}}(\theta)$ as the worst-case sum of squared tracking errors:

$$\mathcal{J}_{\text{rob}}(\theta) = \max_{\Delta \in \mathbf{\Delta}} \sum_{k=0}^N w(k) \left(y_{\text{ref}}(k) - H(q, \Delta)u(k, \theta) \right)^2. \quad (3.4)$$

In (3.4), the template $y_{\text{ref}}(k)$ is the same as in (3.2). Indeed $y_{\text{ref}}(k)$ was constructed with the model $H(q)$ in the condition where $H(q)$ appropriately describes the system (one single drop jetted at rest) and is thus an appropriate description of the desired meniscus velocity.

In order to design the robust actuation pulse, it is important to be able to compute $\mathcal{J}_{\text{rob}}(\theta)$ for any arbitrary value of θ or at least to be able to compute a good approximation for $\mathcal{J}_{\text{rob}}(\theta)$. Obtaining the exact solution of the optimization problem (3.4) is nontrivial, but a good approximation $\mathcal{J}_{\text{rob}}^{LB}(\theta)$ for $\mathcal{J}_{\text{rob}}(\theta)$ can be simply determined by gridding the uncertainty space $\mathbf{\Delta}$.

In our case, as the parameter space of $\mathbf{\Delta}$ is only of dimension two, gridding can be easily and effectively performed. Let the set \mathcal{S} be a fine grid on the parametric

uncertainty Δ , defined as

$$\mathcal{S} = \{\Delta^i, i = 1, \dots, m, \mid \Delta^i \in \Delta\} \quad (3.5)$$

Then a good approximation (lower bound) $\mathcal{J}_{\text{rob}}^{\text{LB}}(\theta)$ of the performance index $\mathcal{J}_{\text{rob}}(\theta)$ can be obtained as the maximum sum squared error over the m grid points, i.e.:

$$\mathcal{J}_{\text{rob}}^{\text{LB}}(\theta) = \max_{\Delta^i \in \mathcal{S}} \sum_{k=0}^N \left(y_{\text{ref}}(k) - H(q, \Delta^i)u(k, \theta) \right)^2. \quad (3.6)$$

Now, the constrained robust actuation pulse parameter is thus the solution θ_{robust} of the following optimization problem

$$\theta_{\text{robust}} = \arg \min_{\theta} \mathcal{J}_{\text{rob}}^{\text{LB}}(\theta) \quad \text{subject to} \quad \theta_{LB} \leq \theta \leq \theta_{UB}, \quad (3.7)$$

where, θ_{LB} and θ_{UB} are vectors containing the lower and the upper bounds on each element of the parameter vector θ .

This is a nonlinear optimization problem which can be solved offline using standard optimization algorithms. Since, we can compute $\mathcal{J}_{\text{rob}}^{\text{LB}}(\theta)$ for each value of θ , we can use gradient-based optimization to find θ_{robust} . Gradient-based optimization is an iterative method. The gradient of $\mathcal{J}_{\text{rob}}^{\text{LB}}(\theta)$ is computed numerically around the current value of θ and then the parameter θ is updated in the gradient direction. We use the MATLAB function `fmincon` for this purpose. This function implements a range of optimization techniques. In our experiments we used the default option which is sequential quadratic programming.

Remark 3.3 *The gridding approach to obtain a tight approximation $\mathcal{J}_{\text{rob}}^{\text{LB}}(\theta)$ for $\mathcal{J}_{\text{rob}}(\theta)$ may pose numerical problems when the dimensions of the parameter space of Δ becomes large or when the dependency of $\mathcal{J}_{\text{rob}}(\theta)$ on θ becomes highly nonlinear. In such scenario, it is important to obtain some confident bounds on $\mathcal{J}_{\text{rob}}(\theta)$ without increasing numerical complexity. In the next section, we will see that for any arbitrary value of θ an upper bound $\mathcal{J}_{\text{rob}}^{\text{UB}}(\theta)$ for $\mathcal{J}_{\text{rob}}(\theta)$, i.e. $\mathcal{J}_{\text{rob}}(\theta) \leq \mathcal{J}_{\text{rob}}^{\text{UB}}(\theta)$, can be obtained as the solution of a convex optimization problem. However, the design of the robust constrained actuation pulse remains a nonlinear optimization problem due to the nonlinear parameterization of $u(k, \theta)$ in θ . We will further see that if we relax the pulse shape constraint, the design of an unconstrained robust actuation pulse is a convex optimization problem (Khalate et al. 2011).*

Remark 3.4 *Due to manufacturing tolerances the dynamical behavior of ink channels inside a printhead may differ. Generally, this is the reason for differences in the performance of inkjet printheads manufactured in a batch. The ink viscosity change caused by temperature change or by slightly different ink can affect the dynamical behavior of a printhead. One can design the uncertainty parameter space of Δ in order to encompass the dynamic variation caused by the manufacturing*

tolerances. Thus, the proposed method to design the robust pulse can be used to tackle the performance degradation due to these manufacturing tolerances.

3.5 Unconstrained Feedforward Control

In the previous section, we have presented a method to design a constrained robust feedforward control for an inkjet system. As discussed Section 3.2, the pulse shape constraint is imposed by the driving electronics of the printhead under consideration. From a theoretical point-of-view, it is nevertheless important to verify whether this shape constraint limits the achieved performance to a small or a large extent. Secondly, for future high-end inkjet printheads this shape constraint on the actuation pulse may restrict the printhead performance. The rapid development in electronics will enable printhead manufacturers to use more sophisticated electronic hardware which can generate an unconstrained actuation pulse. Even presently, for many research and dedicated applications, practitioners are using waveform generators to generate unconstrained actuation inputs. In view of this, it is important to have a simpler method to design unconstrained actuation pulses to tackle the residual oscillations.

In the next section, we will first present a method to compute an unconstrained actuation pulse using the nominal model of the inkjet system and subsequently, we will present a convex optimization-based method to deal with the uncertainty in the nominal model.

3.5.1 Optimal Unconstrained Feedforward Control

Before developing a more rigorous formulation to handle uncertainty, we will first present a simple way to tackle the problem of the residual oscillations in the nominal case. The objective is to develop a method to design the pulse minimizing the difference between the actual meniscus velocity and the desired one when no constraints whatsoever are imposed on the shape of this pulse. One could use for this purpose model predictive control (Maciejowski 2001). However, when the control sequence to be computed is long, this method is computationally expensive. We present a simpler and computationally efficient filtering-based approach to generate the unconstrained actuation waveform in order to damp the residual oscillations. For this purpose, we parameterize the to-be-designed actuation pulse as the pulse response of a Finite Impulse Response (FIR) filter $F(q, \beta)$:

$$u(k, \beta) = F(q, \beta)\delta(k) \quad (3.8)$$

with $F(q, \beta) = \beta_0 + \beta_1 q^{-1} + \dots + \beta_{n_\beta} q^{-n_\beta}$, $\delta(k)$ the unit pulse and $\beta = (\beta_0, \dots, \beta_{n_\beta})^T$ a vector containing the coefficients of the FIR filter. When the dimension of β is chosen equal to the desired length of the actuation pulse, this parametrization allows to generate actuation pulses of arbitrary shapes.

For an arbitrary vector β , the response of the ink channel $H(q)$ to the input

$u(k, \beta)$ is given by:

$$\begin{aligned} y(k, \beta) &= H(q)F(q, \beta)\delta(k) = F(q, \beta)H(q)\delta(k) \\ &= F(q, \beta)h(k) \end{aligned} \quad (3.9)$$

where $h(k)$ is the pulse response of the known ink channel dynamics $H(q)$.

The optimal control $u(k, \beta_{\text{opt}})$ is then the one which minimizes the difference between the desired meniscus velocity trajectory $y_{\text{ref}}(k)$ and the achieved meniscus velocity $y(k, \beta)$. Therefore, the optimal parameter vector β_{opt} is the solution of the following optimization problem :

$$\beta_{\text{opt}} = \arg \min_{\beta} \sum_{k=0}^N w(k) (y_{\text{ref}}(k) - F(q, \beta)h(k))^2 \quad (3.10)$$

Unlike the optimization problem (3.3) which is nonlinear, the optimization problem (3.10) leading to the unconstrained actuation pulse is a weighted linear least-squares problem.

Remark 3.5 *Determining β can be difficult when the least squares problem (3.10) is ill-conditioned. In such cases it is advisable to approximately solve the least squares criterion (3.10) using a truncated Singular Value Decomposition (SVD), to effectively reduce the degrees of freedom in the least squares problem. For more details, see (Golub and van Loan 1989).*

In the next section, we will present a convex optimization based approach to design a robust actuation pulse to deal with the uncertainty in the inkjet system model.

3.5.2 Robust Unconstrained Feedforward Control

In this section, we first present an approach to design the robust actuation pulse using the H_2 feedforward formulation (Zhou and Doyle 1998; Khalate et al. 2011). Further, we provide an extension of (Geromel et al. 2000) to design a robust pulse using a constant Lyapunov function and finally, we give improved conditions using parameter-dependent Lyapunov functions.

Robust actuation pulse using H_2 feedforward control

In Section 3.3, we have designed a meniscus velocity profile $y_{\text{ref}}(k)$ with fast decaying residual oscillations. As shown in Figure 3.3, the reference trajectory $y_{\text{ref}}(k)$ is modeled² as the pulse response of a rational function $H_{\text{ref}}(q)$. The state-space

²In order to obtain the rational function $H_{\text{ref}}(q)$, first we have modeled the reference trajectory $y_{\text{ref}}(k)$ as a FIR transfer function $H_{\text{ref}}^{\text{FIR}}(q)$ with the unit pulse $\delta(k)$ as the input. Further, we have used the model order reduction toolbox of MATLAB to get a lower order rational function $H_{\text{ref}}(q)$ which is the best approximation of $H_{\text{ref}}^{\text{FIR}}(q)$.

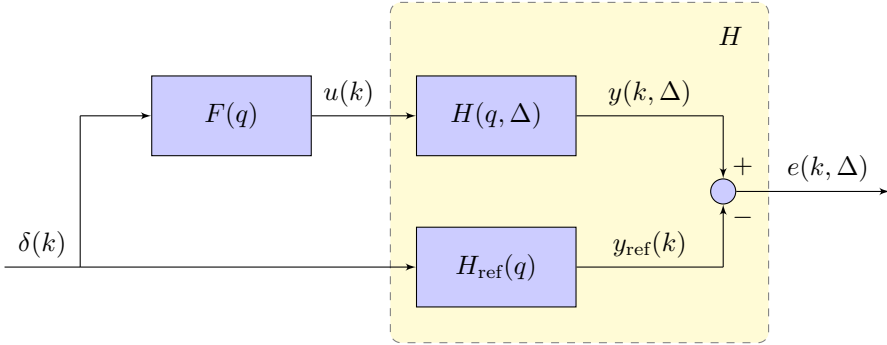


Figure 3.3: Feedforward control problem for the inkjet printhead.

representation of the reference model $H_{\text{ref}}(q)$ is given as follows

$$\begin{aligned} x_R(k+1) &= A_R x_R(k) + B_R \delta(k) \\ y_{\text{ref}}(k) &= C_R x_R(k) \end{aligned} \quad (3.11)$$

where $\delta(k)$ is the unit pulse.

Recall that, if the actuation pulse $u(k)$ is designed in such a way that the meniscus velocity $y(k)$ follows the reference trajectory $y_{\text{ref}}(k)$, then the channel will come to rest very quickly after jetting the ink drop. This will create a condition to jet the ink drops at higher jetting frequencies. In Section 2.4.1, we have presented a compact polytopic uncertainty $\Delta \in \mathbf{\Delta}$ on the coefficients of the inkjet system such that uncertain system $H(q, \Delta)$ represents the set of multiple models obtained at various operating DoD frequencies.

The state-space representation of the system $H(q)$ (see Figure 3.3) with two inputs and the tracking error $e(k, \Delta)$ as output is given as follows:

$$\left[\begin{array}{c|cc} \tilde{A}(\Delta) & \tilde{B}_S(\Delta) & \tilde{B}_R \\ \hline \tilde{C} & 0 & 0 \end{array} \right] = \left[\begin{array}{cc|cc} A_S(\Delta) & 0 & B_S(\Delta) & 0 \\ 0 & A_R & 0 & B_R \\ \hline C_S & -C_R & 0 & 0 \end{array} \right]. \quad (3.12)$$

The uncertainty in the inkjet channel model can now be handled owing to the H_2 filtering formulation. For this purpose, similar to the previous section, we parameterize the actuation pulse as the pulse response of a filter $F(q)$:

$$u(k) = F(q)\delta(k) \quad (3.13)$$

where $\delta(k)$ the unit pulse and the state-space representation of the filter $F(q)$ given as follows:

$$\begin{aligned} x_F(k+1) &= A_F x_F(k) + B_F \delta(k) \\ u(k) &= C_F x_F(k) + D_F \delta(k). \end{aligned} \quad (3.14)$$

The uncertain error dynamics $\nu(q, F, \Delta)$ from the input $\delta(k)$ to the tracking error $e(k, \Delta)$ is defined as follows:

$$\nu(q, F, \Delta) = (H_{\text{ref}}(q) - H(q, \Delta)F(q)), \quad (3.15)$$

and its state-space representation is given as follows:

$$\left[\begin{array}{c|c} A(\Delta) & B(\Delta) \\ \hline C & 0 \end{array} \right] = \left[\begin{array}{cc|c} A_F & 0 & B_F \\ \tilde{B}_s(\Delta)C_F & \tilde{A}(\Delta) & \tilde{B}_s(\Delta)D_F + \tilde{B}_R \\ \hline 0 & \tilde{C} & 0 \end{array} \right]. \quad (3.16)$$

In the sequel, we impose the dimension of A_F to be equal to the one of $\tilde{A}(\Delta)$. It is indeed shown in (Tuan et al. 2001) that the optimal filter has this dimension. As we assume the uncertainty Δ to be of a polytopic nature ($\Delta \in \mathbf{\Delta}$), the state-space matrices of the error system $\nu(q, F, \Delta)$ belong to the following polytope

$$[A(\Delta), B(\Delta), C] = \sum_{i=1}^4 \alpha_i [A_i, B_i, C], \quad (3.17)$$

where the matrices (A_i, B_i, C) are the state-space matrices of the fixed error dynamics $\nu_i(q, F)$ at the i -th vertex of the polytope and α_i are positive scalars such that $\sum_{i=1}^4 \alpha_i = 1$. The matrix C is independent of Δ . Clearly, the uncertain system error dynamics are a convex combination of the fixed systems at the vertices of the polytope $\mathbf{\Delta}$.

For the nominal system, the performance of the filter $F(q)$ can be defined as the H_2 norm of the tracking error. Here, we have an uncertain inkjet system $H(q, \Delta)$ which is perturbed by the uncertainty $\Delta \in \mathbf{\Delta}$. Therefore, we must obtain a robust actuation pulse whose performance is good over the polytopic uncertainty, rather than obtaining an optimal actuation pulse whose performance is only good for the nominal inkjet system. Thus, it is a good choice to define the performance index $\mathcal{J}(\beta)$ as the square of the worst-case H_2 norm of the tracking error transfer function $\nu(q, \beta, \Delta)$:

$$\mathcal{J}(F) = \max_{\Delta \in \mathbf{\Delta}} \|\nu(q, F, \Delta)\|_2^2 = \max_{\Delta \in \mathbf{\Delta}} \|H_{\text{ref}}(q) - H(q, \Delta)F(q)\|_2^2. \quad (3.18)$$

The robust filter F_{robust} , describing the unconstrained robust actuation pulse is, thus, the solution F_{robust} of the following optimization problem

$$[\gamma_{\text{opt}}, F_{\text{robust}}] = \arg \min_{\gamma, F} \gamma, \quad \text{subject to} \quad \mathcal{J}(F) < \gamma, \quad (3.19)$$

where the solution γ_{opt} is the minimal worst-case H_2 norm that can be achieved by a filter $F(q)$ (see Figure 3.3) and F_{robust} is the filter achieving this minimal worst-case H_2 norm.

Remark 3.6 *The objective function defined in the frequency-domain by (3.18) is not precisely same as the objective function defined in the time-domain by (3.10). This is due to the fact that the squared tracking error is weighted by a time-domain weighting filter $w(k)$ in (3.10). Note that the main purpose to use weighting filter $w(k)$ is to emphasis the better tracking requirement of the reference meniscus velocity governing the droplet properties. There is no method available to map $w(k)$ one to one in the frequency domain. One can mimic $w(k)$ by designing a frequency domain weighting filter to penalize the tracking error in the low frequency region. However, for simplicity we have not introduced such frequency domain weighting filter in (3.18).*

It is difficult to obtain the solution of the problem (3.18) as it is not a convex finite dimensional optimization problem. However, it is possible to compute an upper bound on γ_{opt} and a suboptimal filter using convex optimization. In Appendix C, we have presented the LMIs conditions to obtain an upper bound on γ_{opt} with a filter $F(q, \beta)$ restricted to an FIR model structure with β the filter coefficient vector (Khalate et al. 2011). It is observed that the dimension of the to-be-designed vector β will become larger when the actuation pulse is longer and/or when the sampling time T_s is smaller. This may pose numerical problems since the size of the LMI problem, required to obtain the robust filter $F(q, \beta)$, is directly proportional to the dimension of vector β . A general approach to overcome this problem is to chose $F(q)$ as a rational function.

The results for the design of the robust filter F_{robust} are based on the results for the design of a filter F_{opt} for the nominal plant $H(q)$ in (2.5) (i.e. the plant $H(q, \Delta)$ with $\Delta = [0 \ 0]^T$). For simplicity, we first present a methodology to design this nominal filter F_{opt} by solving the following problem

$$\begin{aligned} [\gamma_{\text{opt}}^{\text{nom}}, F_{\text{opt}}] &= \arg \min_{\gamma_{\text{nom}}, F} \gamma^{\text{nom}}, \\ \text{subject to } \mathcal{J}_{\text{nom}}(F) &< \gamma^{\text{nom}}, \end{aligned} \quad (3.20)$$

with $\mathcal{J}_{\text{nom}}(F) = \|H_{\text{ref}}(q) - H(q)F(q)\|_2^2$.

We will see in the following lemma, as opposed to the robust case, the solution of the problem (3.20) can be computed exactly.

Lemma 3.1 *Consider the optimization problem (3.20). The solution $\gamma_{\text{opt}}^{\text{nom}}$ of (3.20) can be exactly computed as the solution of the following LMI optimization problem³*

$$\min_{\gamma^{\text{nom}}, W=W^T, Q=Q^T, Z=Z^T, \tilde{A}_F, B_F, \tilde{C}_F, D_F} \gamma^{\text{nom}}$$

such that

$$\begin{aligned} \text{trace}[W] &< \gamma^{\text{nom}}, \\ \begin{bmatrix} P & S_1 & S_2 \\ * & P & 0 \\ * & * & I \end{bmatrix} &> 0, \end{aligned}$$

³Note that we use * as an ellipsis for terms that can be induced by symmetry.

$$\begin{bmatrix} W & S_3 \\ * & P \end{bmatrix} > 0 \quad (3.21)$$

where

$$\begin{aligned} P &= \begin{bmatrix} (Q - Z) & (Q - Z) \\ * & Q \end{bmatrix}, \\ S_1 &= \begin{bmatrix} \tilde{A}_F & \tilde{A}_F \\ \tilde{B}_S \tilde{C}_F + \tilde{A}(Q - Z) & \tilde{B}_S \tilde{C}_F + \tilde{A}Q \end{bmatrix}, \\ S_2 &= \begin{bmatrix} B_F \\ \tilde{B}_S D_F + \tilde{B}_R \end{bmatrix}, \\ S_3 &= [\tilde{C}(Q - Z) \quad \tilde{C}Q]. \end{aligned} \quad (3.22)$$

The state-space matrices in the above LMIs correspond to the state-space matrices (3.16) of $\nu(q, F, \Delta)$ with $\Delta = [0 \ 0]^T$, i.e. the error dynamics with the nominal system $H(q)$.

The optimal filter $F_{opt}(q)$ achieving $\mathcal{J}_{nom}(F) = \gamma_{opt}^{nom}$ can then be computed with the use of the decision variables Q_{opt} , Z_{opt} , $\tilde{A}_{F_{opt}}$, $B_{F_{opt}}$, $\tilde{C}_{F_{opt}}$ and $D_{F_{opt}}$ solving the above LMI problem

$$F_{opt} = \left[\begin{array}{c|c} A_{F_{opt}} & B_{F_{opt}} \\ \hline C_{F_{opt}} & D_{F_{opt}} \end{array} \right] = \left[\begin{array}{c|c} \tilde{A}_{F_{opt}}(Q_{opt} - Z_{opt})^{-1} & B_{F_{opt}} \\ \hline \tilde{C}_F(Q_{opt} - Z_{opt})^{-1} & D_{F_{opt}} \end{array} \right].$$

Proof: Consider the error dynamics system (3.16) (i.e. the system H augmented with the filter F) without the uncertainty Δ and for one particular $F(q)$. Then, it is well known (Geromel et al. 2000; Xie et al. 2004) that for $\gamma^{nom} > 0$ the inequality $\|\nu(q)\|_2^2 < \gamma^{nom}$ holds if and only if there exist symmetric matrices P and W such that

$$\begin{aligned} \text{trace}[W] &< \gamma^{nom}, \\ \begin{bmatrix} P & AP & B \\ * & P & 0 \\ * & * & I \end{bmatrix} &> 0, \\ \begin{bmatrix} W & CP \\ * & P \end{bmatrix} &> 0, \end{aligned} \quad (3.23)$$

where the matrices A, B, C correspond to the state-space matrices (3.16) of $\nu(q, F, \Delta)$ with $\Delta = [0 \ 0]^T$, i.e. the error dynamics with the nominal system $H(q)$. By using the partition of the Lyapunov function P given in (3.22) and by using the following change of variables $\tilde{A}_F = A_F(Q - Z)$ and $\tilde{C}_F = C_F(Q - Z)$ we can rewrite (3.23) as (3.21). The expression for the optimal filter F_{opt} follows then directly from the definition of \tilde{A}_F and \tilde{C}_F . \square

Remark 3.7 Lemma 3.1 is close to the result of (Geromel et al. 2000). However, we use here another partition of P , see (3.22), which simplifies the derivation of the filter.

Robust actuation pulse design using a rational filter

We have seen that Lemma 3.1 can be used to design an optimal pulse using a rational filter $F(q)$. By extending these results, an upper bound $\gamma_{\text{opt}}^{\text{UB}}$ on the solution γ_{opt} of the problem (3.19) can be obtained by using the following theorem.

Theorem 3.1 Consider the error dynamics given by (3.16) with the polytopic uncertainty (3.17) then, $\gamma_{\text{opt}}^{\text{UB}}$, the solution of the following LMI optimization problem, is guaranteed to be an upper bound of the solution γ_{opt} of the problem (3.19)

$$\min_{\gamma^{\text{UB}}, W=W^T, Q=Q^T, Z=Z^T, \tilde{A}_F, B_F, \tilde{C}_F, D_F} \gamma^{\text{UB}}$$

such that the following LMIs hold for $i = 1, 2, 3, 4$,

$$\begin{aligned} \text{trace}[W] &< \gamma^{\text{UB}}, \\ \begin{bmatrix} P & S_1(\Delta_i) & S_2(\Delta_i) \\ * & P & 0 \\ * & * & I \end{bmatrix} &> 0, \\ \begin{bmatrix} W & S_3 \\ * & P \end{bmatrix} &> 0, \end{aligned} \quad (3.24)$$

where

$$\begin{aligned} P &= \begin{bmatrix} (Q-Z) & (Q-Z) \\ * & Q \end{bmatrix}, \\ S_1(\Delta_i) &= \begin{bmatrix} \tilde{A}_F & \tilde{A}_F \\ \tilde{B}_S(\Delta_i)\tilde{C}_F + \tilde{A}(\Delta_i)(Q-Z) & \tilde{B}_S(\Delta_i)\tilde{C}_F + \tilde{A}(\Delta_i)Q \end{bmatrix}, \\ S_2(\Delta_i) &= \begin{bmatrix} B_F \\ \tilde{B}_S(\Delta_i)D_F + \tilde{B}_R \end{bmatrix}, \\ S_3 &= [\tilde{C}(Q-Z) \quad \tilde{C}Q], \end{aligned} \quad (3.25)$$

and the robust filter $F_{\text{robust}}(q)$ which is guaranteed to achieve (at most) a worst-case norm of $\gamma_{\text{opt}}^{\text{UB}}$ is

$$F_{\text{robust}} = \left[\begin{array}{c|c} A_F & B_F \\ \hline C_F & D_F \end{array} \right] = \left[\begin{array}{c|c} \tilde{A}_F(Q-Z)^{-1} & B_F \\ \hline \tilde{C}_F(Q-Z)^{-1} & D_F \end{array} \right]. \quad (3.26)$$

Proof: The LMI (3.24) for a given i is equivalent to the LMI (3.21) for the error dynamics system $\nu(q, F, \Delta_i)$. Verifying that the LMI (3.24) holds for $i = 1, 2, 3, 4$, is thus equivalent to verify that $\|\nu(q, F, \Delta_i)\|_2^2 < \gamma^{\text{UB}}$ for the systems $\nu(q, F, \Delta_i)$

at the vertices of the polytopic uncertainty Δ . Since the uncertainty Δ enters linearly in the LMI's ($S_1(\Delta)$ and $S_2(\Delta)$ are affine in Δ), the above fact implies that $\|\nu(q, F, \Delta)\|_2^2 < \gamma^{UB}$ for all $\Delta \in \mathbf{\Delta}$ (see e.g. (Boyd et al. 1994)). The construction of the filter is then similar as in (3.26). \square

We observe that the LMI conditions (3.24) proposed to obtain the robust filter F_{robust} should be valid at all vertices $\Delta_i, i = 1, 2, 3, 4$, of the polytope $\mathbf{\Delta}$ with a constant Lyapunov function P . This stringent restriction may lead to conservative results, i.e. $\gamma_{\text{opt}}^{UB} \gg \gamma_{\text{opt}}$. If we allow the Lyapunov function P to be parameter dependent, i.e. $P(\Delta)$, the condition (3.24) will no longer be an LMI because the Lyapunov function P and the state-space variables of the filter $F(q)$ are closely interconnected. Similar to (Tuan et al. 2001), to overcome this difficulty we will utilize a reciprocal variant of the projection lemma (Lemma 3.2) to alleviate the interrelation between P and the filter variables. This result is presented in Theorem 3.2. Prior to this, for readers reference we first present the projection lemma (Tuan et al. 2001) which will be used for the proof of Theorem 3.2.

Lemma 3.2 (Projection lemma (Tuan et al. 2001)) *Given a symmetric matrix $\Psi \in \mathbb{R}^{m \times m}$ and two matrices U, V of column dimension m , the following problem*

$$\Psi + U^T L^T V + V^T L U > 0 \quad (3.27)$$

is solvable in a matrix L of compatible dimension if and only if

$$\mathcal{N}_U^T \Psi \mathcal{N}_U > 0, \quad \mathcal{N}_V^T \Psi \mathcal{N}_V > 0 \quad (3.28)$$

where \mathcal{N}_U and \mathcal{N}_V are any basis of the null space of U and V , respectively.

Proof: See (Tuan et al. 2001). \square

Now, we present the LMI conditions, summarized in the following theorem, to deliver less conservative upper bound γ_{opt}^{UB} on γ_{opt} for certain conditions.

Theorem 3.2 *Consider the error dynamics given by (3.16) with the polytopic uncertainty (3.17). If the following LMI optimization problem is feasible*

$$\min_{\gamma^{UB}, W=W^T, P=P^T, Z, L} \gamma^{UB}$$

such that following LMIs hold for $i = 1, 2, 3, 4$

$$\begin{aligned} & \text{trace}[W] < \gamma^{UB} \\ & \begin{bmatrix} P(\Delta_i) & * & * \\ S_4(\Delta_i) & S_5 - P(\Delta_i) & * \\ S_6(\Delta_i) & S_7 & L_{33} + L_{33}^T - I \end{bmatrix} > 0, \end{aligned} \quad (3.29)$$

$$\begin{bmatrix} W & * \\ S_8(\Delta_i) & P(\Delta_i) \end{bmatrix} > 0 \quad (3.30)$$

where

$$\begin{aligned}
P(\Delta_i) &= \begin{bmatrix} P_1(\Delta_i) & * \\ P_3(\Delta_i) & P_2(\Delta_i) \end{bmatrix}, \\
L &= \begin{bmatrix} L_{11} & L_{12} & L_{13} \\ L_{11} & L_{22} & L_{13} \\ L_{31} & L_{32} & L_{33} \end{bmatrix}, \\
Z &= \begin{bmatrix} Z_{11} & Z_{12} \\ Z_{21} & Z_{22} \end{bmatrix}, \\
S_4(\Delta_i) &= \begin{bmatrix} -Z_{11}^T & -(Z_{21}^T \tilde{B}_S(\Delta_i)^T + L_{12} \tilde{A}(\Delta_i)^T + L_{13} \tilde{B}_R^T) \\ -Z_{11}^T & -(Z_{21}^T \tilde{B}_S(\Delta_i)^T + L_{22} \tilde{A}(\Delta_i)^T + L_{13} \tilde{B}_R^T) \end{bmatrix}, \\
S_5 &= \begin{bmatrix} L_{11} + L_{11}^T & * \\ L_{11} + L_{12}^T & L_{22} + L_{22}^T \end{bmatrix}, \\
S_6(\Delta_i) &= \begin{bmatrix} -Z_{12}^T & -(Z_{22}^T \tilde{B}_S(\Delta_i)^T + L_{32} \tilde{A}(\Delta_i)^T + L_{33} \tilde{B}_R^T) \end{bmatrix}, \\
S_7 &= \begin{bmatrix} L_{31} + L_{13}^T & L_{32} + L_{13}^T \end{bmatrix}, \\
S_8(\Delta_i) &= \begin{bmatrix} \tilde{C}P_3(\Delta_i) & \tilde{C}P_2(\Delta_i) \end{bmatrix}^T, \tag{3.31}
\end{aligned}$$

$$\tag{3.32}$$

then the solution γ_{opt}^{UB} of the above LMI optimization problem is guaranteed to be an upper bound on the solution γ_{opt} of the problem(3.19). Moreover, the robust filter $F_{robust}(q)$ which is guaranteed to achieve (at most) a worst-case norm of γ_{opt}^{UB} is

$$F = \left[\begin{array}{c|c} A_F & B_F \\ \hline C_F & D_F \end{array} \right] = \left[\begin{array}{cc} L_{11}^T & L_{31}^T \\ L_{13}^T & L_{33}^T \end{array} \right]^{-1} \begin{bmatrix} Z_{11} & Z_{12} \\ Z_{21} & Z_{22} \end{bmatrix}. \tag{3.33}$$

Proof: Consider the error dynamics system (3.16) (i.e. the system H augmented with the filter F) for one particular Δ and for one particular $F(q)$, then the inequality $\|\nu(q, F, \Delta)\|_2^2 < \gamma^{UB}$ holds if and only if we can find γ^{UB} such that $\text{trace}[W] < \gamma^{UB}$ and the following inequalities hold

$$\begin{bmatrix} I & A(\Delta) & B(\Delta) \end{bmatrix} \Psi(\Delta)[*]^T > 0, \tag{3.34}$$

$$\begin{bmatrix} W & * \\ S_8(\Delta) & P(\Delta) \end{bmatrix} > 0 \tag{3.35}$$

where $\Psi(\Delta) = \text{diag}(P(\Delta), -P(\Delta), -I)$.

The above conditions are equivalent with those in (3.23). We use the notation $P(\Delta)$ because the Lyapunov matrices P can be different for different values of Δ . Note that the condition (3.35) is an LMI, but the condition (3.34) is not.

In order to obtain a convex robust optimization problem, we need to rewrite (3.34) as a matrix inequality where $P(\Delta)$ does not multiply with any Δ -dependent term. The condition (3.34) can be rewritten using the projection lemma. This projection lemma states that (3.34) holds if and only if there exists a matrix $L(\Delta)$

of appropriate dimension satisfying the following inequality

$$\Psi(\Delta) + U(\Delta)^T L^T(\Delta) V + V^T L(\Delta) U(\Delta) > 0 \quad (3.36)$$

$$\text{with } V = \begin{bmatrix} 0 & I & 0 \\ 0 & 0 & I \end{bmatrix}, U(\Delta) = \begin{bmatrix} -A^T(\Delta) & I & 0 \\ -B^T(\Delta) & 0 & I \end{bmatrix}.$$

The matrices V and $U(\Delta)$ are chosen such that their null spaces satisfies the condition (3.28) of the projection lemma (Lemma 3.2).

Note that $L(\Delta)$ in (3.36) is also function of Δ . However, in sequel we will consider a constant L in order to obtain an LMI formulation. In (3.36), L has no special structure. However, in Theorem 3.2, we impose the special structure on L given by (3.31). If we can find a matrix having this structure, then (3.34) holds. Otherwise, we cannot say anything about (3.34).

Supposing first that a matrix L exists, with $S_4(\Delta), S_5, S_6(\Delta), S_7$ as defined in (3.31) and with the following change of variables

$$\begin{bmatrix} Z_{11} & Z_{12} \\ Z_{21} & Z_{22} \end{bmatrix} = \begin{bmatrix} A_F & B_F \\ C_F & D_F \end{bmatrix} \begin{bmatrix} L_{11}^T & L_{31}^T \\ L_{13}^T & L_{33}^T \end{bmatrix}. \quad (3.37)$$

The condition (3.36) is not an LMI. Hence, we partition $U(\Delta)$ as follows

$$U^T(\Delta) = \begin{bmatrix} 0 & 0 & 0 \\ 0 & -\tilde{A}(\Delta) & -\tilde{B}_R \\ I & 0 & 0 \\ 0 & I & 0 \\ 0 & 0 & I \end{bmatrix} + \begin{bmatrix} -I & 0 \\ 0 & -\tilde{B}_S(\Delta) \\ 0 & 0 \\ 0 & 0 \\ 0 & 0 \end{bmatrix} \begin{bmatrix} A_F & B_F \\ C_F & D_F \end{bmatrix} \begin{bmatrix} I & 0 & 0 \\ 0 & 0 & I \end{bmatrix}. \quad (3.38)$$

Let us analyze the term $U^T(\Delta)L^T V$ of (3.36):

$$U^T(\Delta)L^T V = \begin{bmatrix} 0 & 0 & 0 \\ -(\tilde{A}(\Delta)L_{12}^T + \tilde{B}_R L_{13}^T) & -(\tilde{A}(\Delta)L_{22}^T + \tilde{B}_R L_{13}^T) & -(\tilde{A}(\Delta)L_{32}^T + \tilde{B}_R L_{33}^T) \\ I & 0 & 0 \\ 0 & I & 0 \\ 0 & 0 & I \end{bmatrix} V$$

$$+ \begin{bmatrix} -I & 0 \\ 0 & -\tilde{B}_S \\ 0 & 0 \\ 0 & 0 \\ 0 & 0 \end{bmatrix} \begin{bmatrix} A_F & B_F \\ C_F & D_F \end{bmatrix} \begin{bmatrix} L_{11}^T & L_{31}^T \\ L_{13}^T & L_{33}^T \end{bmatrix} \begin{bmatrix} I & I & 0 \\ 0 & 0 & I \end{bmatrix} V.$$

Now, substituting the change of variable (3.37) in the above expression and with further simplification of (3.36) we get:

$$\begin{bmatrix} P(\Delta) & * & * \\ S_4(\Delta) & S_5 - P(\Delta) & * \\ S_6(\Delta) & S_7 & L_{33} + L_{33}^T - I \end{bmatrix} > 0. \quad (3.39)$$

In (3.39), we observe that $P(\Delta)$ does not multiply terms which are functions of Δ . Moreover, the uncertainty Δ appears linearly in $S_4(\Delta)$ and $S_7(\Delta)$. Finally, (3.39) is affine in the variables $P(\Delta)$, Z and L .

Summarizing, if there exists a matrix L having the special structure given in (3.31), such that $\text{trace}[W] < \gamma^{\text{UB}}$, (3.35) and (3.39) hold then $\|\nu(q, F, \Delta)\|_2^2 < \gamma^{\text{UB}}$ for a given Δ and F . Using the convex combination property (Boyd et al. 1994), we can also say that if there exists L and Z such that $\text{trace}[W] < \gamma^{\text{UB}}$, (3.35) and (3.39) holds for $\Delta = \Delta_i$, $i = 1, 2, 3, 4$, then $\|\nu(q, F, \Delta)\|_2^2 < \gamma^{\text{UB}}$ for all $\Delta \in \mathbf{\Delta}$. Moreover, because of (3.37), the corresponding filter is given as in (3.33). \square

Remark 3.8 *We know that the solution of Theorem 3.1 is an upper bound on the solution γ_{opt} of the problem (3.19), but this does not hold for Theorem 3.2. If the new conditions in Theorem 3.2 with the parameter dependent Lyapunov functions are feasible then, indeed, it delivers an upper bound on the solution γ_{opt} of the problem (3.19). This is due to the fact that Theorem 3.2 eliminates the stringent requirement of satisfying the LMI conditions all vertices $\Delta_i, i = 1, 2, 3, 4$, of the polytope $\mathbf{\Delta}$ with a constant Lyapunov function P . However, when the conditions in Theorem 3.2 are not feasible we cannot say anything about the upper bound. The reason for this is that it is not always possible to obtain L in (3.36) with the proposed special structure to ensure (3.34). Nevertheless, when the LMI problem (3.29)-(3.30) is feasible, in many cases, it will provide a less conservative result (see e.g. (Tuan et al. 2001)).*

3.6 Summary

In this chapter, the drop consistency problem is formulated as a trajectory tracking problem. A method is presented to construct such reference trajectory y_{ref} , i.e. a profile which should be followed to jet an ink droplet and then quickly to bring the ink channel to rest. Now, the actuation pulses can be obtained as a solution of the feedforward control problem. The design methods are characterized in two categories. The first one is constrained actuation pulses obeying the shape constraints and the second one is unconstrained actuation pulses without shape constraints.

For the design of constrained pulse, the set of input signals which can be generated by electronics hardware is parametrized by the pulse parameter vector θ . Using the nominal inkjet system model $H(q)$, an optimal actuation pulse $u(k, \theta_{\text{opt}})$ is designed as the solution of a nonlinear optimization problem. We have seen in the previous chapter that the nominal model $H(q)$ is not sufficient to represent the inkjet system dynamics at all DoD frequencies and that this set of models can be represented by uncertain inkjet system $H(q, \Delta), \Delta \in \mathbf{\Delta}$. In order to tackle this uncertainty, a robust pulse is designed which minimizes the worst-case H_2 norm of the tracking error. A gridding approach is used to compute a lower bound on the the worst-case H_2 norm.

For the design of unconstrained pulse, the input signal is parameterized as the pulse response of the to-be-designed filter $F(q)$. An optimal unconstrained pulse is obtained as the solution of the weighted least-square problem using the FIR model structure for the filter $F(q)$. The design of the robust actuation pulse is formulated as a convex optimization using LMIs. However, use of the FIR model structure poses numerical problem when the pulse duration is longer and/or when the sampling time is smaller. Therefore, we have relaxed the constraint of the FIR model structure on the to-be-designed robust filter presented in Appendix C. Further, we have provided improved conditions to compute the robust filter by allowing parameter dependent Lyapunov functions.

In the next chapter we will investigate the performance of the actuation pulse design method proposed in chapter using simulation and experiments on a real setup.

Feedforward Control of an inkjet channel: Results

Various constrained and unconstrained actuation pulse design techniques are developed in the previous chapter. In this chapter we will evaluate the performance of these design methods in simulations and experiments. We mainly analyze the effect of actuation pulses on the damping of the residual oscillations when a single droplet and multiple droplets are jetted from a single ink channel. Further, we test these pulses on the actual experimental setup to investigate the improvement in the drop consistency.

4.1 Introduction

In the previous chapter we have seen that we are restricted to the use of feedforward control (FFC) for improving the inkjet system performance. This is mainly due to the limitations of the printhead driving electronics, which also restrict the shape of actuation pulses. In Section 3.3, based on the available literature and physical insight the drop consistency problem is formulated as a trajectory tracking problem. A method is presented to construct such reference trajectory y_{ref} , i.e. a profile which should be followed to jet an ink droplet and then quickly bring the ink channel to rest. Now, the actuation pulses can be obtained as solution of the feedforward control problem. The design methods are divided into two categories. The first one leads to constrained actuation pulses obeying the shape constraints in Section 3.2 and the second one is unconstrained actuation pulses without shape constraints. Further, in each category, the actuation pulse designed using the nominal model ($H(q)$ or $G(q)$) is called the optimal actuation pulse. The pulse obtained using the uncertain inkjet system model ($H(q, \Delta)$ or $G(q, \Delta)$), which provides good performance over the operating DoD frequency range is called the robust pulse.

In this chapter, we will validate the actuation pulses designed using the methods presented in the previous chapter. We first present simulation results using the inkjet system model and subsequently, experimental validation will be discussed.

4.2 Simulation Results

We will first consider the (realistic) case where the actuation pulse is constrained to have the trapezoidal shape as discussed in Section 3.2.

4.2.1 Constrained Feedforward Control

It is possible to design the actuation pulses by applying the pulse design techniques, developed in the previous chapter, on the piezo sensor model $G_d(q)$ or on the meniscus velocity model $H(q)$. However, in order to show the performance with a model derived from the first principle approach and to avoid repetition of several results, we restrict to only the meniscus velocity model $H(q)$. In the next chapter, we will discuss the performance with the actuation pulses designed with the piezo sensor model $G_d(q)$. In this section, we present the actuation pulses designed using the meniscus velocity model $H(q)$ and the design methods discussed in Section 3.4.

Optimal Constrained Feedforward Control

The nonlinear optimization problem (3.3) delivering the optimal trapezoidal pulse is solved by using the `fmincon` function of the MATLAB's optimization toolbox. Recall that the goal is to damp the residual oscillations by following the reference trajectory $y_{\text{ref}}(k)$. Therefore, the weighting $w(k)$ is designed to penalize the tracking error more in Part B of the reference trajectory (see Figure 3.2). The initial guess θ_{init} for the optimal parameter vector needed to solve the nonlinear optimization problem (3.3) is chosen as follows:

$$\theta_{\text{init}} = [1.5 \quad 2.5 \quad 1.5 \quad 2.5 \quad 6 \quad 3.6 \quad 1 \quad 1.4 \quad -15]^T.$$

Recall that the pulse parameter vector θ is defined as follows in (3.1):

$$\theta = [t_{rR} \quad t_{wR} \quad t_{fR} \quad V_R \quad t_{dQ} \quad t_{rQ} \quad t_{wQ} \quad t_{fQ} \quad V_Q]^T.$$

The time parameters (t_r, t_w, t_f, t_{dQ}) in θ_{init} are chosen using the recommendations in (Kwon and Kim 2007) and (Kwon 2009a). The optimal parameter vector θ_{opt} obtained after solving the optimization problem (3.3) is given as follows

$$\theta_{\text{opt}} = [2.0 \quad 2.5 \quad 1.3 \quad 22.5 \quad 7.6 \quad 1.3 \quad 0.4 \quad 4.4 \quad -13.2]^T.$$

Note that in the parameter vector θ , the time parameters (t_r, t_w, t_f, t_{dQ}) of the actuation pulse are expressed in μs .

We compare the standard pulse (see Section 3.3) and the optimal actuation pulse in the bottom panel of Figure 4.1. As expected, the optimal piezo actuation pulse contains two components, the resonating pulse and the quenching pulse. The quenching pulse deflects the piezo actuator in order to damp the residual oscillations. This enables the meniscus velocity to track the reference trajectory very closely and brings the ink channel to rest soon after jetting the ink drop as seen in the top panel of Figure 4.1 where we compare $y_{\text{opt}}(k) = H(q)u(k, \theta_{\text{opt}})$

to the meniscus velocity corresponding to the standard pulse. As discussed in Section 2.3.3, the starting time for the quenching pulse is approximately $12\mu\text{s}$, which is the fundamental period corresponding to the first resonant frequency at 80kHz (see Figure 2.2). The energy spectral density of the tracking error for the standard pulse and the optimal pulse is shown in Figure 4.2. It is evident that considerable error reduction is achieved by the optimal pulse at the two dominant resonant frequencies of the inkjet printhead, i.e. at 0.5×10^6 rad/sec (or 80 kHz) and 1×10^6 rad/sec (or 160 kHz), and at low frequencies in general.

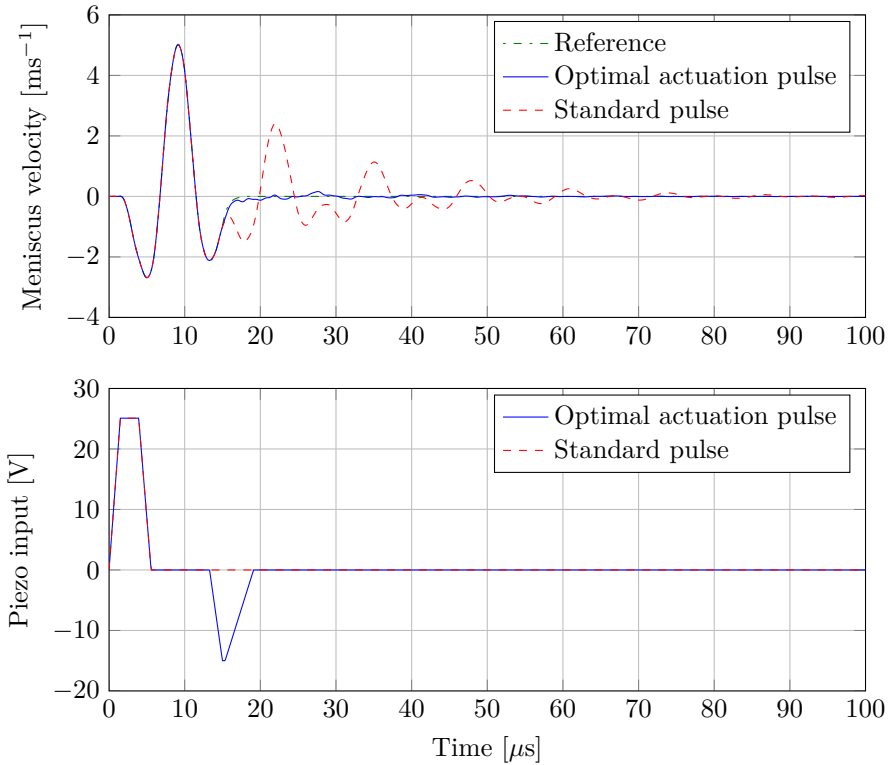


Figure 4.1: Response of the meniscus velocity to the standard pulse and the optimal actuation pulse.

Given the behavior in Figure 4.1, ink drops in theory can be jetted with higher frequencies using the optimal actuation pulse. Figure 4.3 shows the response of the ink channel when ten ink drops are jetted at DoD frequency 38 kHz, i.e., the time interval between the initiation of two actuation pulses is $(1/38)$ ms. In this figure, we compare the behavior when the standard and the optimal pulses are used. For the standard actuation pulse, the meniscus velocity does not quickly come to rest after jetting the ink drop. Therefore, the initial conditions differ when applying the subsequent actuation pulses. This causes the velocity-peaks to change for subsequent drops as indeed observed in Figure 4.3 where they are not equal to 5 ms^{-1} as in Figure 3.2. Recall that the meniscus velocity peak is an important feature

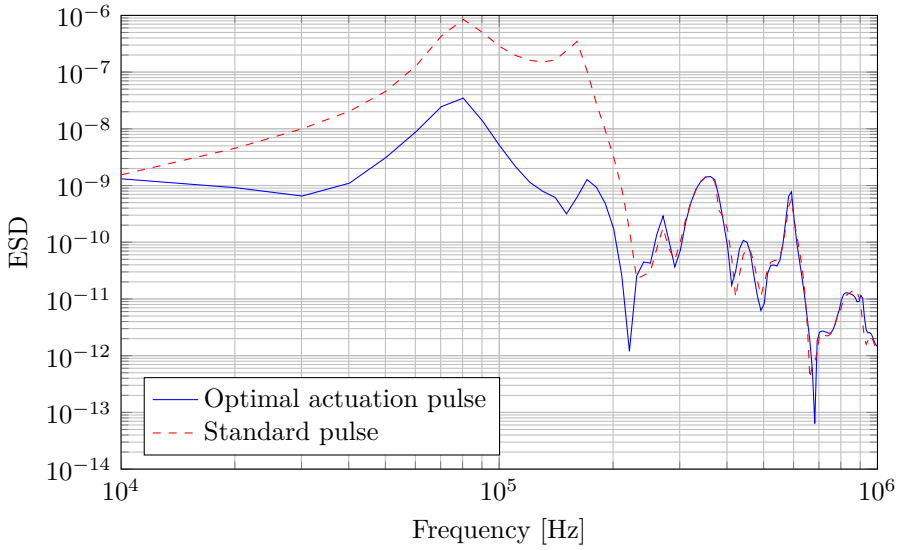


Figure 4.2: Energy spectral density of the error signal ($y_{\text{ref}} - y$).

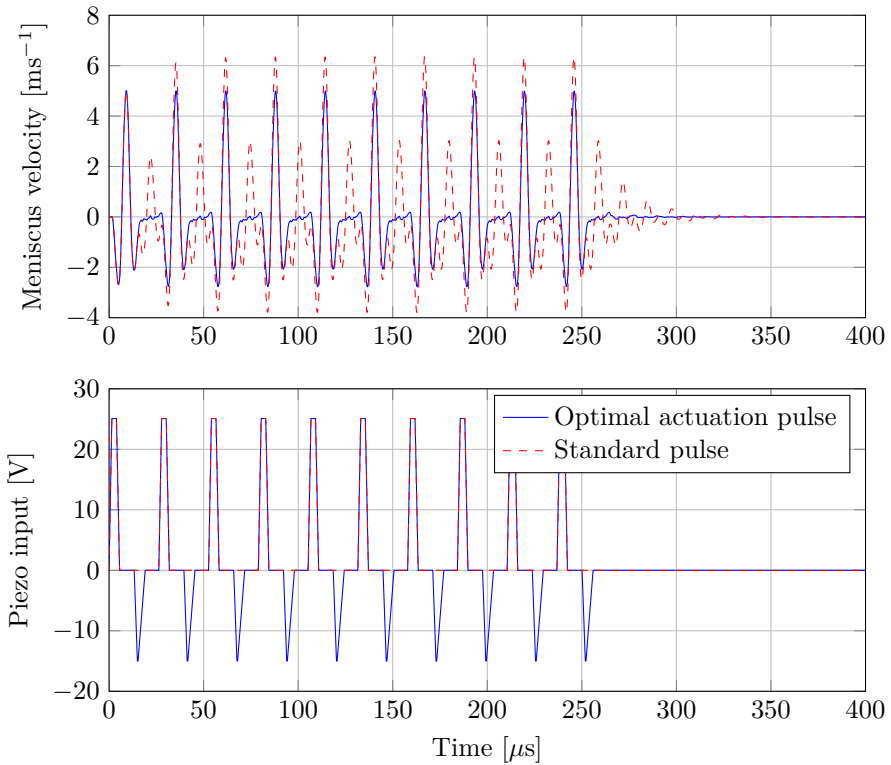


Figure 4.3: Simulation for jetting of ten drops at DoD frequency 38kHz.

and that a changed velocity-peak will result in drops having different velocities. These shortcomings are not seen with the optimal piezo actuation pulse. It ensures similar initial conditions before the application of the resonating pulse for each ink drop. The difference in the velocity-peaks for the optimal actuation pulse are almost negligible. This will result into ink drops having almost the same velocity.

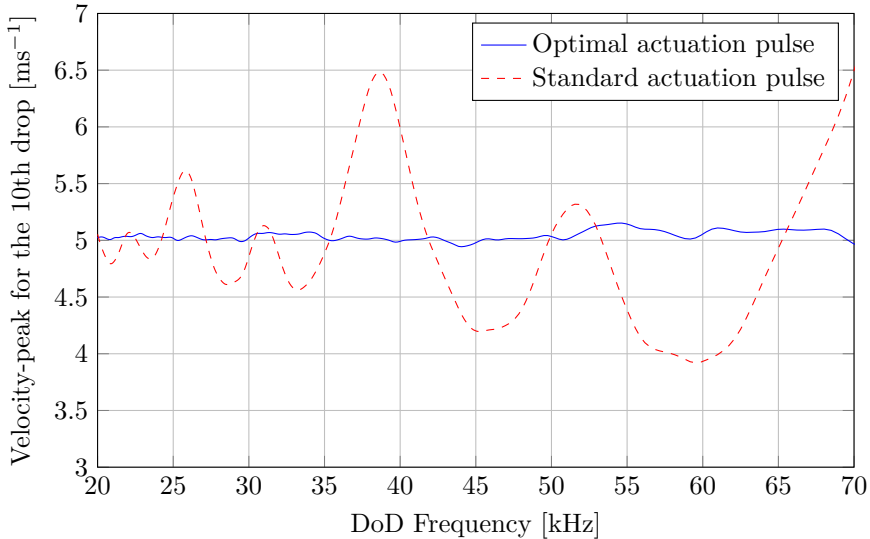


Figure 4.4: Simulated DoD curve.

We have done similar experiments at different DoD frequencies to analyze the improvement in the performance of the inkjet printhead. To summarize all the results, in Figure 4.4 we have only plotted the velocity-peak of the tenth drop against the DoD frequency. As the velocity-peak is almost equal to the velocity of the jetted drop, Figure 4.4 is equivalent to the ‘DoD-curve’, which is the benchmark introduced in Section 1.2.3. We have seen previously that the standard pulse is not able to quickly bring the ink channel to a rest. The time allowed for the residual oscillation to settle down will reduce as we increase the DoD frequency. Therefore, as shown in Figure 4.4, the variation in the peak meniscus velocity becomes larger at higher DoD frequencies when we consider the standard pulse. As opposed to this, the variation of the velocity-peak with the optimal pulse is very limited.

Remark 4.1 *By adding an extra quenching pulse, the duration of the optimal pulse will always be longer than the standard pulse. The duration of the standard pulse is $5.5 \mu\text{s}$ while the one of the optimal pulse ($u(k, \theta_{opt})$) is $19.5 \mu\text{s}$. A consequence of the longer duration of the pulse is that, within the range $[0 \text{ } 70\text{kHz}]$ for the DoD frequency, the optimal pulses will overlap from a DoD frequency $(1/19.5 \mu\text{s})=51 \text{kHz}$. This does not happen for the standard pulse. For $f_{DoD} > 51 \text{kHz}$, we have decided to superimpose the overlapping pulses. This means that, if we want to jet*

a series of N_D drops at a DoD frequency f_{DoD} larger than 51 kHz, we in fact apply the following voltage $u_{overlap}(k)$ to the piezo unit

$$u_{overlap}(k) = \sum_{i=0}^{N_D-1} u_{opt}(k - iD_k) \quad (4.1)$$

where $u_{opt}(k) = u(k, \theta_{opt})$ the optimal pulse of duration $19.5 \mu s$, and D_k is the number of samples between two actuation pulses. If T_s is the sampling time and $\text{round}(x)$ rounds a real number x to the nearest integer, D_k is then equal to $\text{round}(\frac{1}{T_s f_{DoD}})$. Indeed, at a DoD frequency of f_{DoD} , the time separating two successive actuation pulses is $\frac{1}{f_{DoD}}$ second and D_k must be an integer since $u_{opt}(k)$ is a discrete-time signal.

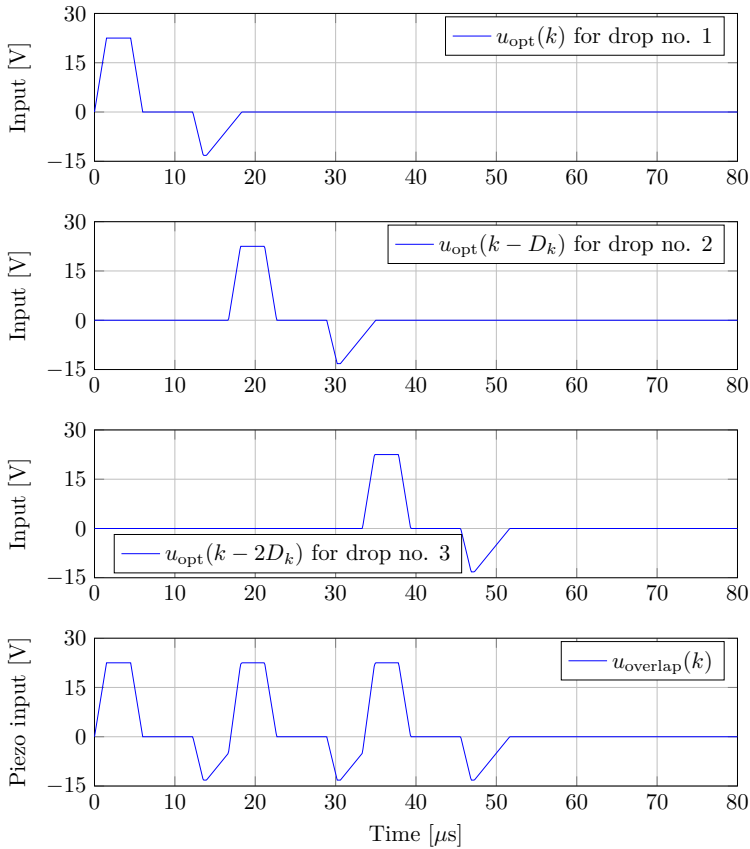


Figure 4.5: Computation of the overlapping pulse $u_{overlap}(k)$ for jetting three ink drops at DoD frequency 60 kHz.

In Figure 4.5 we have shown the computation of the overlapping pulse $u_{overlap}(k)$ for jetting three ink drops at DoD frequency 60 kHz using equation (4.1). It can be seen that the actuation pulse for the second and the third drop is same as the

actuation pulse for the first drop and the only difference is that they are delayed by time duration (in seconds) $D_k T_s$ and $2D_k T_s$ respectively. Recall that k indicate discrete time index and it has to be multiplied by the sampling time T_s to obtain time in seconds. The overlapping pulse $u_{overlap}(k)$ to jet three ink drops is obtained by adding the three pulses $u_{ot}(k)$, $u_{opt}(k - D_k)$ and $u_{opt}(k - 2D_k)$.

Robust Constrained Feedforward Control

In the previous Section, we have seen that the optimal pulse designed using the method presented in Section 3.4.1 effectively damps the residual oscillations in the nominal inkjet system $H(q)$. However, inkjet system is subjected to parametric uncertainty $\Delta \in \mathbf{\Delta}$. In Section 3.4.2, the robust constrained actuation pulse design is presented to reduce the residual oscillations in the uncertain system $H(q, \Delta)$. In this section, we present simulation results with the robust pulse.

The nonlinear optimization problem (3.7) is solved by using the command `fmincon` of the optimization toolbox of MATLAB. The robust actuation pulse parameter vector θ_{robust} obtained after solving the optimization problem (3.7) is

$$\theta_{robust} = [1.5 \ 2.5 \ 1.5 \ 23.0 \ 6.93 \ 2.74 \ 0.4 \ 3.75 \ -13.22]^T$$

The robust pulse $u_{robust}(k) = u(k, \theta_{robust})$ designed in such a manner is shown in Figure 4.6 by the solid blue line.

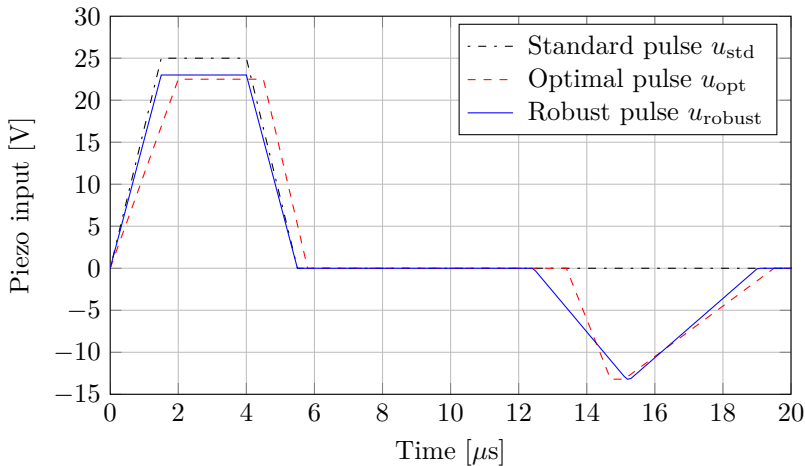


Figure 4.6: Actuation pulses.

We compare the response of the inkjet system with the robust actuation pulse and the optimal actuation pulse in Figure 4.7. As expected, the optimal actuation pulse damps the residual oscillations effectively for the nominal plant. However, for the worst-case uncertain inkjet system in $H(q, \Delta)$, $\Delta \in \mathbf{\Delta}$, the amplitude of the residual oscillations is quite large. For the nominal inkjet system, the robust

actuation pulse does not damp the residual oscillations so effectively as the optimal pulse. However, for the worst-case uncertain inkjet system, the deviation from the nominal response is smaller compared to the optimal pulse. This enables the meniscus velocity to track the reference trajectory closely and brings the ink channel to rest soon after jetting the ink drop even in the presence of parametric uncertainty.

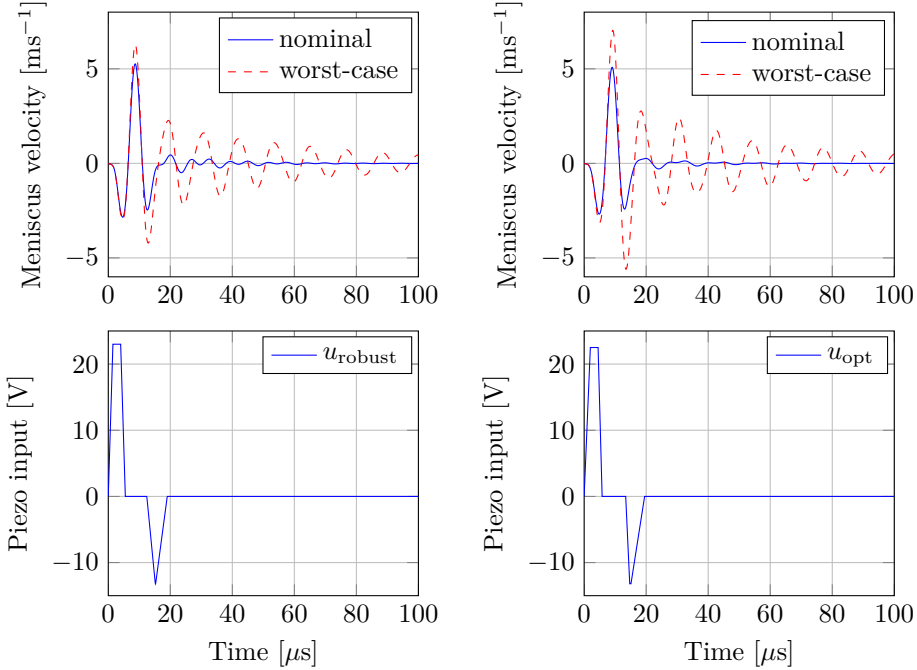


Figure 4.7: Response for the meniscus velocity to the robust and the optimal actuation pulse.

In Figure 4.7, it appears that the robust pulse is fairly better than the optimal pulse for the worst-case scenario. However, it is important to analyze the ink drop consistency when numerous drops are jetted at a high DoD frequency with both the pulses. Figure 4.8 shows the response of the nominal and the worst-case uncertain inkjet channel when ten ink drops are jetted at DoD frequency 38 kHz, i.e., the time interval between the initiation of two actuation pulses is $(1/38)\text{ms}$. For the worst-case uncertain ink channel in $H(q, \Delta)$, $\Delta \in \mathbf{\Delta}$, the deviation in the meniscus velocity-peak of the tenth drop is smaller by 2ms^{-1} with the robust pulse compared to the optimal pulse. This is a considerable improvement.

We have done similar experiments at different DoD frequencies to analyze the improvement in the performance of the inkjet printhead. To summarize all the results, we have only plotted the velocity-peak of the tenth drop against the DoD frequency in Figure 4.9. Since, for the nominal case the optimal actuation pulse damps the residual oscillations effectively, the DoD-curve is relatively flat for the

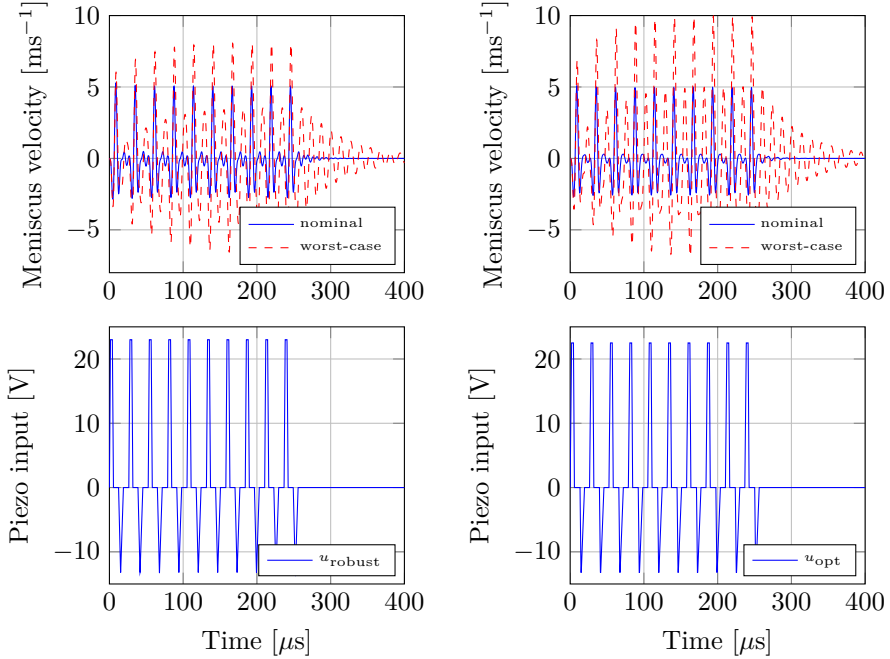


Figure 4.8: Simulation for jetting ten drops at DoD frequency 38kHz.

optimal actuation pulse. However, we have seen previously that the optimal actuation pulse does not effectively damp the residual oscillations for the worst perturbed inkjet system. We have simulated the response of uncertain inkjet system $H(q, \Delta)$, $\Delta \in \mathbf{\Delta}$ with a fine grid $\mathcal{S} = \{\Delta^i, i = 1, \dots, m, \mid \Delta^i \in \mathbf{\Delta}\}$ on $\mathbf{\Delta}$. The region in which the velocity-peak (of the 10th drop) for uncertain inkjet system $H(q, \Delta)$, $\Delta \in \mathbf{\Delta}$ may lie is shown by the gray shaded area in Figure 4.9. It is observed that the bounds obtained on the DoD-curve for the optimal actuation pulse after simulating the perturbed inkjet systems $H(q, \Delta)$, $\Delta \in \mathbf{\Delta}$, are wider compared to the robust actuation pulse. This indicates that in the presence of parametric uncertainty the performance of the robust pulse will not degrade similar to the optimal actuation pulse.

We have seen that the constrained actuation pulse is effective in reducing the residual oscillations. In the next section we present the simulation results to access the effectiveness of the unconstrained pulses to damp the residual oscillations.

4.2.2 Unconstrained Feedforward Control

In Section 3.5 we have seen that the rapid development in electronics may enable printhead manufacturers to use more sophisticated electronic hardware which can generate an unconstrained actuation pulse. A method is proposed Section 3.5.1 to compute unconstrained actuation pulse using the nominal model of the inkjet

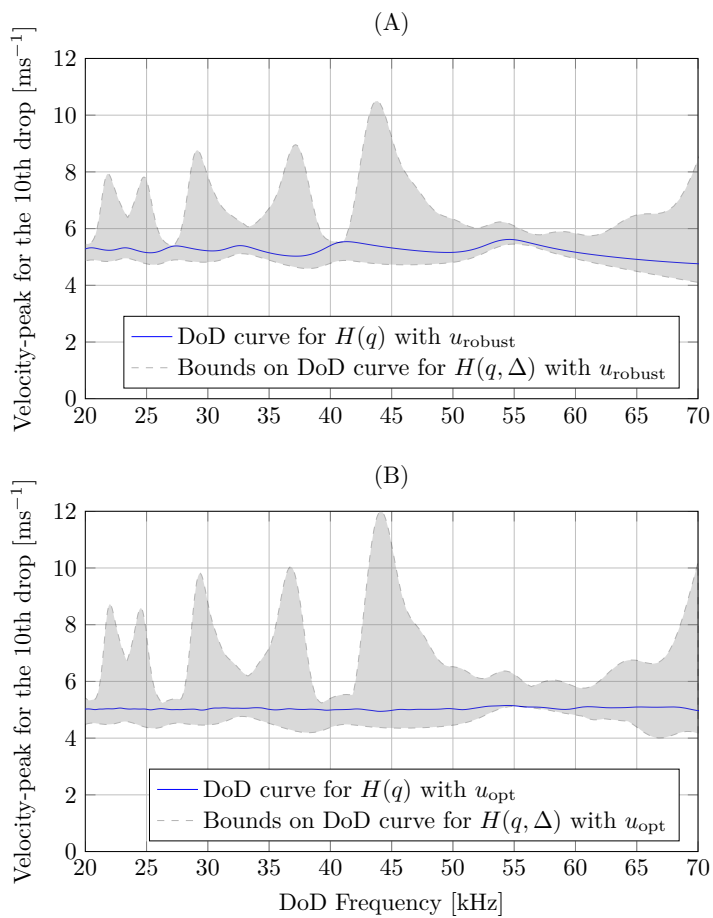


Figure 4.9: Simulated DoD curve.

system. Furthermore, in Section 3.5.2, the design of a robust unconstrained pulse is formulated as a convex optimization problem using the uncertain inkjet system $H(q, \Delta)$. We subsequently present the simulation results to show the improvement with the unconstrained actuation pulses.

Optimal Unconstrained Feedforward Control

In Figure 4.1 we observe that the optimal trapezoidal shape allows to reduce significantly the residual oscillations. By considering the approach in Section 3.5.1, we will now verify whether an even better performance can be achieved if we relax the trapezoidal shape constraint on the actuation pulse. For this purpose, we have solved the least-square problem (3.10) with a FIR filter $F(q, \beta)$ of length 930 to improve the performance. In Figure 4.10, we compare the meniscus velocity resulting from the application of the optimal unconstrained pulse obtained by solving (3.10) and the meniscus velocity resulting from the application of the optimal constrained pulse obtained by solving (3.3) (i.e. the trapezoidal pulse). By analyzing the unconstrained pulse (see the bottom of Figure 4.10,), we must first observe that this unconstrained pulse is very similar to the optimal constrained pulse. The main difference between these two pulses is the oscillating behavior after $15\mu\text{s}$ in the unconstrained pulse. However, from a practical point of view, the increase of complexity of the pulse (the oscillatory behavior) outweighs the improvement of performance (the performance with the optimal trapezoidal pulse is already very satisfactory). Considering this, the optimal trapezoidal pulse delivered by the optimization problem (3.3) seems the best compromise between performance and complexity for the printhead under consideration. It also indicates that the nonlinear optimization (3.3) yields an actuation pulse which is very similar to the unconstrained actuation pulse and therefore it is close to the global optimum.

Robust Unconstrained Feedforward Control

In the previous section we have obtained an unconstrained optimal pulse using the solution of a simple least-square problem. It is also possible to design an unconstrained optimal actuation pulse $u_{\text{opt}}(k)$ for the nominal model $H(q)$ using Lemma 3.1 (i.e., without considering the polytopic uncertainty). For this purpose, we use the desired meniscus velocity $y_{\text{ref}}(k)$ designed in Section 3.3, i.e., a template for the meniscus velocity with fast decaying residual oscillations. The black dash-dot line in Figure 4.11 shows the unconstrained optimal pulse $u_{\text{opt}}(k) = F_{\text{opt}}(q)\delta(k)$ obtained after solving the optimization problem of Lemma 3.1 using the LMI Control Toolbox of MATLAB. The H_2 norm of the error dynamics $\nu(q, F_{\text{opt}})$ is found to be $\gamma_{\text{opt}}^{\text{nom}} = 0.1172$. Note that the optimal filter $F_{\text{opt}}(q)$ obtained here is a rational filter unlike in the previous section which was a FIR filter.

We know that this optimal pulse may not perform satisfactorily in practice because the inkjet dynamics changes considerably while jetting at different DoD frequencies. Therefore, it is interesting to compute the worst-case H_2 norm of the error dynamics $\nu(q, F_{\text{opt}}, \Delta)$ for the polytopic uncertainty $\Delta \in \mathbf{\Delta}$ with the optimal filter $F_{\text{opt}}(q)$ to analyze the performance degradation (see Section 3.5.2). For the

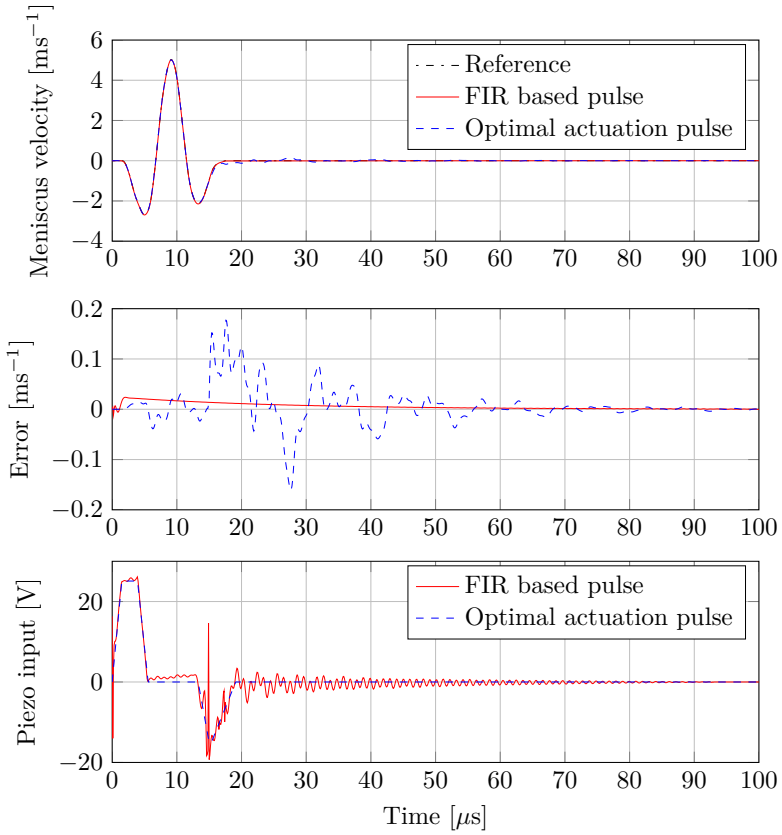


Figure 4.10: Response of the meniscus velocity to the optimal constrained pulse and the optimal unconstrained actuation pulse.

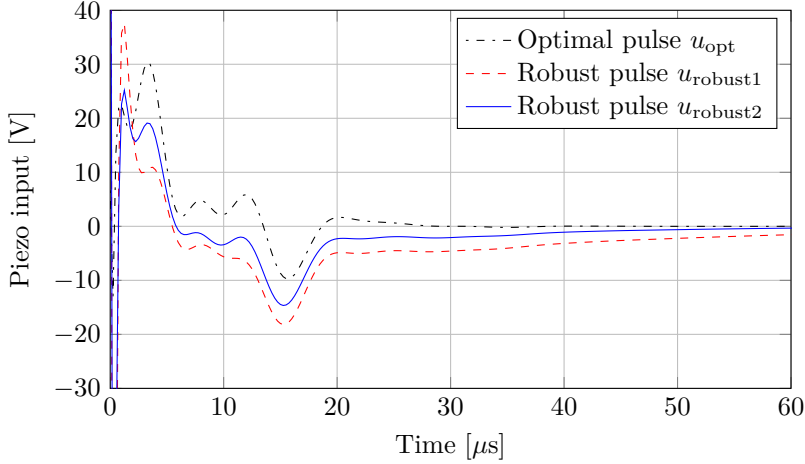


Figure 4.11: Comparison of the actuation pulses $u_{\text{opt}}(k) = F_{\text{opt}}(q)\delta(k)$ obtained using Lemma 3.1, Theorem 3.1 and Theorem 3.2.

given filter $F_{\text{opt}}(q)$, we can compute a lower bound γ^{LB} on the worst-case H_2 norm by evaluating H_2 norm of $\nu(q, F_{\text{opt}}, \Delta)$ at fine grid points on the parametric uncertainty Δ . We found that the lower bound γ^{LB} on the worst-case H_2 norm with the optimal filter F_{opt} is 189.53.

In Section 3.5.2, we have proposed Theorems 3.1 and 3.2 to obtain robust pulses. The LMI conditions for Theorem 3.1 are more stringent due to use of a constant Lyapunov function resulting in more conservative solution. In Theorem 3.2 we have relaxed these condition by allowing the Lyapunov function to be parameter dependent and thus, it is expected to deliver a less conservative results. We have solved the LMI optimization problem in Theorems 3.1 and 3.2 and the resulting robust pulses, $u_{\text{robust1}}(k)$ and $u_{\text{robust2}}(k)$, respectively, are shown in Figure 4.11. Figures 4.12 and 4.13 shows simulation results with these pulses. Note that in these figures the solid blue line shows the response of the nominal system $H(q)$. The shaded area shows the bounds on the uncertain system $H(q, \Delta)$ response obtained with a fine grid on the polytopic uncertainty Δ (as discussed in Section 3.4.2.) A numerical comparison of the worst-case H_2 norm of the error dynamics $\nu(q, \Delta)$ with these robust actuation pulses is presented in Table 4.1. In Table 4.1, we give also corresponding lower bound on γ_{opt} computed with a fine grid on the polytopic uncertainty Δ . Compared to the nominal filter F_{opt} achieving a worst-case norm of at least 189.53, the robust filters F_{robust1} and F_{robust2} achieve a much smaller worst-case norm. This is especially true with the pulse u_{robust2} obtained with Theorem 3.2. This is expected as Theorem 3.2 uses parameter-dependent Lyapunov function reducing the conservatism in Theorem 3.1 which uses parameter-independent Lyapunov function (see Section 3.5.2). We also observe that the upper bound given by Theorem 3.2 is close to the lower bound, which shows its efficacy for conservatism reduction.

The response of the meniscus velocity to the robust actuation pulses $u_{\text{robust1}}(k)$

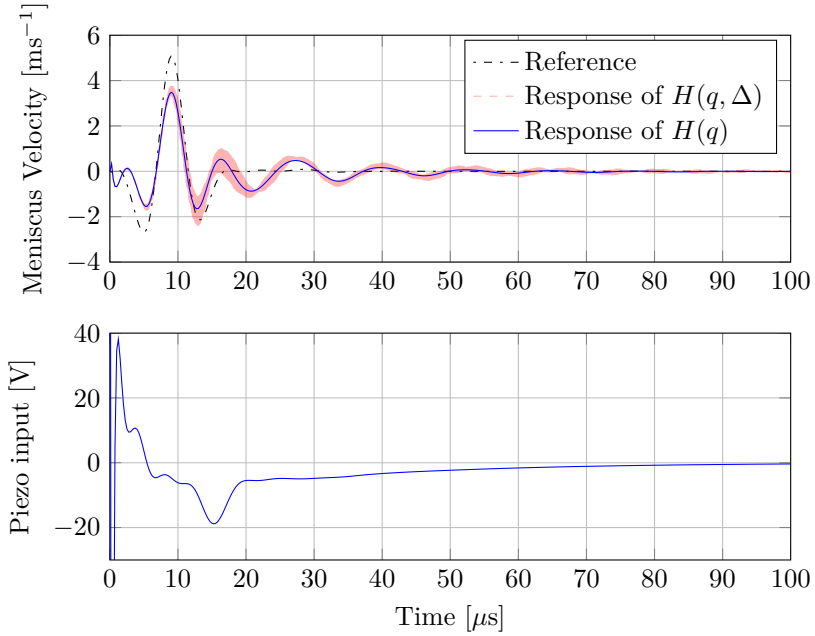


Figure 4.12: Simulation results with the robust pulse $u_{\text{robust1}}(k)$ obtained with Theorem 3.1.

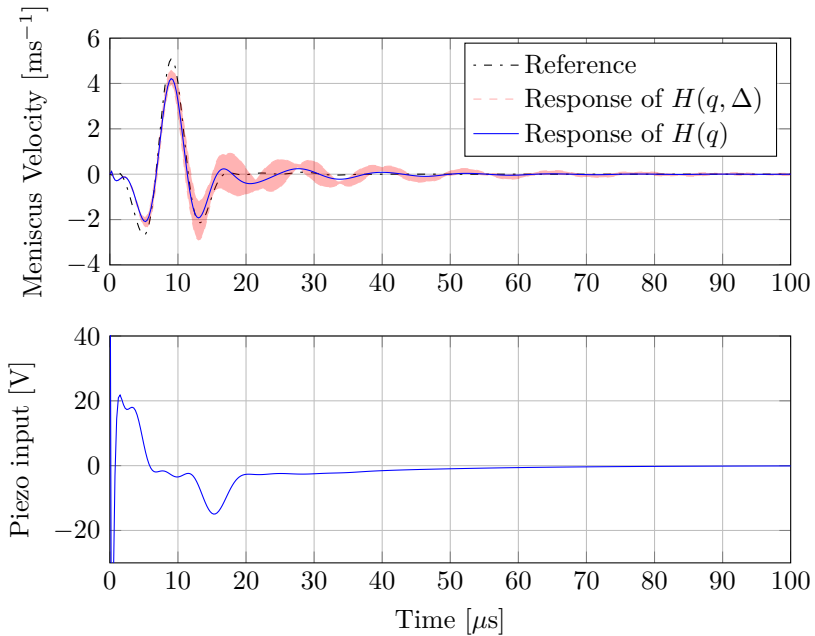


Figure 4.13: Simulation results with the robust pulse $u_{\text{robust2}}(k)$ obtained with Theorem 3.2.

Table 4.1: Comparison of the worst-case H_2 norm of the error dynamics $\nu(q, \Delta)$

	γ^{LB}	$\gamma_{\text{opt}}^{\text{UB}}$
Robust pulse $u_{\text{robust1}}(k)$ with Theorem 3.1	104.27	143.68
Robust pulse $u_{\text{robust2}}(k)$ with Theorem 3.2	52.21	70.82

and $u_{\text{robust2}}(k)$ is shown in Figures 4.12 and 4.13 respectively. For the nominal $H(q)$ system, it can be observed that the meniscus velocity with $u_{\text{robust2}}(k)$ follows the reference trajectory $y_{\text{ref}}(k)$ more closely compared to $u_{\text{robust1}}(k)$. The major difference is that the velocity-peak is tracked by $u_{\text{robust2}}(k)$ better than $u_{\text{robust1}}(k)$. Furthermore, for uncertain system $H(q, \Delta)$, the response of the meniscus velocity with $u_{\text{robust2}}(k)$ does not deviate much from its nominal response and remains close to $y_{\text{ref}}(k)$. This validates our approach to design the robust unconstrained actuation pulse based on less conservative LMI conditions with parameter dependent Lyapunov functions.

4.3 Experimental Results

The simulation results show that considerable improvements can be achieved by using the constrained and unconstrained pulses derived in the previous section. However, as only a constrained actuation pulse can be used in the current printhead, we have not used the unconstrained actuation pulse for the experiment. In this section we present experimental results obtained with the optimal constrained pulse $u_{\text{opt}}(k)$ and the robust constrained pulse $u_{\text{robust}}(k)$ (derived in Section 4.2.1) to observe the drop consistency.

4.3.1 Optimal Constrained Feedforward Control

Conventionally, the performance of a DoD inkjet printhead is analyzed by the DoD-curve, i.e. variation of the drop velocity against the increase in the DoD frequency. For a given DoD frequency, the drop velocity is classically measured for a continuous stable jetting (see Section 1.2.3). Thus, the transient information at the start of the jetting is lost. Even though it is ideally required to have the consistent drop velocity while jetting any bitmap, it is not possible to test several bitmaps to construct the performance metric. Therefore, we will extend the classical concept of the DoD curve to be a better instrument to analyze the drop consistency. For a given DoD frequency, we will jet 10 ink drops and measure the drop velocities of all drops to analyze the effect of transient behavior on the drop velocity. Thus, the DoD-curve obtained in this way will demonstrate the transient behavior in the continuous jetting at different DoD frequencies.

The details of the experimental setup is discussed in Appendix B. The experimental setup is equipped with a CCD camera which can capture the images at an interval of $10 \mu\text{s}$ of jetted drops. A single image shows the locations of jetted

drops with respect to the nozzle and the paper location at a fixed instant in time. Now, in each experiment we have jetted 10 ink drops from the inkjet channel at a fixed DoD frequency. Several images of the jetted drops, traveling towards the paper location, are collected after every $10\ \mu\text{s}$. All these images are then placed adjacent to each other in the order of the time instant when they are captured. The composite image constructed in this manner for a DoD frequency equal to 28 kHz is shown in Figure 4.14. This image shows the flight profile of the ten drops from the nozzle to the paper. The vertical axis represents the position of the ink drop. The starting position is the nozzle level and the paper is placed at the end position. The distance between the nozzle and the paper is approximately 2 mm.

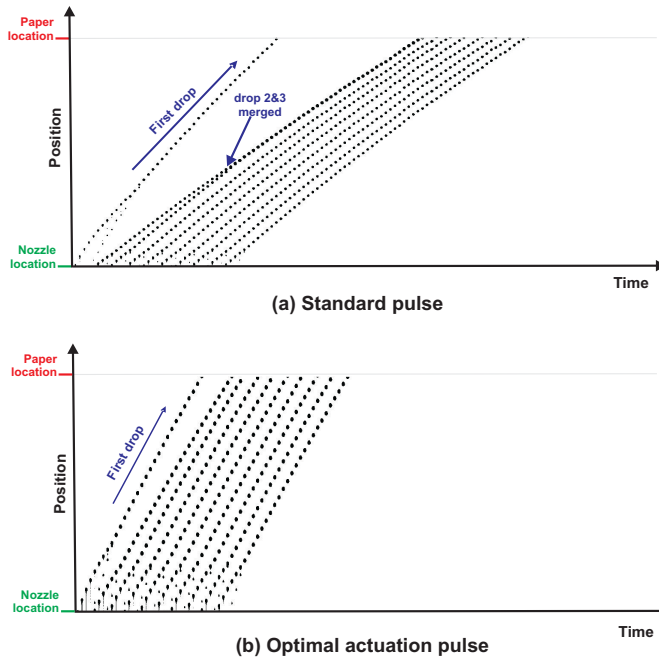


Figure 4.14: Experimental results: 10 drops jetted at DoD frequency 28kHz.

Ideally, it is required that the 10 drops are placed at an equal distance on the paper. In Figure 4.14, we compare the result obtained with the standard pulse (Figure 4.14a) and with the optimal pulse (Figure 4.14b) at a DoD frequency equal to 28 kHz. Figure 4.14a shows that, for the standard pulse, the first drop travels to the paper, but the second drop is slower than the first drop and gets merged in the third drop. Only nine drops reach the paper and the first drop is placed far away from the rest of the drops. However, for the optimal pulse, all the ten drops travel with almost the same velocity and they are placed at an equal distance on the paper.

The printhead performance degrades severely when the standard pulse is used at a DoD frequency of 46kHz as shown in Figure 4.15. Figure 4.15a shows that

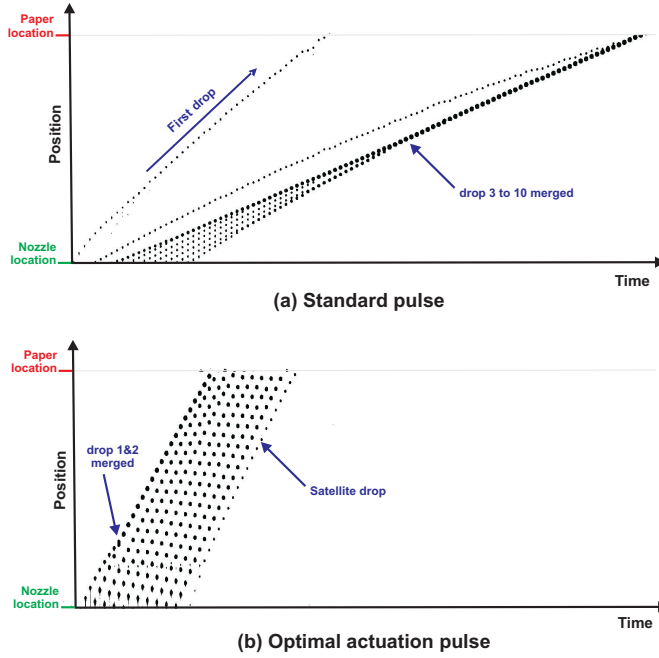


Figure 4.15: Experimental results: 10 drops jetted at DoD frequency 46kHz.

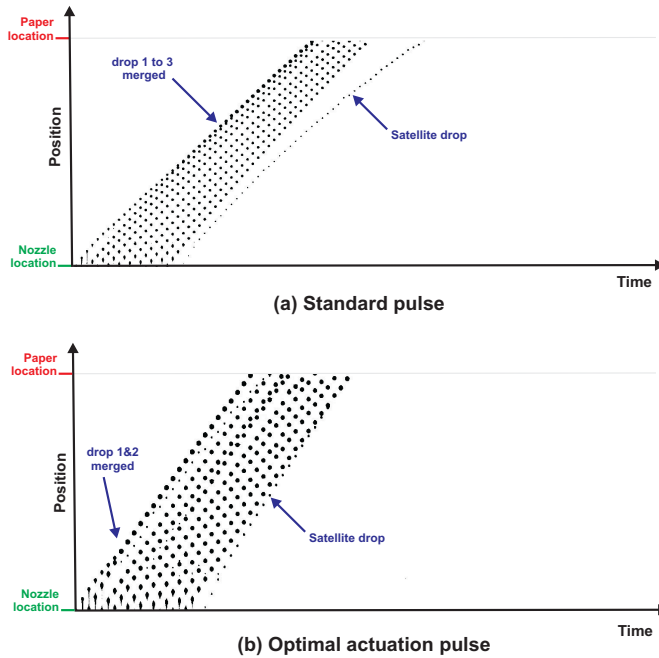


Figure 4.16: Experimental results: 10 drops jetted at DoD frequency 54kHz.

for the standard pulse, the first drop travels to the paper. However, the drops jetted subsequently have different velocities and they are slower than the first drop. Therefore, they get merged into a single drop before reaching the paper. Consequently, only two drops eventually reach the paper and they are placed far away from each other. For the optimal actuation pulse, all the jetted drops have almost the same velocity (see Figure 4.15b). Since they have similar velocities, the drops are placed at an equal distance on the paper. The first drop is however slower and hence caught by the second drop. A small satellite drop is also visible after the tenth drop.

Now let us consider the case of a DoD frequency equal to 54kHz (see Figure 4.16). In this case, as opposed to the previous cases, the first drop is slower than drops 2, 3 and 4 when the standard pulse is used (see Figure 4.16a). This has the consequence that the first four drops merge (just before reach the paper) and only seven drops reach the paper. With the optimal pulse, only the first two drops merge. Another advantage of the optimal actuation is that the drops, which do not merge, have similar velocities while these velocities are disparate with the standard pulse.

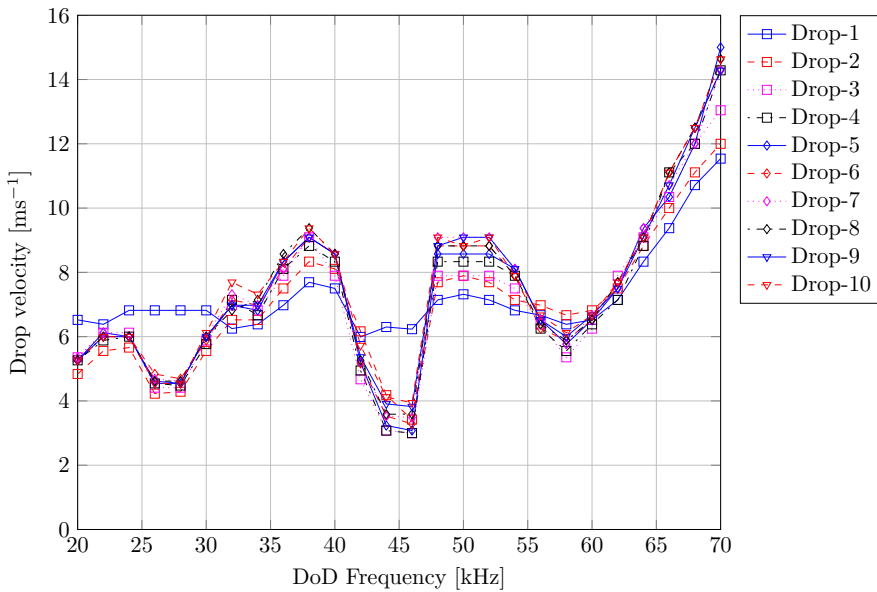


Figure 4.17: Experimental DoD curve with the standard pulse.

Besides the experiments at these three DoD frequencies, other experiments were carried out for different DoD frequencies ranging from 20 kHz to 70 kHz with the step of 2 kHz. The drop velocities of each of the 10 drops are shown in Figures 4.17 and 4.18 as a function of the DoD frequency (DoD curve). Figure 4.17 is obtained when the standard pulse is used and Figure 4.18 shows the results when the optimal pulse is used. As we will show in the sequel, these figures confirm the observations made for Figures 4.14-4.16. We evaluate the performance observed in these two

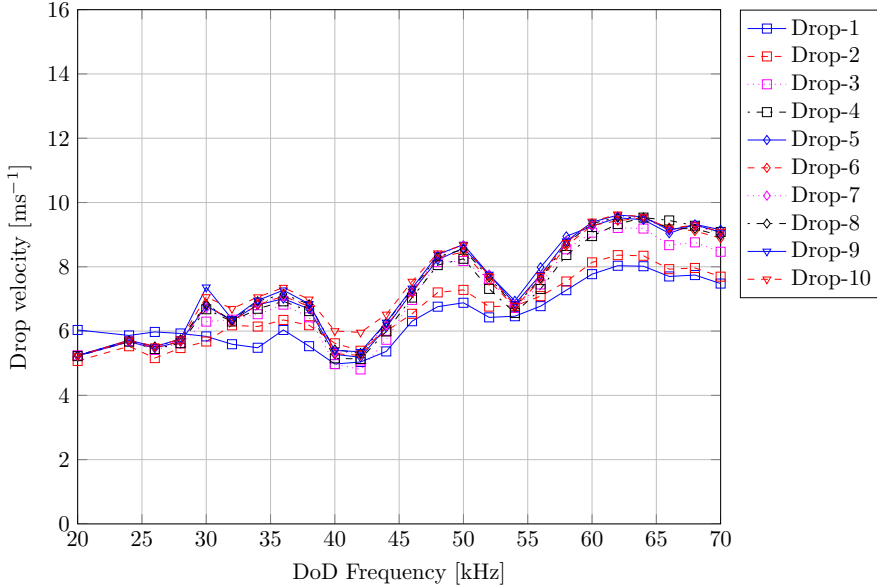


Figure 4.18: Experimental DoD curve with the optimal actuation pulse.

new figures based on three aspects. First, we compare the velocity variation of the tenth drop over the DoD frequency range. The velocity of the tenth drop for the standard pulse varies from 5.5 ms^{-1} to 14.5 ms^{-1} . For the optimal actuation pulse, this variation is considerably smaller: the velocity of the tenth drop varies from 5.5 ms^{-1} to 9.8 ms^{-1} . Second, at each DoD frequency we look at the velocities of the individual drops. It is very clear that at a fixed DoD frequency, the velocities of the ten drops are quite different for the standard pulse. On the other hand, individual drop velocities are very similar when the optimal pulse is applied to the inkjet printhead. Third, the behavior of the first drop is analyzed over the DoD frequency range. In Figure 4.17, we observe that, for the standard pulse, the first drop behaves very differently compared to the subsequent nine drops. This can severely affect the print quality, as it appears like a shadow of the printed bitmap to human eyes. When the optimal pulse is used, the difference between the first and the subsequent drops is much less significant. Hence, a bitmap printed with the optimal pulse will not suffer from the shadow effect. The overall improvement in the velocity consistency achieved using the optimal piezo actuation pulse has far-reaching consequences for the print quality. This is because the distance between the inkjet printhead and the printing paper which is relatively large (approximately 2 mm) and the relative speed between is the printhead carriage and the paper is around 1 ms^{-1} .

In the simulation results, we observe that the optimal pulse allows us to almost completely remove the residual oscillations. This should imply a flat DoD curve. However, even though we observe significant improvements, the DoD curve is not completely flattened when using the optimal pulse. This could be explained by

the changing dynamics of ink channel with the DoD frequency, as discussed in Section 2.4.1. The optimal constrained pulse does not take into account this DoD frequency dependency of the inkjet channel dynamics and this is the main reason the experimental DoD curve is not completely flat.

In the next section we present experimental results for the robust constrained pulse which uses information of the DoD dependency (i.e. the uncertainty on the nominal model).

4.3.2 Robust Constrained Feedforward Control

In this section, we present experimental results to show the improvements in the drop consistency with the robust actuation pulse $u_{\text{robust}}(k)$ presented in Section 4.2.1 (using the method discussed in Section 3.4.2). We have done similar experiments as mentioned in the previous section with the robust pulse $u_{\text{robust}}(k)$ and obtained the DoD-curve as shown in Figure 4.19. This DoD-curve is much flatter compared to the DoD curves shown in Figure 4.17 and Figure 4.18. Since the robust pulse $u_{\text{robust}}(k)$ is designed to give a good average performance over the set of models represented by $H(q, \Delta)$, it delivers better results than the optimal pulse. Now, the drop velocity variation is even less than 2 ms^{-1} .

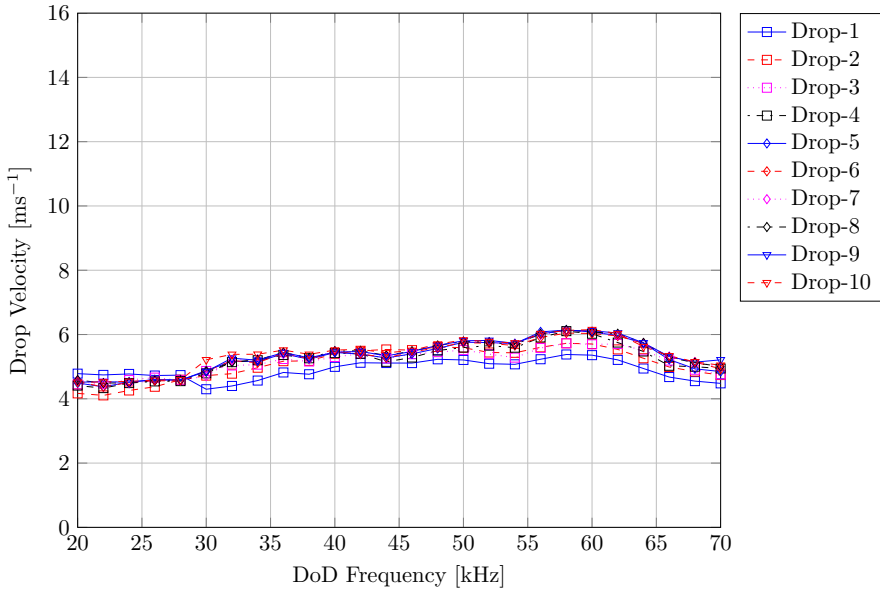


Figure 4.19: Experimental DoD curve with the robust pulse $u_{\text{robust}}(k)$.

Let us now focus on a single DoD frequency of 48 kHz and let us compare the performance of the three pulses (i.e., the standard pulse, the optimal pulse and the robust pulse) at that frequency. Consider for this purpose the flight profile of 10 drops jetted at that frequency. This flight profile, from the nozzle to the paper,

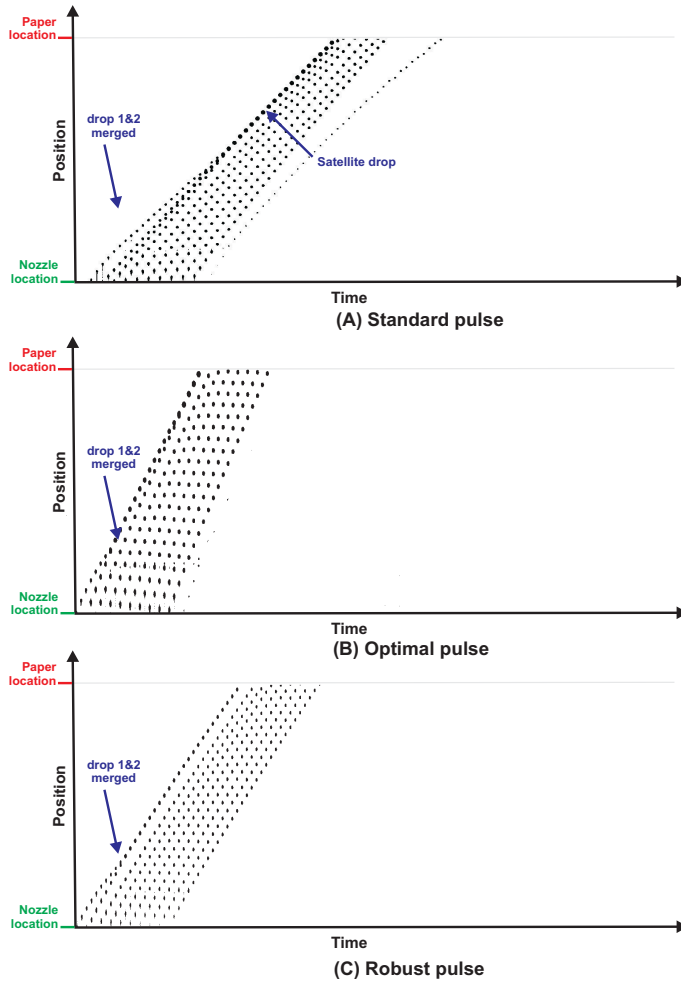


Figure 4.20: Experimental result: 10 drops jetted at DoD frequency 48 kHz.

is represented in Figure 4.20. The vertical axis represents the position of the ink drop. The starting position is the nozzle level and the paper is placed at the end position. The distance between the nozzle and the paper is approximately 2mm.

Ideally, it is required that the 10 drops should be placed at an equal distance on the paper. For the standard pulse (Figure 4.20.A), the first four drops are slower and they are merged together and finally, only seven drops reach the paper. Most of the jetted drops have different velocities. Also, a small and slower satellite drop is generated after the 10th drop. For the optimal pulse (Figure 4.20.B), the first two drops are slower and they are caught by the faster third drop. The remaining seven drops have similar velocities. The satellite drop generated after the 10th drop is faster and gets merged in 10th drop. With the robust pulse (Figure 4.20.C¹), except for the first two drops, the drop velocities of the remaining drops are very similar to each other. There is also no satellite drop generated after the 10th drop.

The proposed robust actuation pulse reduces the drop velocity variation to 2.0ms^{-1} compared to a drop velocity variation equal to 4.5ms^{-1} with the optimal constrained pulse (see Section 4.3.1). This reduction in the drop velocity variation can reduce the drop placement error by approximately 40% compared to the optimal constrained pulse (when the inkjet printhead to the printing paper distance is 2 mm and the relative speed between is the printhead carriage and the paper is around 1ms^{-1}).

Remark 4.2 *Note that the robust pulse (designed using uncertain ink channel dynamics) has reduced the drop velocity variation significantly but an upward slope in the drop velocity with increase in DoD frequency is visible in Figure 4.19. In the future, it is worth investigating the reasons for the inability of a single actuation pulse to completely flatten the DoD curve despite fairly capturing the refill dynamics in uncertain inkjet system model. Based on the physical model and the data-based model, we may relate this phenomenon to two factors related to the printhead geometry.*

The first one is the actuator used in the current printhead design. The length of the piezo actuator is very long and it is placed in the middle of the channel. This may pose restrictions in the profile of pressure wave which can be generated at the nozzle entrance. Thus, while jetting at different DoD frequencies, the average meniscus position at the moment of the drop formation cannot be controlled accurately with a single actuation pulse and the resulting drops have different properties. Indeed, it is shown in (Ezzeldin 2012) with experimental results that one has to use more than one actuation pulse to reduce the drop velocity variation to a very small value.

The second factor is the proximity of the fundamental resonant mode with the second resonant mode. Let us define the ratio of the second resonant mode frequency to the fundamental/jetting resonant mode frequency as the frequency separation ratio. As the frequency separation ratio reduces, the influence of the second acoustic mode on the meniscus behavior increases. In the current printhead design, the

¹Note that the ink drops with the robust pulse appear smaller compared to the standard pulse and the optimal pulse. The reason for this is that the setting for the image capture system is different for the robust pulse compared to other pulse.

second acoustic resonant mode is approximately twice of the primary jetting resonant mode (i.e. the frequency separation ratio is two) and its damping is very low compared to the primary jetting resonant mode. Thus, the second acoustic mode, significantly, influences the meniscus behavior and the drop formation process. This is evident from the shape of the quenching pulse needed to damp the residual oscillations.

The ability to generate a more complex pressure profile in order to control the meniscus behavior will not only provide tighter control on specific drop properties but it will also allow the users to modulate the drop sizes (to deliver high print quality or high productivity as per requirement). Note that one has to use separate actuation pulses for jetting droplet of different drop volume. In order to obtain actuation pulse for a specific drop volume, one should use the proposed robust feedforward control with the $y_{\text{ref}}(t)$ profile corresponding to the drop sizes.

4.4 Summary

In this chapter, we have presented simulation and experimental results to evaluate the improvement in the inkjet system performance with the constrained and the unconstrained pulses. Simulation with the constrained pulse show that the proposed method can very effectively damp the residual oscillations enabling the ink channel to jet ink drops at higher jetting frequencies. Experimental results with this pulse have demonstrated that considerable improvements in the ink drop consistency (maximum drop velocity variation 4.5 ms^{-1}) can be achieved compared to the standard pulse (maximum drop velocity variation 12 ms^{-1}). However, the DoD-curve is not completely flat. This is mainly due to the fact that the optimal pulse design does not take into account the DoD dependency of the inkjet system. The robust constrained pulse obtained by using the uncertain inkjet system $H(q, \Delta)$ (i.e. a good representation of changing inkjet system dynamics) overcomes this drawback. With the robust constrained pulse maximum drop velocity variation is reduced to 2 ms^{-1} . The simulation of the unconstrained optimal pulse shows that the trapezoidal pulse delivered by the optimization problem (3.3) seems the best compromise between performance and complexity for the printhead under consideration. It also indicates that the nonlinear optimization (3.3) yields an actuation pulse which is very close to the global optimum. The robust unconstrained pulses obtained by solving the LMI problems in Theorem 3.1 and Theorem 3.2 improve the worst-case H_2 norm of the tracking error. Especially, the use of parameter-dependent Lyapunov functions in Theorem 3.2 helps to reduce the conservatism in the estimation of the upper bound on the worst-case H_2 norm.

MIMO Feedforward Control of a DoD Inkjet Printhead

In Chapter 3, we have discussed various control methods to design actuation pulses for a single ink channel and in Chapter 4 we have evaluated their performance using simulation and experimental results. In Chapter 2, we have seen that apart from the residual oscillations within the ink channel, the cross-talk induced by the simultaneous actuation of neighboring channels can influence the drop properties. Thus, it is essential to consider the effect of the cross-talk during the design of actuation pulses. For this purpose, we can use the multi-input multi-output (MIMO) model of the inkjet printhead developed in Section 2.3. The actuation pulse design for several ink channels can be formulated as MIMO feedforward control problem. In this chapter we present a constrained MIMO feedforward controller which has lower implementation complexity. Furthermore, we develop an unconstrained MIMO feedforward controller which improves the printhead performance. Effectiveness of the proposed methods is demonstrated through simulation and experimental results.

5.1 Introduction

Generally, inkjet practitioners rely extensively on experimental tuning, see (Bogy and Talke 1984; Chung et al. 2005; MicroFab Technologies Inc. 1999; Gan et al. 2009; Dong et al. 2006; Kwon and Kim 2007; Kwon 2009a), to fine tune the printhead performance. This is due to insufficient knowledge of the geometry and the dynamics of the inkjet printhead. The designers of these printheads often use simple physical models to predict the system behavior. In Chapter 2, we have seen that it is not always possible to obtain a reasonably accurate physical model for an ink channel. Especially, physical modeling of a multi-input multi-output (MIMO) inkjet printhead, including the cross-talk effects, is a difficult and a time consuming task. In Section 2.3, we have constructed a MIMO model of the inkjet printhead

using identification SISO models with experimental data. In this chapter, we extend the methods proposed in Chapter 3 to handle the MIMO feedforward problem. This method will be useful for printhead designers to quickly design the actuation pulse for the MIMO inkjet printhead. Moreover, inkjet practitioners can first obtain a printhead model using the data-based modeling (see Section 2.3) and then can use the MIMO feedforward techniques, proposed in this chapter, to design the actuation pulses. Such a procedure will be very useful for inkjet practitioners as they can improve the system performance via an appropriate design of the actuation pulse without knowing the geometry of the printhead.

In order to improve the print quality, we focus on addressing the issues of residual oscillations and cross-talk using a systems and control approach. In Section 3.2, we have discussed in detail the limitations of the control hardware which allows one to use only feedforward control policies and presented an optimization-based technique to design the actuation pulse for the SISO case. In theory, it is possible to use any off-the-shelf feed-forward MIMO control method to obtain a good actuation pulse. In (Ezzeldin 2012), model predictive control is used to design unconstrained actuation signals for the ink channels. However, we are faced with a practical constraint. The driving electronics hardware of our printhead can only use trapezoidal pulses (see Section 3.2). To overcome this constraint, in Section 3.2 we have defined the actuation pulse so that it contains a positive trapezoidal pulse used for jetting a droplet and a negative trapezoidal pulse to damp the residual oscillations in an ink channel. Now, in order to reduce the cross-talk effect we apply the same actuation pulse to all the ink channels but introduce an actuation delay t_a between the actuation of the neighboring channels. This ensures that cross-talk is reduced as no two neighboring channels are excited at the same time. This is a good choice because it reduces the complexity of the implementation and hence, cheaper electronics hardware can be used. The actuation delay for a pre-specified number of neighboring channels and the actuation pulse parameters are obtained as a solution to an optimization problem. These optimized parameters guarantee a minimum performance over all the models in the uncertain inkjet system $G(q, \Delta)$, $\Delta \in \mathbf{\Delta}$. Furthermore, we investigate the possibilities to design unconstrained actuation pulses. In order to validate the proposed methodology, we use an experimental small-droplet printhead, developed by Océ Technologies. Simulation and experimental results are presented to show the usefulness of the proposed method.

In the next section we present the design of actuation pulses for the MIMO printhead dynamics obeying the pulse shape constrained discussed in Section 3.2.

5.2 Robust Constrained MIMO Feedforward Control

In order to design actuation pulses to compensate the cross-talk effect and the residual oscillations we need a MIMO model of the DoD inkjet printhead. Since we do not have a fairly accurate MIMO physical model (i.e. a model from the piezo inputs to the meniscus velocities of ink channels) we will use the MIMO model

from the piezo inputs to the piezo sensor outputs of ink channels obtained using the data-based modeling in Section 2.3. This model is constructed with two identified SISO models, the first one being the direct dynamics $G_d(q)$ of an ink channel and the second one the cross-talk dynamics $G_c(q)$ or the effect of the actuation of the immediate neighboring channel (see Figure 2.1). In Section 2.3.4, we have seen that the direct dynamics G_d depend on the DoD frequency and furthermore, in Section 2.4.2 we have represented the set of multiple models obtained for the direct dynamics at different DoD frequencies by $G_d(q, \Delta)$, i.e., the nominal model $G_d(q)$ with a compact uncertainty $\Delta \in \mathbf{\Delta}$. In Section 3.4.2, a method is presented which uses this uncertain ink channel dynamics $G_d(q, \Delta)$ to design a robust actuation pulse when a single channel is jetting (SISO case). This robust pulse ensures a minimum performance for all systems in the uncertainty $\mathbf{\Delta}$ rather than obtaining an optimal actuation pulse whose performance is only good for one single element of this set (see Section 3.4.1). In this section, we present the extension of this robust pulse design method to the MIMO case (Khalate et al. 2012) in order to minimize the effect of the residual oscillations and the cross-talk (i.e. when multiple channels are jetting).

Our goal is now to design an actuation pulse $u(k, \theta)$, with the pulse parametrization θ proposed in Figure 3.1, to damp the oscillations in an ink channel caused due to transient effects (i.e. the residual oscillations) and due to the cross-talk effect. We discussed in Section 2.1 that an ink channel is mainly influenced by the cross-talk from the immediate neighbors. One may think of using advanced control techniques to design complex actuation waveform to jet all ink channels simultaneously ensuring the drop consistency. However, this would lead to a complex implementation which may not be feasible due to electronic hardware limitations. Therefore, avoiding simultaneous actuation of immediate neighbors is a simple and an effective solution to minimize the cross-talk influence from the implementation point of view. A common practice in the printing industry is to delay the actuation of immediate neighbors by time t_a . The actuation delay t_a is generally obtained through trial and error. Here we propose to optimize the value of t_a using the identified model.

Now, we club all the even number of ink channels as one group and all the odd number of ink channels as another group. We apply $u(k, \theta)$ to both even and odd channels, but the actuation of even channels is delayed by time t_a (μs). Thus, the piezo sensor output of even channels (except for the 128th channel) is given as follows

$$\begin{aligned} y_n(k, \Delta, t_a, \theta) &= G_d(q, \Delta)u_n(k - t_a, \theta) \\ &+ G_c(q)u_{n-1}(k, \theta) + G_c(q)u_{n+1}(k, \theta), \\ n &= 2, 4, \dots, 126, \Delta \in \mathbf{\Delta}. \end{aligned} \quad (5.1)$$

The piezo sensor output of the odd channels (except for the 1st channel) is given as follows:

$$\begin{aligned} y_{n+1}(k, \Delta, t_a, \theta) &= G_d(q, \Delta)u_{n+1}(k, \theta) \\ &+ G_c(q)u_n(k - t_a, \theta) + G_c(q)u_{n+2}(k - t_a, \theta), \end{aligned}$$

$$n = 2, 4, \dots, 126, \Delta \in \mathbf{\Delta}. \quad (5.2)$$

For the first and the last channel, only one neighbor will contribute to the cross-talk.

As discussed in Section 3.4.2, the dimension of the parameter space of $\mathbf{\Delta}$ is only two and hence, we can easily grid the parametric uncertainty $\mathbf{\Delta}$. Recall that the set \mathcal{S} represents the grid on the parametric uncertainty $\mathbf{\Delta}$, defined by (3.5)

$$\mathcal{S} = \{\Delta^i, i = 1, \dots, m, \mid \Delta^i \in \mathbf{\Delta}\}$$

In order to minimize the residual oscillations and the cross-talk and achieve drop consistency it is important that the piezo sensor signals should follow the reference signal closely. Similar to Section 3.4.2, for a given parameter vector θ and the actuation delay t_a , we define the performance index $\mathcal{J}(t_a, \theta)$, for even and odd channels, as the worst-case sum of squared error computed at each of the m grid elements, i.e.:

$$\begin{aligned} \text{for even channel: } \mathcal{J}_e(t_a, \theta) &= \max_{\Delta^i \in \mathcal{S}} \sum_{k=0}^N w_e(k) \left(y_{\text{ref}}(k - t_a) - y_n(k, \Delta^i, t_a, \theta) \right)^2, \\ \text{for odd channel: } \mathcal{J}_o(t_a, \theta) &= \max_{\Delta^i \in \mathcal{S}} \sum_{k=0}^N w_o(k) \left(y_{\text{ref}}(k) - y_n(k, \Delta^i, t_a, \theta) \right)^2, \end{aligned} \quad (5.3)$$

where $N = \frac{T}{T_s}$, T_s is the sampling time chosen equal to $0.1 \mu\text{s}$, T is chosen equal to $100 \mu\text{s}$. The reference trajectory $y_{\text{ref}}(k)$ for the piezo sensor signal is designed using the approach discussed in Section 3.3. The time-domain weighting filter for even and odd channels are $w_e(k)$ and $w_o(k)$ respectively. For control purposes, we have changed the sampling time of the identified models in Section 2.3 from $1.6 \mu\text{s}$ to $0.1 \mu\text{s}$ using MATLAB command `d2d`.

Note that since the input for the even channel $u_n(k - t_a, \theta)$ is delayed by t_a , if we do not delay y_{ref} then the value of \mathcal{J}_e will increase largely. Therefore, in (5.3) y_{ref} for the even channel is also delayed by t_a .

Now, depending on whether the neighboring channels are actuated or not, we have four scenarios for an even channel given in Table 5.1 and similarly for an odd channel given in Table 5.2. Note that ‘1’ indicates jetting with actuation pulse $u(k, \theta)$ and ‘0’ indicates non-jetting, i.e. actuation pulse is not applied or $u(k) = 0$. For the i -th case, the performance index $\mathcal{J}_e(t_a, \theta)$ evaluated as described in (5.3) is denoted as $\mathcal{J}_{e,i}(t_a, \theta)$, $i = 1, \dots, 4$.

Table 5.1: Jetting pattern for even channels

	u_{n-1}	u_{n+1}	$\mathcal{J}_e(t_a, \theta)$
Case-1	0	0	$\mathcal{J}_{e,1}(t_a, \theta)$
Case-2	0	1	$\mathcal{J}_{e,2}(t_a, \theta)$
Case-3	1	0	$\mathcal{J}_{e,3}(t_a, \theta)$
Case-4	1	1	$\mathcal{J}_{e,4}(t_a, \theta)$

Table 5.2: Jetting pattern for odd channels

	u_n	u_{n+2}	$\mathcal{J}_o(t_a, \theta)$
Case-1	0	0	$\mathcal{J}_{o,1}(t_a, \theta)$
Case-2	0	1	$\mathcal{J}_{o,2}(t_a, \theta)$
Case-3	1	0	$\mathcal{J}_{o,3}(t_a, \theta)$
Case-4	1	1	$\mathcal{J}_{o,4}(t_a, \theta)$

One can observe that Case-1 represents the SISO case wherein we have to damp the oscillations caused solely by the transients in the ink channel (or the residual oscillations). The remaining cases involve both the residual oscillations and the cross-talk. Note that in (5.2)-(5.1) the cross-talk effect from the left and the right neighbor is modeled by the same transfer function $G_c(q)$. Hence, Case-2 and Case-3 are effectively the same. Based on (5.2) and (5.1) we can also conclude that the Case-4 is the worst-case as the cross-talk disturbance is maximum in this case. Particularization of (5.3) to the cases in Table 5.1 and 5.2 is constituted as follows:

$$\begin{aligned}
\mathcal{J}_1(t_a, \theta) &= \mathcal{J}_{e,1}(t_a, \theta) = \mathcal{J}_{o,1}(t_a, \theta), \\
\mathcal{J}_2(t_a, \theta) &= \max\left(\mathcal{J}_{e,2}(t_a, \theta), \mathcal{J}_{o,2}(t_a, \theta)\right), \\
\mathcal{J}_4(t_a, \theta) &= \max\left(\mathcal{J}_{e,4}(t_a, \theta), \mathcal{J}_{o,4}(t_a, \theta)\right).
\end{aligned} \tag{5.4}$$

It is clear that $\mathcal{J}_1(t_a, \theta)$ represents the worst-case the SISO case and $\mathcal{J}_4(t_a, \theta)$ is the worst-case for the MIMO case. Considering the fact that we need a single actuation pulse which should perform well for both the SISO and the MIMO case, using only $\mathcal{J}_4(t_a, \theta)$ for optimization may lead to a pulse which may not perform fairly good for the SISO case. Therefore, we propose to optimize t_a and θ as solution of the following multi-objective optimization problem:

$$\begin{aligned}
&\min_{t_a, \theta} \mathcal{J}(t_a, \theta) && (5.5) \\
&\text{subject to } 0 \leq t_a \leq t_a^{\text{UB}} \quad \text{and} \quad \theta_{\text{LB}} \leq \theta \leq \theta_{\text{UB}},
\end{aligned}$$

where $\mathcal{J}(t_a, \theta) = \lambda \mathcal{J}_1(t_a, \theta) + (1 - \lambda) \mathcal{J}_4(t_a, \theta)$, $\lambda \in [0, 1]$ is the user defined weighting, t_a^{UB} is the upper bound on the actuation delay and θ_{LB} and θ_{UB} are the vectors containing the lower and the upper bounds on each element of the parameter vector θ .

Similar to (3.7), this is a constrained nonlinear optimization problem and can be solved off-line using standard algorithms. We use the MATLAB function `fmincon`. This function implements a range of optimization techniques. In our experiments we used the default option which is sequential quadratic programming. The value of the upper bound on the actuation delay t_a^{UB} depends on the print quality requirement for a given application, we have chosen it equal to $10 \mu\text{s}$.

In the next section we present a method to design unconstrained actuation

pulses to minimize the residual oscillations and the cross-talk.

5.3 Unconstrained MIMO Feedforward Control

In Section 3.5, we have seen that with the rapid developments in electronics it may be possible in future to use unconstrained actuation pulses to improve the inkjet performance. Subsequently, in Section 3.5.1 we have developed a simple method to construct unconstrained actuation pulse for an ink channel using the nominal model of the system. In the next section we present an extension of this method to handle the MIMO feedforward control problem.

5.3.1 Optimal Unconstrained MIMO Feedforward Control

It is important to have a simpler method to design unconstrained actuation pulses to tackle the residual oscillations and the cross-talk. Note that for simplicity we will here not consider the uncertainty on the direct dynamics G_d and we will just extend the filter-based approach to design an unconstrained actuation pulse for a single ink channel of Section 3.5.1.

Contrary to the constrained MIMO feedforward control discussed in Section 5.2, the improved printhead electronics would certainly allow the use of a different pulse for even and odd channels. Moreover, it would be also possible to use different actuation pulses for each case in Table 5.2 and 5.2 (instead of one pulse for all the cases as in Section 5.2). Here, we present the methodology for Case-4 (the other cases can be determined similarly).

Let $u_e(k) = u_n(k)$ and $u_o(k) = u_{n+1}(k)$ be the actuation pulses for even and odd ink channels respectively with $n = 2, 4, \dots, 126$.

Now, for Case-4, we can write the sensor outputs of even and odd channels in the following compact representation using (5.1) and (5.2)

$$\begin{bmatrix} y_e(k) \\ y_o(k) \end{bmatrix} = \begin{bmatrix} G_d(q) & 2G_c(q) \\ 2G_c(q) & G_d(q) \end{bmatrix} \begin{bmatrix} u_e(k) \\ u_o(k) \end{bmatrix} \quad (5.6)$$

Similar to Section 3.5.1, we parameterize the to-be-designed actuation pulses as the pulse response of a finite impulse response(FIR) filter:

$$\begin{bmatrix} u_e(k, \beta^e) \\ u_o(k, \beta^o) \end{bmatrix} = \begin{bmatrix} F(q, \beta^e) \\ F(q, \beta^o) \end{bmatrix} \delta(k) \quad (5.7)$$

where $F(q, \beta) = \beta_0 + \beta_1 q^{-1} + \dots + \beta_{n_\beta} q^{-n_\beta}$, $\beta^e = [\beta_0^e, \dots, \beta_{n_\beta}^e]^T$ and $\beta^o = [\beta_0^o, \dots, \beta_{n_\beta}^o]^T$ are vectors containing the coefficients of the FIR filter and $\delta(k)$ is the unit pulse. When the dimensions of β^e and β^o are chosen equal to the desired length of the actuation pulse, this parametrization allows to generate actuation pulses of arbitrary shapes.

For an arbitrary vector β^e and β^o , the responses of the even and odd ink channel to the input $u(k, \beta^e)$ and $u(k, \beta^o)$ are given by

$$\begin{aligned} \begin{bmatrix} y_e(k, \beta^e, \beta^o) \\ y_o(k, \beta^e, \beta^o) \end{bmatrix} &= \begin{bmatrix} G_d(q) & 2G_c(q) \\ 2G_c(q) & G_d(q) \end{bmatrix} \begin{bmatrix} F(q, \beta^e) \\ F(q, \beta^o) \end{bmatrix} \delta(k) \\ \begin{bmatrix} y_e(k, \beta^e, \beta^o) \\ y_o(k, \beta^e, \beta^o) \end{bmatrix} &= \begin{bmatrix} F(q, \beta^e)g_d(k) + 2F(q, \beta^o)g_c(k) \\ 2F(q, \beta^e)g_c(k) + F(q, \beta^o)g_d(k) \end{bmatrix} \end{aligned} \quad (5.8)$$

where $g_d(k)$ and $g_c(k)$ are the pulse responses of the known direct dynamics $G_d(q)$ and cross-talk dynamics $G_c(q)$.

The optimal actuation pulses $u_e(k, \beta_{\text{opt}}^e)$ and $u_o(k, \beta_{\text{opt}}^o)$ are then the ones which minimize the difference between the desired sensor signal $y_{\text{ref}}(k)$ and the actual sensor signal $y(k, \beta)$. In order to get better performance we can use the additional freedom to delay y_{ref} of the even channel by time t_a with respect to y_{ref} of the odd channel. Therefore, the optimal delay t_a^{opt} and the optimal parameter vectors β_{opt}^e and β_{opt}^o are the solution of the following optimization problem :

$$\begin{aligned} \min_{t_a, \beta^e, \beta^o} \sum_{k=0}^N W(k) \|Y_{\text{ref}}(k, t_a) - Y(k, \beta^e, \beta^o)\|_2^2 \quad (5.9) \\ \text{subject to} \quad 0 \leq t_a \leq t_a^{\text{UB}} \end{aligned}$$

where $Y(k, \beta^e, \beta^o) = [y_e(k, \beta^e, \beta^o) \ y_o(k, \beta^e, \beta^o)]^T$, $Y_{\text{ref}}(k, t_a) = [y_{\text{ref}}(k-t_a) \ y_{\text{ref}}(k)]^T$, $W(k) = [w_e(k) \ w_o(k)]^T$ and t_a^{UB} is the upper bound on the actuation delay.

The above problem (5.9) leading to the unconstrained actuation pulse is a nonlinear optimization problem similar to (5.5). However, for a given actuation delay t_a the optimization problem (5.9) leading to the unconstrained actuation pulse will reduce to a linear least-squares problem and thus, can be solved easily. One can then do a line search to obtain the optimal delay t_a . Note that the optimization problem (5.9) uses the nominal model of the direct dynamics and leads to an optimal actuation pulse. Readers interested in the design of robust unconstrained actuation pulse can use the method presented in Section 3.5.2.

5.4 Simulation results

In the previous sections, we have presented design methods for the constrained and the unconstrained MIMO feedforward control of a DoD inkjet printhead. In this section, simulation results are presented to evaluate their effectiveness. We first consider the constrained feedforward control wherein the actuation pulse is constrained to have the trapezoidal shape of Figure 3.1. We solved the nonlinear optimization problem (5.5) with $\lambda = 0.8$ delivering the robust trapezoidal pulse (based on the piezo sensor model $G(q, \Delta)$) and the robust actuation delay using the `fmincon` function of the MATLAB's optimization toolbox. The robust actuation delay t_a^{rob} obtained by solving the optimization problem (5.5) is equal to $7.93 \mu\text{s}$

and the robust parameter vector θ_{rob} is given as follows

$$\theta_{\text{rob}} = [1.50 \ 3.00 \ 1.50 \ 24.06 \ 6.23 \ 3.18 \ 0.76 \ 3.17 \ -11.87]^T.$$

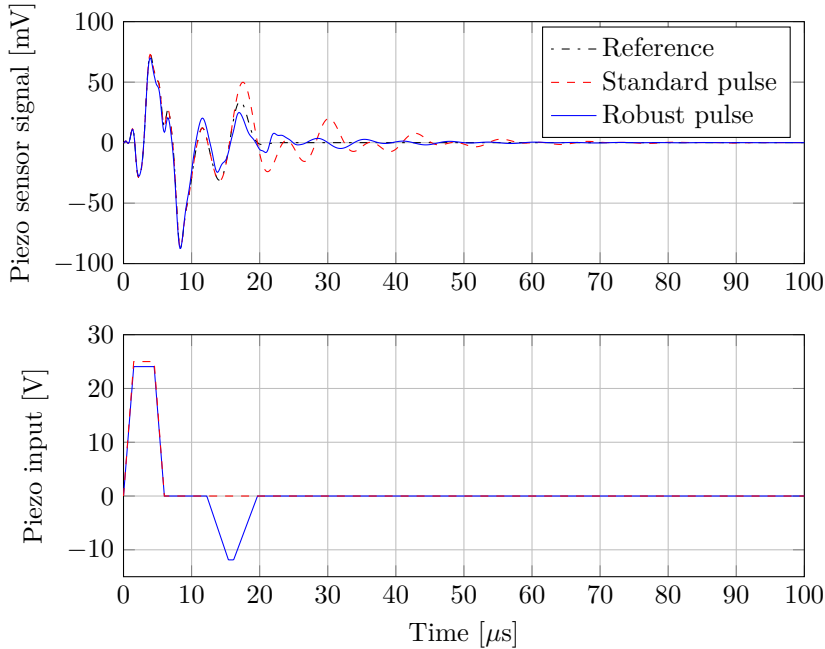


Figure 5.1: Response of the sensor signal to the standard $u_{\text{std}}(k)$ and the optimal actuation pulse $u_{\text{rob}}(k)$.

In order to see the improvement with the proposed method we compare its results with the standard pulse which we designed with only the knowledge about the first resonant mode. In Figure 5.1 we compare the standard pulse $u_{\text{std}}(k)$ and the robust pulse $u_{\text{rob}}(k) = u(k, \theta_{\text{rob}})$. At the top of Figure 5.1, we compare the piezo sensor signals generated by the nominal direct dynamics $G_d(q)$ in response to the robust pulse and the standard pulse. As expected, we observe at the top of Figure 5.1 that the robust pulse $u_{\text{rob}}(k)$ is more effective in damping the residual oscillations. This enables the sensor signal to track the reference trajectory very closely and thus brings the ink channel to rest soon after jetting the ink drop.

Prior to discuss the results with the proposed unconstrained pulse, we first analyze the conventional use of the standard pulse with no compensation for the cross-talk. In Figure 5.2 we show the simulation of Case-4 (see Tables 5.2 and 5.2) with the standard pulse, in which the two immediate neighbors of an ink channel are jetting. It is clear that due to the residual oscillations and the cross-talk effect, the piezo sensor signals do not track the reference signal nicely.

In Figure 5.3, we show the simulation of Case-4 (see Table 5.2 and 5.2) with $u_{\text{rob}}(k)$ and t_a^{rob} . Here, it can be observed that the actuation of the even channel

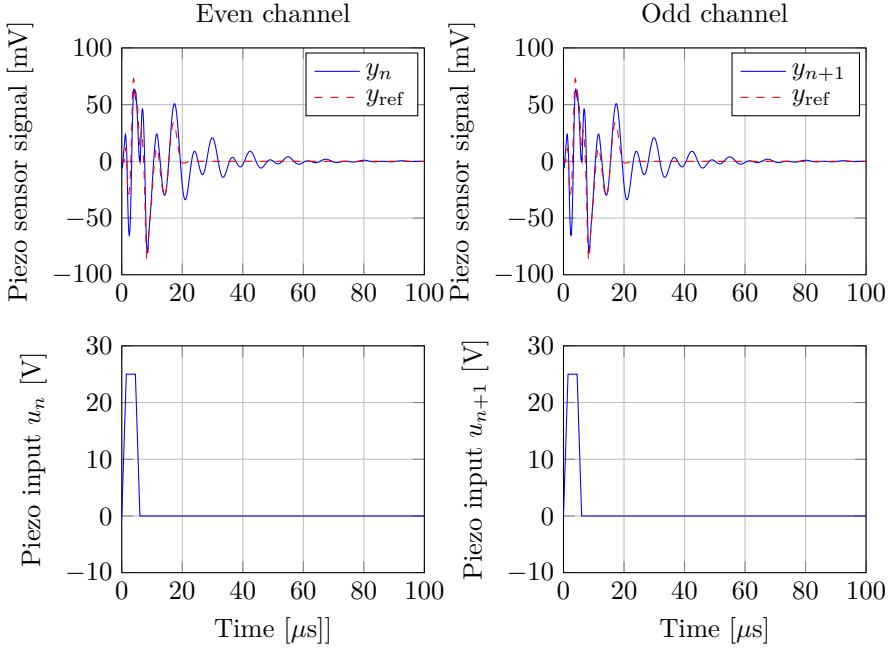


Figure 5.2: Response of the even and the odd channel to the standard pulse for Case-4.

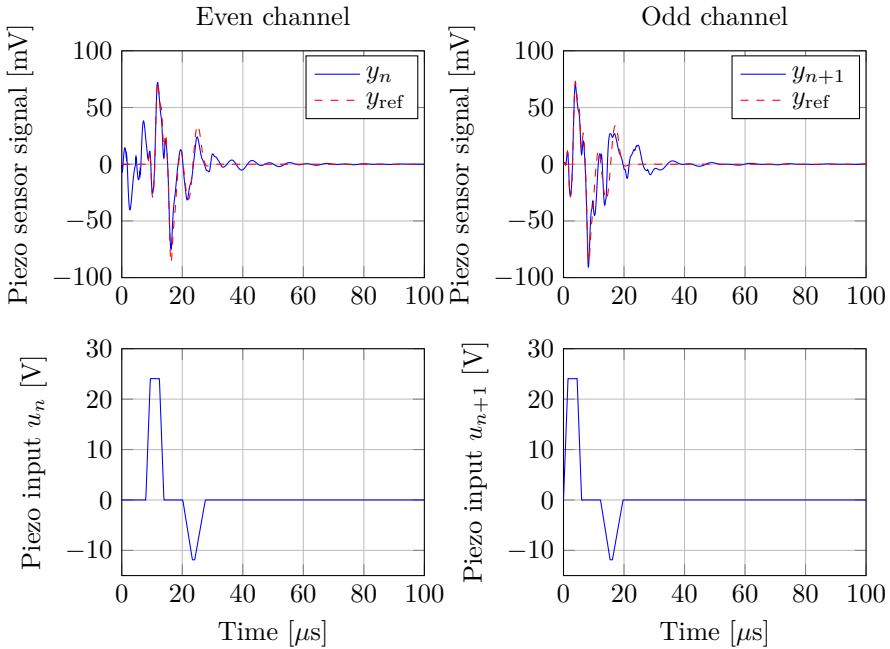


Figure 5.3: Response of the even and the odd channel to the robust constrained MIMO feedforward control for Case-4.

$u_n(k)$ is delayed by t_a^{rob} compared to the actuation of odd channel $u_{n+1}(k)$. This helps to minimize effect of the cross-talk and allows the sensor signal to follow the reference signal closely.

In Figure 5.3, we observe that the constrained MIMO feedforward control considerably reduces the residual oscillations and the cross-talk. For robust constrained MIMO feedforward control, the performance index $\mathcal{J}_4(t_a^{\text{rob}}, \theta_{\text{rob}})$ is 4.254×10^4 whereas for the standard pulse, the performance index $\mathcal{J}_4(0, \theta_{\text{std}})$ is 8.075×10^4 . By considering the unconstrained approach in Section 5.3.1, we will see whether an even better performance could be achieved with unconstrained MIMO feedforward control. For this purpose, we have solved the problem (5.9) with a FIR filter $[F(q, \beta^e) \ F(q, \beta^o)]^T$, where the length of the vectors β^e and β^o is chosen to be equal to 930. The optimal actuation delay t_a^{opt} obtained after solving (5.9) is $6.6 \mu\text{s}$. The optimal unconstrained pulses obtained by solving (5.9) may contain high frequency signals and sudden transients due to numerical problems. Therefore, these pulses are filtered through a anti-causal second order low-pass filter with a cutoff frequency of 500kHz. We have used the MATLAB function `filtfilt` for this purpose. The resulting actuation pulses are presented in Figure 5.4. In this figure, we show the simulation of Case-4 (see Table 5.2 and 5.2) with these optimal unconstrained pulses. Note that the reference sensor signal for even channels is delayed by t_a^{rob} . Comparing Figure 5.3 and Figure 5.4, we can see that for the nominal case (i.e. when uncertainty in the inkjet system is neglected) unconstrained feedforward control can provide a better tracking compared to robust constrained MIMO feedforward control as expected. For the unconstrained pulse, the performance index $\mathcal{J}_4(t_a^{\text{rob}}, \beta^e, \beta^o)$ is 2.200×10^4 . As mentioned in Section 5.3, readers are recommended to use the method presented in Section 3.5.2 to design the robust unconstrained actuation pulse in the presence of uncertainty in the inkjet system.

5.5 Experimental results

The simulation results show that improvements can be achieved by using robust constrained MIMO feedforward control. In this section, we present experimental results to show the improvements in the drop consistency with the proposed approach. As the printhead under consideration can only generate trapezoidal actuation pulses, we will not present experimental results with the unconstrained actuation pulses of Figure 5.4. As discussed in Section 4.3 the experimental setup is equipped with a CCD camera which can capture the images of jetted drops at an interval of $10 \mu\text{s}$.

We first present the results with the robust pulse for Case-1 (the SISO case) to see the effectiveness of $u_{\text{rob}}(k)$ to damp the residual oscillations in a single ink channel. Similarly as in Section 4.3, in each experiment we have jetted 10 ink drops from an ink channel at a fixed DoD frequency. We have done several such experiments for different DoD frequencies ranging from 20 kHz to 70 kHz, with a step of 2 kHz. The drop velocities of each of the 10 drops are shown in Figure 5.5 as a function of the DoD frequency (DoD curve). We observe that the robust pulse almost flattens the DoD-curve, as desired. The drop velocity variation with the

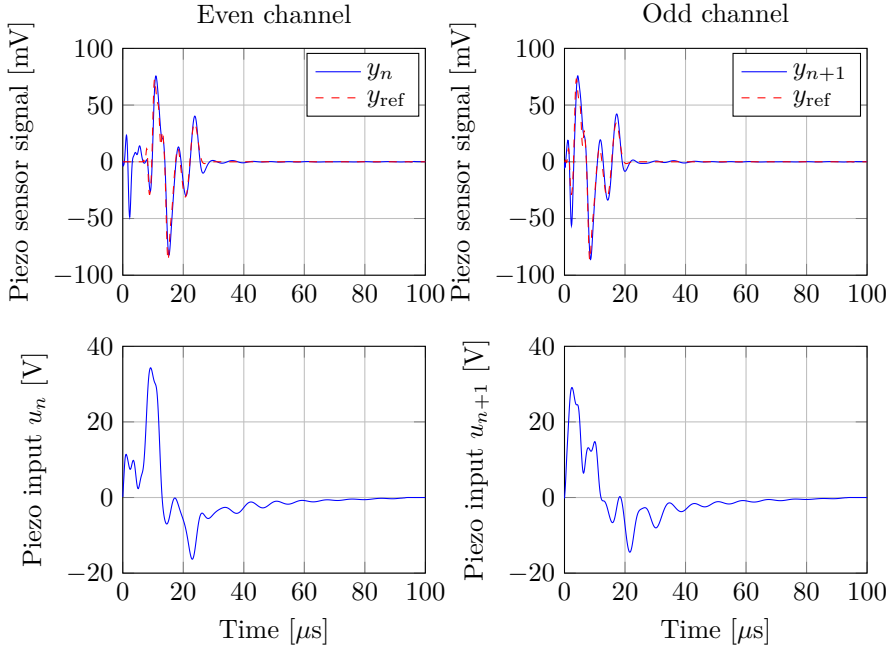


Figure 5.4: Response of the even and the odd channel to the optimal pulse generated through unconstrained feedforward control for Case-4.

robust pulse proposed in this paper is 2.5 ms^{-1} where as the drop velocity variation for the robust pulse in Section 4.3.2 is 2 ms^{-1} . This performance with the robust pulse based on identified models is not only significantly better compared to the standard pulse (see Section 4.3.1) ,but it is also fairly comparable to the robust pulse designed with a physical model, see Section 4.3.2. This indicates that, with the proposed method, practitioners can achieve a similar performance than when using a physical model of the printhead.

Now, we present the experimental results to prove the efficacy of the proposed method to minimize the cross-talk effect. One can analyze the influence of the cross-talk on the drop velocities with a DoD curve obtained by the procedure mentioned above. However, plotting drop velocities of all 10 drops, with and without cross-talk, as a function of DoD frequencies, may be difficult to read. Therefore, we only analyze the influence of the cross-talk on the ink drop velocity of a continuous jetting process at different DoD frequencies (similar to conventional DoD-curve discussed in Section 1.2.3). It means several thousands drops are jetted at a given DoD frequency before measuring the drop velocity. Due to the limitations of the experimental setup we cannot measure the DoD-curve for a continuous jetting sequence when the DoD frequency exceeds 51 kHz. Therefore, we have obtained the DoD-curve for the DoD frequency range of 10 kHz to 50 kHz. Figures 5.6 and 5.7 show such type of DoD-curve of the even channel, no. 66, and the neighboring odd channel, no. 67 obtained for Case-4 (see Section 5.2) with the robust pulse u_{rob} , shown in Figure 5.3. In Figure 5.5, we can see that the drop velocities for the first

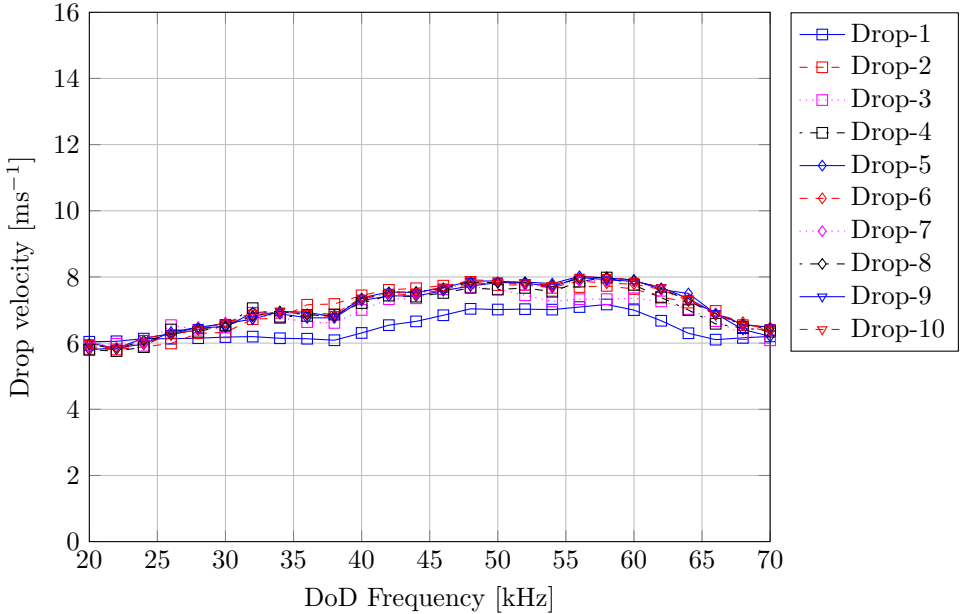


Figure 5.5: Experimental DoD curve with the robust pulse $u_{\text{robust}}(k)$.

few drops are different from the rest of drops due to the transient effects. This transient effect decays after jetting of the first few drops and hence, it does not influence the measured drop velocity with continuous jetting. Therefore, the DoD-curves in Figures 5.6-5.7 (obtained by a continuous jetting) for the no-cross-talk case are not exactly similar to Figure 5.5. Note that the drop velocity of the 10th drop should be close to the drop velocity with continuous jetting. Comparing the DoD-curve of the 10th drop in Figure 5.5 with the DoD-curves for the no cross-talk case in Figures 5.6-5.7 we can see a close match.

From Figures 5.6 and 5.7, it can be seen that when immediate neighbors are actuated simultaneously ($t_a = 0$), the maximum deviation in the drop velocity of the even channel over the DoD frequency range is almost 0.80 ms^{-1} due to the cross-talk effect. Whereas, the maximum deviation in the drop velocity of the odd channel is almost 0.83 ms^{-1} . Once we introduce the robust delay t_a^{rob} , as discussed in Section 5.2, the cross-talk effect is minimized. It can be observed in Figures 5.6 and 5.7 that the drop velocities of the even and odd channels are almost brought back to the drop velocities without the cross-talk. This shows that the proposed method is effective in minimizing the cross-talk effect.

In order to get a realistic insight about the performance improvements with the constrained MIMO feedforward control we jetted the sample bitmap pattern shown in Figure 5.8. Figure 5.9 shows the image captured by the CCD camera when the bitmap pattern is jetted with the standard pulse without the actuation delay (which is the initial step of actuation pulse design). For each nozzle, it can be seen that except for the first two drops, the remaining drops are very slow and get

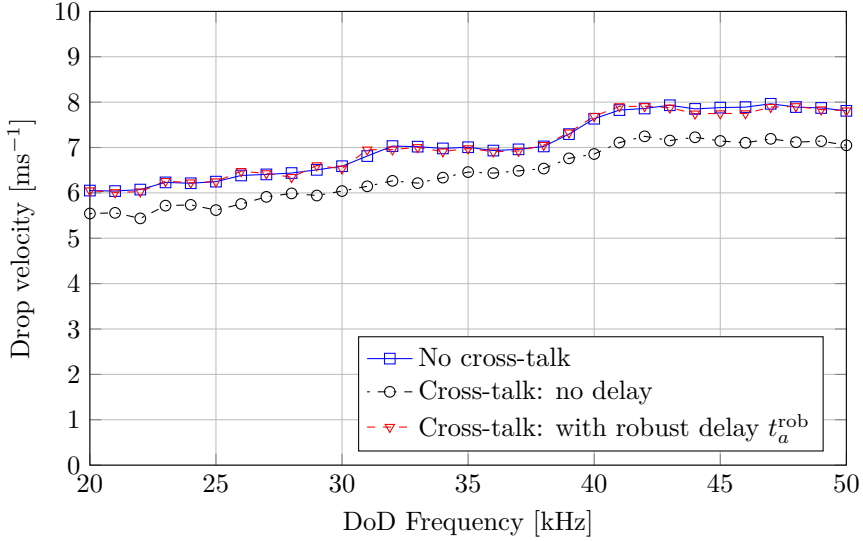


Figure 5.6: DoD curve for an even channel with the robust pulse $u_{\text{rob}}(k)$.

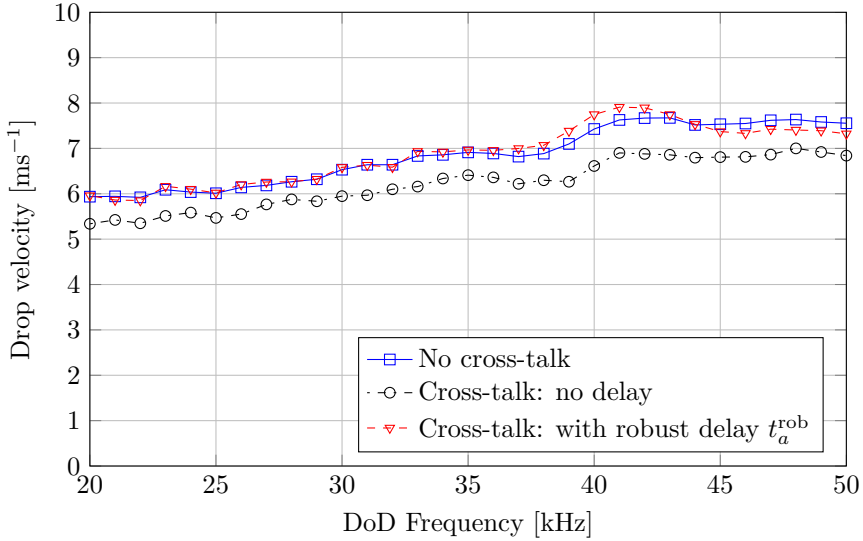


Figure 5.7: DoD curve for an odd channel with the robust pulse $u_{\text{rob}}(k)$.

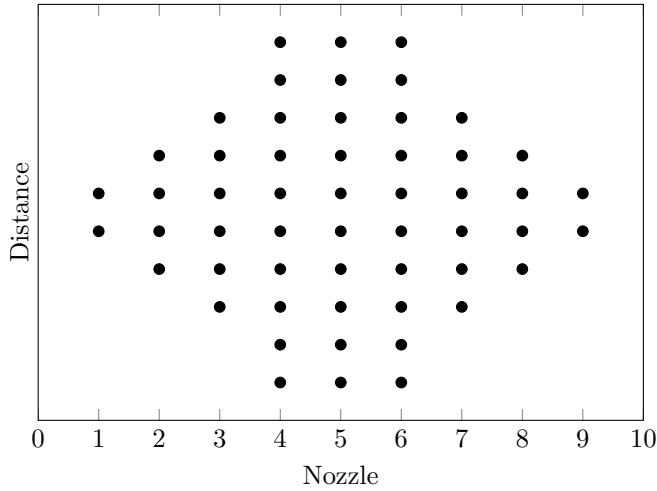


Figure 5.8: Bitmap to be printed.

merged into each other. This has distorted the jetted bitmap pattern considerably. Figure 5.10 shows the image captured by the CCD camera of the bitmap pattern jetted by the robust pulse $u_{\text{rob}}(k)$ with the robust actuation delay t_a^{rob} . It can be seen that except for the slower first drop, which is caught by the faster second drop, the remaining drops travel with similar velocities. The satellite drops observed in this figure are slower compared to the last drops but their volume is small compared to the satellite drops with the standard pulse and thus their influence on the print quality is negligible. As we have measured drop velocities in Figure 5.5, we can measure the drop velocities in the jetted pattern. Figures 5.11 and 5.12 shows the drop velocities of all drops corresponding to each nozzle when the bitmap pattern is jetted. Figure 5.11 is obtained with the standard pulse and Figure 5.12 with robust constrained MIMO control. For the standard pulse, it is observed that the average drop velocity variation is 38% (i.e. the average drop velocity for all nozzles is 4.9 ms^{-1} compared to the nominal drop velocity of 8 ms^{-1} at the DoD frequency of 50 kHz.). The robust MIMO feedforward control has improved the drop consistency and, now, the average drop velocity variation is reduced to 10% (i.e. the average drop velocity of all nozzles is 7 ms^{-1} compared to the nominal drop velocity of 7.8 ms^{-1} at the DoD frequency of 50 kHz.). Moreover, the drop velocity variation among individual nozzles is 1.7 ms^{-1} for the robust MIMO feedforward control compared to 2.5 ms^{-1} for the standard pulse. Note that the average drop velocity with the robust pulse is higher compared to the average drop velocity with the standard pulse. This may be the effect of the different tail and satellite droplets in the drop formation process. However, one can manipulate the drop velocity in a narrow range by scaling the amplitude of the robust pulse. It is evident from Figures 5.10 and 5.12 that the proposed method is very effective to minimize the residual oscillations and the cross-talk influence.

It would be interesting to test other bitmaps containing some more complicate patterns to further validate the proposed actuation procedure. If some degradation

is observed with these bitmaps, the model of the printhead could be refined as proposed in Remark 2.5. In (Ezzeldin 2012), it is shown that the design of actuation pulses based on the input bitmap pattern can improve the print quality. In principle it is possible to the design of bitmap-dependent actuation pulses with proposed method by using a bitmap-dependent model obtained using system identification for a given bitmap pattern.



Figure 5.9: Bitmap image with the standard pulse.



Figure 5.10: Bitmap image with the constrained MIMO feedforward control.

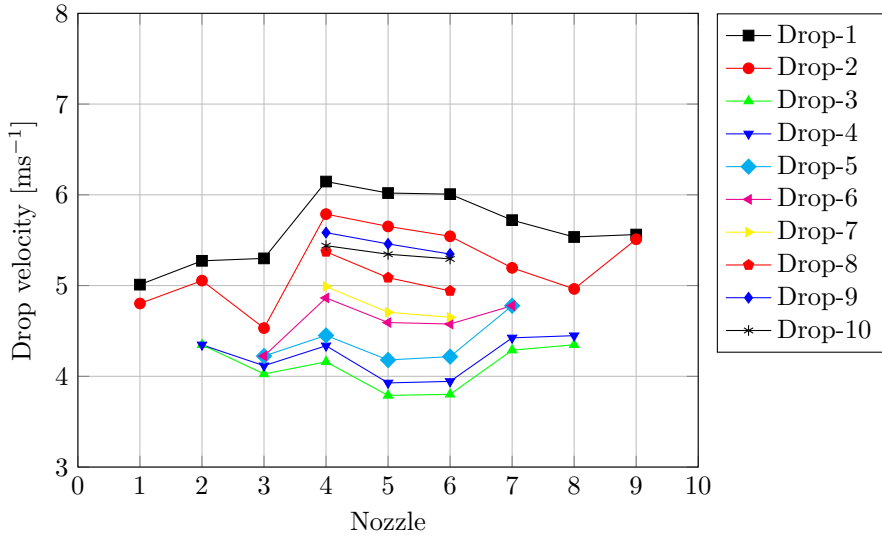


Figure 5.11: Drop velocities in the jetted bitmap with the standard pulse.

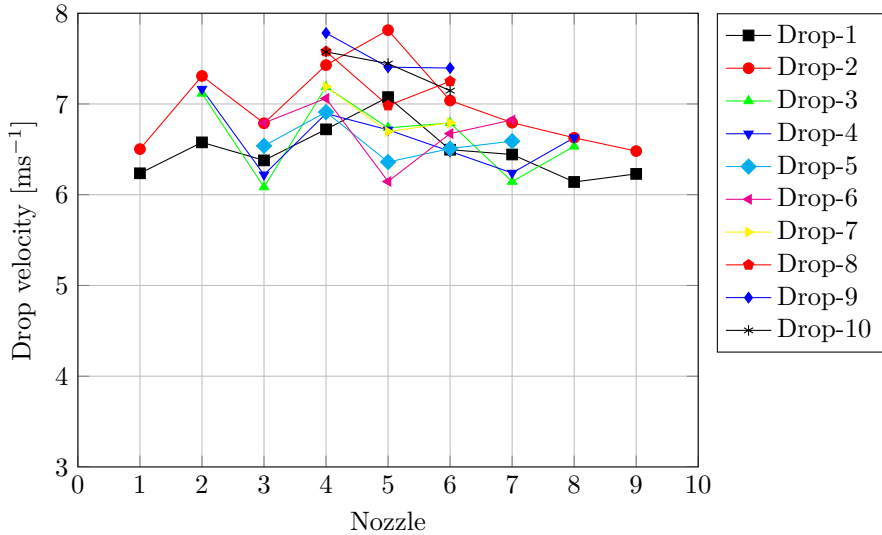


Figure 5.12: Drop velocities in the jetted bitmap with the robust constrained MIMO feedforward control.

5.6 Summary

In this chapter we have presented a model-based approach to improve the performance of a DoD inkjet printhead. The model developed using experimental system identification is used for control purposes. This is an advantage for printhead practitioners who do not have information about the printhead architecture and dynamics. It may also be useful for the printhead designers to validate their physical models or to obtain quickly a MIMO model of the printhead. In order to tackle the residual oscillations and the cross-talk in the printhead with trapezoidal waveforms, we proposed to use constrained MIMO feedforward control. The solution of the robust optimization problem delivers the robust actuation pulse $u_{\text{rob}}(k)$ and the robust actuation delay t_a^{rob} . The robust actuation pulse effectively damps the residual oscillations in a single ink channel in the presence of parametric uncertainty. Further, this robust pulse is applied to all ink channels but the actuation of the group of even ink channels is delayed by t_a^{rob} with respect to the actuation of the group of odd ink channels. This effectively reduces the cross-talk effect by avoiding simultaneous actuation of immediate neighboring ink channels. Simulation and experimental results have demonstrated that a considerable improvement in the ink drop consistency can be achieved with the proposed constrained feedforward control compared to the standard pulse which was the starting point of the pulse design.

Conclusions and Recommendations

In the first chapter, we have discussed the emergence of inkjet technology as a promising micro-fabrication tool. We have seen that the application of inkjet technology is limited by operational issues. Based on the state of art in the inkjet printhead control, we have formulated the research question and have proposed a model-based control approach. In this thesis, we have shown that data-based modeling can deliver a model of an inkjet printhead close to the working conditions. This model comprises of the nominal model and polytopic uncertainty on its parameters. It is observed that this model not only enables the waveform design, but also simplifies the robust feedforward control design greatly, thanks to the choice of uncertainty description. Subsequently, this approach is validated through simulations and experiments. In this chapter, we look back to the proposed approach and present the conclusions on the conducted research. Further, we provide recommendations for the printhead design, data-based modeling and performance monitoring of the printhead for the future research.

6.1 Conclusions

The contributions of this thesis are mainly in the modeling of an inkjet printhead and in the design of a robust actuation pulse to provide better performance over the operating range. In this section, we first present the improvements in printhead modeling using a data-based approach and later present the efficacy of the robust feedforward control.

6.1.1 Data-based modeling of Inkjet printhead

In the first chapter, we have formulated the research question, ‘is it possible to obtain a model of inkjet printhead in different operating regimes, sufficiently compact to enable model-based control’. In order to achieve a solution for this and

achieve the objectives of the thesis, an inkjet printhead model should satisfy several requirements. Primarily, the model should represent the printhead dynamics close to its working conditions. Furthermore, the model should have low complexity and should be compact to enable the use of control techniques. Currently available models do not satisfy the requirements mentioned above and thus, a suitable modeling approach is needed.

It is difficult to obtain a good physical model for an inkjet system either, due to inability to capture the system dynamics in compact analytical equations or due to insufficient knowledge of various complex interactions (e.g., the refill dynamics and the cross-talk effect). It is easier to use experimental measurements to develop a model. Therefore, in this thesis, we have proposed a data-based modeling approach, to obtain a model of the inkjet system under consideration, close to its operating conditions. We have exploited the self-sensing mechanism of the piezo-unit and have used it simultaneously as an actuator and a sensor. The dynamics between the piezo input of an ink channel and its piezo sensor output (when none of the neighboring channels are actuated) is called the direct dynamic model of an ink channel, G_d . We have observed that the direct dynamic model G_d of an ink channel is significantly influenced by the nonlinearities in the drop formation. Hence, to obtain G_d we have applied the input signal which is used in practice to jet ink drops, i.e. a series of positive trapezoidal pulses at a given DoD frequency. These experimental data are used in the prediction error identification to deliver a ink-channel model under working conditions.

The local inkjet model is influenced by the jetting frequency and the refill dynamics. Thus, to capture the behavior of the printhead over the operating regime, we have obtained several local models at different DoD frequencies. We have found that, for the printhead under investigation, the variation in the first resonant mode is more significant for the actuation pulse design compared to the variations in the second resonant mode. We have used the information of the first mode dynamics variation to construct a polytopic uncertainty set Δ on the parameters of the nominal model G_d . Now, the uncertain system $G_d(q, \Delta)$, $\Delta \in \Delta$, represents the set of local inkjet models obtained at different DoD frequencies. The use of the polytopic description for uncertainty in the inkjet system offers us a compact representation of the printhead behavior. Furthermore, this system description effectively simplifies the design of robust feedforward control. It is observed that the cross-talk dynamics between the piezo inputs of the immediate neighboring channels and the piezo sensor output of the considered channel are not influenced by the DoD frequency.

In this thesis, in order to reduce the model complexity, we have made two assumptions. The first assumption is that the geometry of all the ink-channels is identical, leading to very similar input-output relation G_d . In practice, however, the variation in the direct dynamics of ink channels may be considerable due to higher manufacturing tolerance. Although it is not explicitly demonstrated in this thesis, it is possible to capture this variation in the printhead geometry using polytopic uncertainty. The second assumption is that the cross-talk effects due to the left and the right neighboring ink-channels are similar and higher manufacturing tolerance affects it. As recommended for the direct dynamics, the variation in the

cross-talk dynamics due to manufacturing tolerance can be captured by introducing parametric uncertainty on the cross-talk G_c as well.

6.1.2 Robust feedforward control inkjet printhead

In Section 1.2.2, we have discussed that the prime performance metric for a DoD inkjet printhead is the drop consistency and the productivity. The performance is adversely affected by two operational issues: the residual oscillations and the cross-talk. In order to improve the performance, we have designed the actuation pulses using a model-based control approach utilizing the polytopic model of the inkjet printhead. We have developed a constrained robust feedforward control method to design the actuation pulse subjected to the shape constraints, due to limitations of the driving electronics (ASICs). The actuation pulse parameters are obtained as the solution of a nonlinear optimization problem. It is observed that this solution is less sensitive to the initial guess of the pulse parameters. The implementation complexity of the proposed method is very low as the hardware limitations are taken into account during the pulse design step. Use of such systematic procedure will reduce the development time as one does not have to conduct several time consuming experiment. The performance of this model based method depends on the model accuracy. When sufficiently accurate model is not available, in (Ezzeldin 2012) an experimental method is proposed, which delivers very good performance. For such scenarios, one can also easily modify the proposed method to use the experimental setup (see Remarks 3.1 and 3.2). However, in this thesis, we have proposed another simple approach to obtain fairly accurate printhead model based on system identification. As discussed in the earlier section, the advantage of this data-based modeling approach is that it can provide some insight in the printhead functioning (which is very useful for inkjet practitioners who do not have the information about the printhead geometry and the dynamics).

The robust pulse designed with the proposed approach provides good performance over the printhead operating frequency range rather than at only one particular DoD frequency. By comparing the simulation results with the constrained and the unconstrained pulses, we have observed that, the performance degradation caused by the pulse shape constraints is, in fact, quite limited.

Conventionally, the performance of a DoD inkjet printhead is analyzed by the DoD-curve, i.e. variation of the drop velocity against the increase in the DoD frequency. For a given DoD frequency, the drop velocity is classically measured for a continuous stable jetting. Thus, the transient information at the start of the jetting is lost. Even though it is ideally required to have the consistent drop velocity while jetting any bitmap, it is not possible to test several bitmaps to construct the performance metric. Therefore, we have extended the classical concept of the DoD curve to be a better instrument to analyze the drop consistency. For a given DoD frequency, we have jetted 10 ink drops and measured the drop velocities of all drops to analyze the effect of transient behavior on the drop velocity. Thus, the DoD-curve presented in this thesis demonstrate the transient behavior in the continuous jetting at different DoD frequencies.

For a better print quality, even though not sufficient, it is at least expected to have a flat DoD-curve. For the standard trapezoidal pulse, the maximum drop velocity variation over the operating range (i.e. up to 70 kHz) is 12 ms^{-1} . The robust actuation pulse has reduced the maximum drop velocity variation substantially, and it is less than 2 ms^{-1} . We have seen that, for the printhead under consideration, the drop consistency is also affected by the cross-talk. Conventionally, the effect of the cross-talk is reduced by introducing actuation delay between the immediate neighboring channels. In this thesis, we have demonstrated that this actuation delay can be obtained through an optimization (MIMO feedforward control) problem, unlike the trial and error method used in practice. The actuation delay is a result of the robust MIMO feedforward control that uses the uncertain inkjet printhead model. Thus, this delay is robust against the variation in the inkjet operating conditions and hence called the robust actuation delay. This robust MIMO feedforward control is tested by jetting a bitmap image at a DoD frequency of 50 kHz. For the standard pulse, it is observed that the average drop velocity variation is 38% (i.e. the average drop velocity for all nozzles is 4.9 ms^{-1} compared to the nominal drop velocity of 8 ms^{-1} at the DoD frequency of 50 kHz). The robust MIMO feedforward control has improved the drop consistency and, now, the average drop velocity variation is reduced to 10% (i.e. the average drop velocity of all nozzles is 7 ms^{-1} compared to the nominal drop velocity of 7.8 ms^{-1} at the DoD frequency of 50 kHz). Moreover, the drop velocity variation among individual nozzles is 1.7 ms^{-1} for the robust MIMO feedforward control compared to 2.5 ms^{-1} for the standard pulse. In (Ezzeldin 2012), it is shown that the design of actuation pulses based on the input bitmap pattern can improve the print quality.

Although, it is not demonstrated in this thesis, the design of bitmap-dependent actuation pulses is possible with the framework that we have proposed in this thesis by either using a better physical nonlinear printhead model (which can capture the refill dynamics) or by using a bitmap-dependent model obtained using system identification for a given bitmap pattern. In this case, one would have to use a different pulse for each bitmap to be printed. However, if one would like to apply only a single pulse for all bitmap patterns, then the pulse should be robust against the bitmap dependent dynamics variation. For this purpose, one has to construct the uncertainty on the nominal model by considering the set of models identified with different bitmaps. Further, one has to use the proposed robust feedforward control to obtain a single pulse which will be robust against bitmap pattern changes.

6.2 Recommendations

Based on the model-based inkjet control presented in this thesis, we have identified three areas for further improvements: printhead design, data-based modeling and printhead control. In this section, we present the recommendations for the further research in these areas.

6.2.1 Inkjet printhead design

In this thesis we have presented the application of the systems and control approach for the given inkjet printhead design. However, utilizing a system and control approach in the inkjet printhead design can improve the sensing and controllability of the system for broadening the operating regimes. In this section, we present the following recommendations to improve the printhead design.

Improvement in the controllability of the jetting process

The ability to generate more complex pressure profiles in order to control the meniscus behavior will not provide tighter control on specific drop properties but it will also allow the user to modulate the drop sizes (to deliver high print quality or high productivity as per requirement).

- *Acoustic dynamics*

For a chosen fundamental jetting resonant frequency, the proximity of the second resonant frequency to the primary jetting mode limits the achievable performance (see Remark 4.2). As the frequency separation ratio reduces, the influence of the second acoustic mode on the meniscus behavior increases. This limits the flexibility in the drop formation as the meniscus movement can be controlled only in a restricted regime. This influence can be minimized by a complex actuation pulse leading to expensive driving electronics. For very small frequency separation ratio, it is fundamentally not possible to avoid influence of the second resonant mode. In the current printhead design, the second acoustic resonant mode is approximately twice the primary jetting resonant mode (i.e. the frequency separation ratio is two). Therefore, it is recommended to increase the frequency separation ratio (approximately above five to six) by the redesign of the ink channel geometry for a better control.

- *Printhead actuation*

In the current design, the controllability of the jetting process is considerably restricted by the actuation(see Remark 4.2). The actuator is very long and is placed in the middle of the channel. Thus, it is difficult to control the refill dynamics and to generate complex pressure profile at the nozzle entrance. Using multiple actuators over the channel length can improve the ability to generate more complex pressure profiles inside the channel and at the nozzle entrance. In Figure 6.1, we have shown possible locations to add two more piezo units to have better control on the jetting process. These piezo units can be used as simultaneous actuators and sensors, as proposed in this thesis. The piezo unit S_3 can be used to effectively influence the ink flow close to the ink reservoir (providing better control on the refill process) and the piezo unit S_2 can be used to shape complex pressure profile at the nozzle entrance.

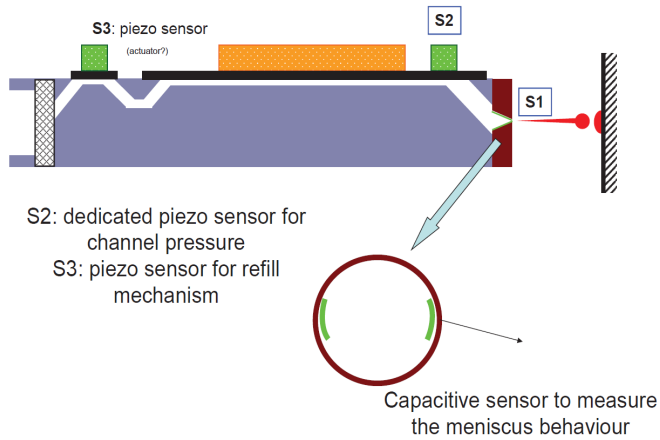


Figure 6.1: Proposed actuator and sensor functionality in the inkjet printhead.

Improvement of sensing functionality of the jetting process

The sensor functionality available in the current printhead is significantly limiting the observability of the jetting process. Firstly, the piezo sensor location is not optimal to monitor the drop formation close to the nozzle and the refill phenomena closer to the ink reservoir. Secondly, the current piezo sensor measures the average pressure over the long length of the piezo unit. This restricts the measurement of the pressure waves whose net pressure over the surface is zero. In Figure 6.1, we have recommended addition of three sensors to improve the observability of the inkjet process. In order to predict drop properties more accurately, it is important to measure the system behavior as close to the drop formation as possible. Therefore, it is recommended to include a capacitive sensor S_1 in the nozzle to provide a signal proportional to the meniscus movement. With the recent developments in the design of inkjet printheads using MEMS technology, inclusion of such a meniscus capacitive sensor is possible (Wei et al. 2012). To avoid averaging the pressure waves over a long area, it is recommended to include two short piezo units on both ends of the ink channel. The sensor S_3 will provide more information on the refill dynamics and the sensor S_2 will provide more information on the pressure profile at nozzle entrance.

6.2.2 Data-based modeling

We have seen that the data-based modeling approach is a useful tool to obtain fairly accurate inkjet printhead models. Further improvements in the data gathering and model structure can open new possibilities to use these models for the printhead design and system health monitoring.

- *Experimental modeling*

In the previous section, we have proposed an addition of a new sensor functionality to improve the observability of the jetting process. However, for the inkjet printheads which do not have these functionalities, even better models can be obtained by improving the experimental data collection. In the current experimental setup, it is only possible to measure the piezo sensor signal. However, obtaining a data-based model for meniscus dynamics will provide more information on the jetting process. However, it is difficult to measure the meniscus behavior with a laser vibrometer during the jetting. It is recommended to explore other measurement methods to monitor the meniscus behavior during the jetting. One way is to collect high resolution images (with laser light source instead LED stroboscopic light source (Bos 2011)) of the nozzle from different angles and reconstructing the meniscus motion in 3-dimension using image processing softwares.

- *Data-based nonlinear model development*

During the design phase of the inkjet printhead, complex numerical (Ansys + CFD) models are used to analyze the behavior of the printhead. These models can predict the nonlinear behavior of inkjet printhead with a very high accuracy. However, these models are computationally very expensive and, hence, are not used for control purposes. By utilizing the simulation data of these complex models, it is possible to obtain computationally efficient black-box non-linear models (Bos 2006) for control purposes. Note that all the relevant internal variables of the inkjet system can be monitored in the Ansys/CFD models. Thus, it is possible to obtain fairly accurate models for the relevant variables which cannot be measured practically. Moreover, these computationally efficient black-box models can be used to develop real-time soft-sensors for monitoring health of the inkjet system.

- *Linear parameter varying (LPV) model development*

A favorable description of nonlinear system for control design is the linear parameter varying (LPV) system. For this class of nonlinear systems, the system behavior depends on external scheduling variable. For a constant value of the scheduling variable, the nonlinear system reduces to a linear system. Further research is required to explore the possibility of data-based LPV modeling of a DoD inkjet printhead.

6.2.3 Control and performance monitoring of inkjet printhead

In this thesis, we have seen that the robust feedforward control is an effective method to tackle the system variations in the operating regime. Further research is needed to explore possibilities to extend its use in the inkjet printing system and also to introduce new control concepts to deliver high performance inkjet systems.

- *Reduction in manufacturing cost through robust control*

The printhead dynamics are sensitive to the channel geometry, the materials

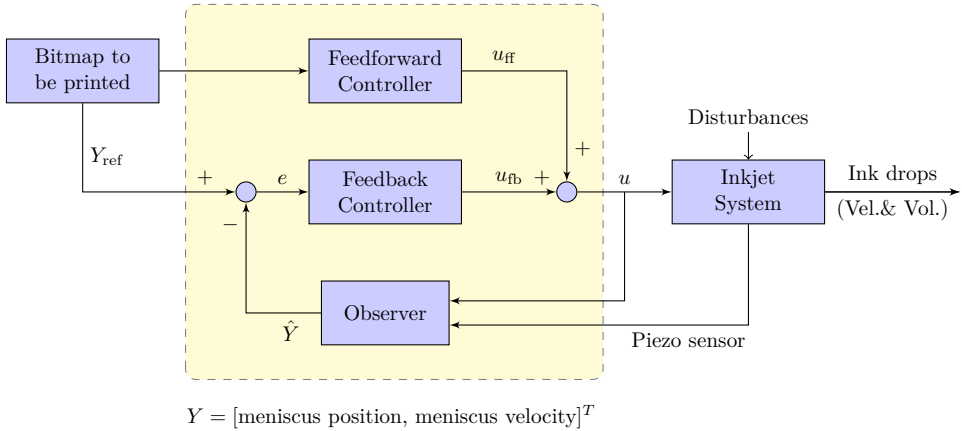


Figure 6.2: Proposed feedforward and feedback control system for a high performance inkjet printhead.

used and the manufacturing processes. Therefore, during production, the material properties are strictly regulated and high precision machining is used to ensure uniformity in a inkjet printhead. During the printhead operation, high quality ink is used with very low tolerances on its properties. These measures increase the production and the operational cost. Conventionally, the pulse design does not take into account the manufacturing tolerances. Although, it is not demonstrated in this thesis, it is possible to represent the effect of manufacturing tolerances on the inkjet dynamics using the polytopic uncertainty set Δ . Using such inkjet model, it would be possible to design an actuation pulse which is robust against the manufacturing tolerances. This can substantially reduce the manufacturing and the operational cost as the tolerances on the material properties and the manufacturing process variations can be increased. Further research is required to demonstrate the impact of robust feedforward control on the printhead manufacturing.

- *Drop size modulation (DSM)*

It is well known that print quality can be significantly improved if the inkjet can deliver ink droplets of different volumes as per requirement. Even though it is not demonstrated in this thesis, the proposed robust feedforward approach is suitable for DSM. It can be achieved by suitable selection of the reference trajectory y_{ref} . Further research is needed to incorporate the insight from Ansys/CFD models in the design of the reference trajectories.

- *Health monitoring and adaptive control*

The piezo sensor signal is fairly sensitive to various changes in the inkjet printhead, such as: air bubble entrapment, intrusion of dirt in the nozzle, wetting on the nozzle plate, change in the ink viscosity, piezo aging, back pressure change and printhead temperature change. To provide optimal jetting it is important to detect system deviation and diagnose its cause. Moreover, after

detecting the deviation in the system properties, the actuation pulses should be adapted to restore the optimal performance. It is highly important to investigate application of systems and control theory for inkjet performance monitoring and adaptive control.

- *High performance through Feedforward and Feedback control system*
Application of inkjet technology to micro-manufacturing demands high productivity and high accuracy. Currently, various unknown disturbance and system changes limits the achievable performance. Providing a very fast feedback control loop in addition to feedforward control (see Figure 6.2) can provide high performance for applications where accurate placement of each droplet is critical (e.g. printed electronics, manufacturing integrated circuits with inkjet etc.). Further research is need on this topic to explore performance improvements and limitations.

Performance measures of a DoD Inkjet Printhead

In Section 1.2.2, we have discussed the primary drop properties i.e. the drop velocity, the drop volume and their consistency. In this section, we represent other critical drop quality metrics.

- *Satellite drops.*

The drop is generated from an initial liquid column which comes out of the nozzle to form a leading droplet and an elongated tail. The separation of the leading droplet and the elongated tail can lead to the formation of satellite drops (Derby 2010). If the satellite drops are faster than the main droplet, then they get merged into the main droplet before reaching the print media. However, if the satellite drops are slower than the main droplet, then they are deposited on the print media deteriorating the resolution and the accuracy. Therefore, it is essential to avoid generation of satellite drops.

- *Jet straightness.*

The droplets have to be deposited in a straight line on the substrate, typically with an accuracy of 5 to 18 mrad. Note that, as the drop volume decreases, this requirement becomes even more important.

As discussed in Section 1.2.2, the throughput and the yield of an inkjet printhead is influenced by the productivity of a DoD inkjet printhead. Another factor which contributes to the throughput and yield is the *reliability* of a printhead, which is related to the jetting stability. The jetting stability depends on the compatibility of the ink with the printhead. Generally, the reliability of a printhead is defined as the absence of nozzle failure for a certain amount of jetted drops, e.g. one failure per one million jetted drops.

The designers of the inkjet-based micro-manufacturing application have to appropriately choose a DoD inkjet printhead based on the requirements of their applications (e.g. resolution, yield etc.). In Table A.1, we have summarized the relationship between the application requirements and the performance metrics of a DoD inkjet printhead.

Application requirements	Performance metric of a DoD inkjet printhead
Throughput, productivity	Number of usable jets Jetting frequency Reliability
Feature size	Drop volume Drop spread (mostly substrate)
Feature precision	Drop placement accuracy Drop volume control
Yield	Consistency and Reliability

Table A.1: Relationship between the application requirements and the performance metrics of a DoD inkjet printhead.

B

APPENDIX

Experimental Setup

Generally, experimental setup used for investigating the performance of a DoD printhead consists of several sensors which may not be available when in the actual inkjet printer. Figure B.1 shows a schematic overview of the experimental setup and Figure B.2 shows the actual experimental setup. Two sensors are available in this setup. We can utilize the electro-mechanical coupling in a piezo-unit in order to use it as a sensor. Further, a Charge-Coupled Device (CCD) camera along with a microscope is used to analyze the properties of jetted drops. The setup can be functionally divided into two parts, a part responsible for controlling the printhead and a part responsible for monitoring the jetting process (Wijshoff 2008).

As discussed in Section 2.1, the printheads under investigation is a hot-melt inkjet printhead and solid ink balls are heated in the printhead to get the liquid ink. The temperature of the printhead is maintained to around 130° C by a simple feedback loop which utilizes a thermocouple as a sensor and a PID controller (Eurotherm 2408) to manipulate the input to the heating elements. A level sensor is incorporated in the printhead to monitor ink level in the reservoir. Similar to its position in a real printer, the printhead is mounted vertically with its nozzles facing downward. This can cause leaking of ink through the nozzle due to gravity. Hence, an air pressure unit (TS 9150G) is provided to ensure that the pressure inside the ink reservoir remains below the ambient pressure.

The setup is connected to a personal computer that is equipped with National Instruments IMAQ PCI 1409 and PCI GPIB cards for image processing and communication, respectively. A Newport MM3000 motion controller is used for automatic positioning of the printheads in the measuring positions with Newport xy-tables (Wijshoff 2008). A Labview software is used to control the setup and for data acquisition. Note that in order to directly send the piezo actuation waveform to the amplifier we need a data acquisition system with very high sampling frequency, which is mostly not available in the market. Therefore, once the actuation signal is defined, this digital information is sent to an arbitrary waveform generator (Philips PM 5150/Wavetek 75A). The waveform generator generates the analogue actuation signal and sends it to an amplifier (Krohn-Hite 7602) as the piezo-unit needs higher amplitude signal. The amplified signal is fed to a so-called switch-

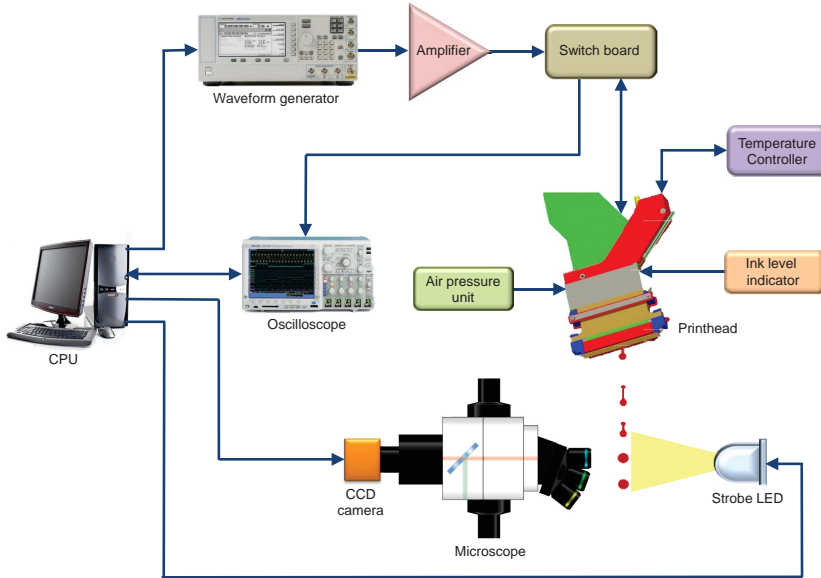


Figure B.1: Schematic overview of the experimental setup.

board which directs the actuation signal to an appropriate channel instructed by the personal computer. An oscilloscope (Tektronix TDS 420/TDS 3034B) is used to measure the applied actuation signal and the piezo sensor signal. As the personal computer can communicate to the oscilloscope, it can directly store the displayed data on the oscilloscope.

Measurement of the drop properties

In Section 2.3.1 we have discussed the piezo sensor functionality in the experimental setup. In this section we present the second sensor functionality, i.e. the CCD camera. This functionality is quite important as it gives the direct information about the ink drop properties which is crucial for performance assessment of the printhead. A standard CCD camera (jAi progressive scan) is used to capture the images from a microscope (Olympus SZH-10) of the drop formation with a frame rate 25 images/sec. A stroboscopic LED light source produces flashes of very short duration (typically 100 ns). Once the the strobe frequency chosen equal to the DoD frequency then we can see the repeatable part of the drop formation, as the images are integrated over many droplets (depending on the DoD frequency up to several hundred). In order to capture the non-repeatable part of the drop formation one has to use a high-speed camera. The images collected at different time instants of the drop formation are be processed to show the flight path of the droplet traveling towards the print media. The drop velocity can be easily determine from this flight path of the droplet. Furthermore, it is possible to estimate the drop volume using

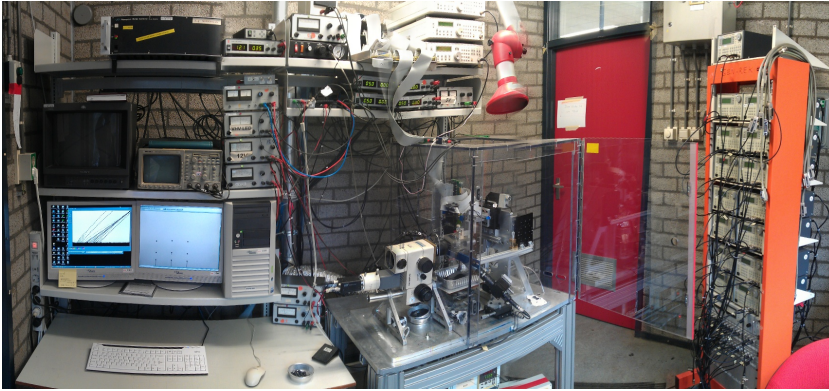


Figure B.2: The experimental setup.

the measured droplet diameter in the captured images. However, accuracy of the droplet volume estimate is limited due to the lower resolution of the camera. Apart from this, one can measure droplet jetting angle, the behavior of satellites drops and the stability of the jetting process. The image processing used for estimation of drop properties is sensitive to the black and white contrast of the images which is influenced by the stroboscopic light source. In (Bos et al. 2011) a laser light source is used instead of LED light source for high intensity and short flash duration which enhances the captured image quality significantly.

Robust Unconstrained Feedforward Control using FIR Filters

As discussed in Section 3.5.2 we formulate the feedforward control problem as a filtering problem. We use the model $H_{\text{ref}}(q)$ to generate the reference trajectory $y_{\text{ref}}(k)$ (see Figure 3.3.). Design of the model $H_{\text{ref}}(q)$ is simpler once we chose a finite impulse response (FIR) model structure for it.

Recall that the state-space representation of the reference model $H_{\text{ref}}(q)$ is given as follows

$$\begin{aligned}x_R(k+1) &= A_R x_R(k) + B_R \delta(k) \\ y_{\text{ref}}(k) &= C_R x_R(k) + D_R \delta(k)\end{aligned}\tag{C.1}$$

where $\delta(k)$ is the unit pulse.

Now, we parameterize the actuation pulse as the pulse response of a FIR filter $F(q, \beta)$:

$$u(k) = F(q, \beta) \delta(k)\tag{C.2}$$

with $F(q, \beta) = \beta_0 + \beta_1 q^{-1} + \dots + \beta_{n_f} q^{-n_f}$, $\beta = [\beta_0, \dots, \beta_{n_f}]^T$ a vector containing the coefficients of the FIR filter and $\delta(k)$ the unit pulse. The state-space representation of $F(q, \beta)$ is given as follows

$$\begin{aligned}x_F(k+1) &= A_F x_F(k) + B_F \delta(k) \\ u(k, \beta) &= C_F(\beta) x_F(k) + D_F(\beta) \delta(k)\end{aligned}\tag{C.3}$$

where

$$\begin{aligned}A_F &= \begin{bmatrix} 0 & 0 \\ I_{n_f-1} & 0 \end{bmatrix}, & B_F &= \begin{bmatrix} 1 \\ 0 \end{bmatrix} \\ C_F(\beta) &= [\beta_1 \quad \dots \quad \beta_{n_f}], & D_F(\beta) &= \beta_0.\end{aligned}$$

The choice of the filter structure is important, as it determines the length and the shape of the actuation pulse. One can choose the filter $F(q)$ as a rational function, however, this would result in an actuation pulse of an infinite length because the rational filter has an infinite pulse response. However, in our problem, it is required to obtain a finite length actuation pulse. The use of the FIR structure allows us to set the length of the actuation pulse a-priori. In addition, the to-be-designed filter coefficient vector β only appears in the state-space matrices C_F and D_F . This property greatly simplifies the optimization problem to design the filter $F(q)$.

Note that the inkjet system $H(q, \Delta)$ is a single input single output (SISO) system. Hence, the uncertain error dynamics $\nu(q, \beta, \Delta) = (H_{\text{ref}}(q) - H(q, \Delta)F(q, \beta))$ will not be changed if we interchange $H(q, \Delta)$ and $F(q)$, i.e. $\nu(q, \beta, \Delta) = (H_{\text{ref}}(q) - F(q, \beta)H(q, \Delta))$, see Figure 3.3. Thus, the state-space representation of the error dynamics $\nu(q, \beta, \Delta)$ is given as follows

$$\begin{aligned} x(k+1) &= A(\Delta)x(k) + B(\Delta)\delta(k) \\ e(k, \beta, \Delta) &= C(\beta, \Delta)x(k) + D(\beta, \Delta)\delta(k), \end{aligned} \quad (\text{C.4})$$

where

$$\begin{aligned} A(\Delta) &= \begin{bmatrix} A_S(\Delta) & 0 & 0 \\ B_F C_S(\Delta) & A_F & 0 \\ 0 & 0 & A_R \end{bmatrix}, B(\Delta) = \begin{bmatrix} B_S(\Delta) \\ B_F D_S(\Delta) \\ B_R \end{bmatrix} \\ C(\beta, \Delta) &= \begin{bmatrix} -D_F(\beta)C_S(\Delta) & -C_F(\beta) & C_R \end{bmatrix}, \\ D(\beta, \Delta) &= \begin{bmatrix} D_R - D_F(\beta)D_S(\Delta) \end{bmatrix}. \end{aligned}$$

Note that the inkjet system dynamics $H(q)$ in (2.6) and the reference model $H_{\text{ref}}(q)$ do not have direct feed through, i.e. D matrix is null. However, to provide general results we have considered here. Therefore, while solving the problem for the inkjet system considered in this thesis we will assign matrix D as null matrix.

It can be seen that thanks to the particular choice of the FIR structure for the filter $F(q)$, only the matrices C and D of (C.4) depend on the filter coefficient vector β . Also, as we assume the uncertainty Δ to be of a polytopic nature ($\Delta \in \mathbf{\Delta}$), the state-space matrices of the error system $\nu(q, \beta, \Delta)$ belong to following polytope

$$\begin{aligned} & \left(A(\Delta), B(\Delta), C(\beta, \Delta), D(\beta, \Delta) \right) \\ &= \sum_{i=1}^4 \alpha_i (A_i, B_i, C_i(\beta), D_i(\beta)). \end{aligned} \quad (\text{C.5})$$

where the matrices $(A_i, B_i, C_i(\beta), D_i(\beta))$ are the state-space matrices of the fixed error dynamics $\nu_i(q, \beta)$ at the i -th vertex of the polytope and α_i are positive scalars such that $\sum_{i=1}^4 \alpha_i = 1$. Clearly, the uncertain system error dynamics is a convex combination of the fixed systems at the vertices of the polytope $\mathbf{\Delta}$.

As discussed in Section 3.5.1, the performance index (3.10) for the actuation

pulse is defined as the square of the H_2 norm of the tracking error. Now, the inkjet system is perturbed by the uncertainty $\Delta \in \mathbf{\Delta}$. Therefore, we define the performance index $\mathcal{J}(\beta)$ as the square of the worst-case H_2 norm of the tracking error transfer function $\nu(q, \beta, \Delta)$:

$$\begin{aligned} \mathcal{J}(\beta) &= \max_{\Delta \in \mathbf{\Delta}} \|\nu(q, \beta, \Delta)\|_2^2 \\ &= \max_{\Delta \in \mathbf{\Delta}} \|H_{\text{ref}}(q) - H(q, \Delta)F(q, \beta)\|_2^2. \end{aligned} \quad (\text{C.6})$$

The filter coefficient vector β_{robust} , describing the unconstrained robust actuation pulse is thus the solution β_{robust} of the following optimization problem

$$\begin{aligned} \beta_{\text{robust}} &= \arg \min_{\gamma, \beta} \gamma \\ \text{subject to} \quad &\mathcal{J}(\beta) < \gamma. \end{aligned} \quad (\text{C.7})$$

It is difficult to obtain the solution of the above problem (C.7) as it is semi-infinite optimization problem. However, it is possible to obtain a relaxation for the robust H_2 problem such that we obtain an upper bound γ_{opt} for the performance index $\mathcal{J}(\beta)$. In order to compute an upper bound on γ_{opt} and a suboptimal filter $\beta_{\text{robust}}^{\text{UB}}$ we can use the convex optimization described in the following theorem (Khalate et al. 2011).

Note that we use $*$ as an ellipsis for terms that can be induced by symmetry.

Theorem C.1 *Consider the error dynamics given by (C.4) then, the optimal coefficient vector $\beta_{\text{robust}}^{\text{UB}}$ for the robust actuation pulse can be determined by solving the following LMI optimization*

$$\beta_{\text{robust}}^{\text{UB}} = \min_{\gamma^{\text{UB}}, \beta, K=K^T} \gamma^{\text{UB}}$$

$$\text{subject to} \quad \begin{bmatrix} \gamma^{\text{UB}} - B_i^T K B_i & * \\ D_i(\beta) & 1 \end{bmatrix} > 0 \quad (\text{C.8})$$

$$\begin{bmatrix} K - A_i^T K A_i & * \\ C_i(\beta) & 1 \end{bmatrix} > 0, \quad i = 1, 2, 3, 4, \quad (\text{C.9})$$

where A_i, B_i, C_i, D_i are the system matrices of the inkjet system at the vertices of the polytope $\mathbf{\Delta}$.

Indeed, the above optimization problem delivers an upper bound $\gamma_{\text{opt}}^{\text{UB}}$ for the optimal γ of the problem (C.7).

Proof: Consider the system (C.4) for one particular Δ and for one particular β . Then, following the same reasoning as e.g. in the proof of Proposition 2 in (Bombois et al. 2010), it can be shown that $\|\nu(q, \beta, \Delta)\|_2^2 < \gamma^{\text{UB}}$ if there exists a

positive definite symmetric matrix K such that

$$\begin{aligned} B(\Delta)^T K B(\Delta) + D^2(\beta, \Delta) &< \gamma^{\text{UB}} \\ A(\Delta)^T K A(\Delta) + C^T(\beta, \Delta) C(\beta, \Delta) &< K \end{aligned} \quad (\text{C.10})$$

These two LMIs can also be rewritten as follows using the Schur complement

$$\begin{bmatrix} \gamma^{\text{UB}} & * & * \\ B(\Delta) & K^{-1} & * \\ D(\beta, \Delta) & 0 & 1 \end{bmatrix} > 0, \quad \begin{bmatrix} K & * & * \\ A(\Delta) & K^{-1} & * \\ C(\beta, \Delta) & 0 & 1 \end{bmatrix} > 0. \quad (\text{C.11})$$

The LMIs (C.11) are affine in Δ because the matrices $A(\Delta)$, $B(\Delta)$, $C(\beta, \Delta)$, $D(\beta, \Delta)$ are affine in Δ . In (Boyd et al. 1994), it is shown that (C.11) hold for all $\Delta \in \Delta$ if (C.11) hold for $\Delta = \Delta_i$, $i = 1, \dots, 4$; in other words if the following LMIs hold

$$\begin{bmatrix} \gamma^{\text{UB}} & * & * \\ B_i & K^{-1} & * \\ D_i(\beta) & 0 & 1 \end{bmatrix} > 0, \quad \begin{bmatrix} K & * & * \\ A_i & K^{-1} & * \\ C_i(\beta) & 0 & 1 \end{bmatrix} > 0, \quad (\text{C.12})$$

for $i = 1, 2, 3, 4$. Using the Schur complement, (C.12) reduces to (C.8) and (C.9).

Note finally that the expressions (C.8) and (C.9) are LMIs in β since C and D in (C.4) are affine in C_F and D_F in (C.3). The matrices C_F and D_F are indeed also linear function of β . \square

Remark C.1 *Major drawback of this method is that the dimension of the to-be-designed vector β will become larger when the actuation pulse is longer and/or when the sampling time T_s is smaller. This may pose numerical problems since the size of the LMI problem, required to obtain the robust filter $F(q, \beta)$, is directly proportional to the dimension of vector β .*

Bibliography

- Basten, T., R. Hamberg, F. Reckers and J. Verriet (Eds.) (2013). *Model-Based Design of Adaptive Embedded Systems*. Springer New York.
- Beltman, W.M. (1998). *Viscothermal wave propagation including acoustoelastic interaction*. Ph. D. thesis, University of Twente, The Netherlands.
- Berger, S. S. and G. Recktenwald (2003). Development of an improved model for piezo-electric driven ink jets. In *International Conference on Digital Printing Technologies*, Springfield, USA, pp. 323–327.
- Bogy, D.B. and F.E. Talke (1984). Experimental and theoretical study of wave propagation phenomena in drop-on-demand ink jet devices. *IBM J. Res. Dev.* **28**(3), 314–321.
- Boland, T., T. Xu, B. Damon and X. Cui (2006). Application of inkjet printing to tissue engineering. *Biotechnology Journal* **1**(9), 910–917.
- Bombois, X., H. Hjalmarsson and G. Scorletti (2010). Identification for robust H_2 deconvolution filtering. *Automatica* **46**(3), 577 – 584.
- Bos, A. van der (2011). *Air entrapment and drop formation in inkjet printing*. Ph. D. thesis, University of Twente, The Netherlands.
- Bos, A. van der, T. Segers, R. Jeurissen, M. van den Berg, H. Reinten, H. Wijshoff, M. Versluis and D. Lohse (2011). Infrared imaging and acoustic sizing of a bubble inside a micro-electro-mechanical system piezo ink channel. *Journal of Applied Physics* **110**(3), 034503.
- Bos, R. (2006). *Model based monitoring of large scale processes in process industry*. Ph. D. thesis, Delft University of Technology, The Netherlands.
- Boyd, S., L. El Ghaoui, E. Feron and V. Balakrishnan (1994). *Linear Matrix Inequalities in System and Control Theory*, Volume 15 of *Studies in Applied Mathematics*. SIAM.
- Brandt, R. (2010). Reduction of effects of residual dynamics and cross coupling in drop-on-demand inkjet printhead. Master’s thesis, Delft University of Technology.

- Calvert, P. (2001). Inkjet printing for materials and devices. *Chemistry of Materials* **13**(10), 3299–3305.
- Chappell, J., D.A. Hutt and P.P. Conway (2008). Variation in the line stability of an inkjet printed optical waveguide-applicable material. In *2nd Electronics System-Integration Technology Conference*, Greenwich, UK, pp. 1267–1272.
- Chung, J., S. Ko, C.P. Grigoropoulos, N.R. Bieri, C. Dockendorf and D. Poulikakos (2005). Damage-Free low temperature pulsed laser printing of gold nanoinks on polymers. *Journal of Heat Transfer* **127**(7), 724–732.
- Clayton, G.M., S. Tien, K.K. Leang, Q. Zou and S. Devasia (2009). A review of feedforward control approaches in nanopositioning for high-speed spm. *Journal of Dynamic Systems, Measurement, and Control* **131**(6), 061101–061101–19.
- Cox, W.R., D.J. Hayes, T. Chen, D.W. Ussery, D.L. MacFarlane and E. Wilson (1995). Fabrication of micro-optics by microjet printing. *SPIE Proceedings* **2383**, 110–115.
- de Jong, J. (2007). *Air entrapment in piezo inkjet printing*. Ph. D. thesis, University of Twente, The Netherlands.
- Delaney, J.T., P.J. Smith and U.S. Schubert (2009). Inkjet printing of proteins. *Soft Matter* **5**(24), 4866–4877.
- Derby, B. (2010). Inkjet printing of functional and structural materials: Fluid property requirements, feature stability, and resolution. *Annual Review of Materials Research* **40**(1), 395–414.
- Desoer, C. A. and M. Vidyasagar (1975). *Feedback Systems: Input-Output Properties*. Academic Press, New York.
- Devasia, S. (2002). Should model-based inverse inputs be used as feedforward under plant uncertainty? *IEEE Transactions on Automatic Control* **47**(11), 1865–1871.
- Dijksman, J.F. (1984). Hydrodynamics of small tubular pumps. *Journal of Fluid Mechanics* **139**, 173–191.
- Dijksman, J. F., P.C. Duineveld, M.J.J. Hack, A. Pierik, J. Rensen, J.-E. Rubingh, I. Schram and M.M. Vernhout (2007). Precision ink jet printing of polymer light emitting displays. *Journal of Materials Chemistry* **17**(6), 511–522.
- Dong, H., W.W. Carr and J.F. Morris (2006). An experimental study of drop-on-demand drop formation. *Physics of Fluids* **18**(7), 072102.
- Ezzeldin, M. (2012). *Performance improvement of professional printing systems: from theory to practice*. Ph. D. thesis, Eindhoven University of Technology, The Netherlands.

- Fakhfouri, V., N. Cantale, G. Mermoud, J.Y. Kim, D. Boiko, E. Charbon, A. Martinoli and J. Brugger (2008). Inkjet printing of SU-8 for polymer-based MEMS a case study for microlenses. In *IEEE 21st International Conference on Micro Electro Mechanical Systems*, Tucson, USA, pp. 407–410.
- Fujimoto, H., Y. Hori and A. Kawamura (2001). Perfect tracking control based on multirate feedforward control with generalized sampling periods. *IEEE Transactions on Industrial Electronics* **48**(3), 636–644.
- Gan, H.Y., X. Shan, T. Eriksson, B.K. Lok and Y.C. Lam (2009). Reduction of droplet volume by controlling actuating waveforms in inkjet printing for micro-pattern formation. *Journal of Micromechanics and Microengineering* **19**(5), 055010.
- Geromel, J.C., J. Bernussou, G. Garcia and M.C. de Oliveira (2000). H_2 and H_∞ robust filtering for discrete-time linear systems. *SIAM J. Control Optim.* **38**, 13531368.
- Geromel, J.C., M.C. de Oliveira and J. Bernussou (2002). Robust filtering of discrete-time linear systems with parameter dependent lyapunov functions. *SIAM J. Control Optim.* **41**, 700–711.
- Giusto, A. and F. Paganini (1999). Robust synthesis of feedforward compensators. *IEEE Transactions on Automatic Control* **44**(8), 1578–1582.
- Goldmann, T. and J.S. Gonzalez (2000). DNA-printing: utilization of a standard inkjet printer for the transfer of nucleic acids to solid supports. *Journal of Biochemical and Biophysical Methods* **42**(3), 105–110.
- Golub, G.H. and C.F. van Loan (1989). *Matrix Computations* (second ed.). John Hopkins Univ. Press, Baltimore, USA.
- Groot Wassink, M.B. (2007). *Inkjet printhead performance enhancement by feedforward input design based on two-port modeling*. Ph. D. thesis, Delft University of Technology, The Netherlands.
- Hitoshi, U. (2006). *Digital Printing of Textiles*. Woodhead Publishing Ltd.
- Jo, B.W., A. Lee, K.H. Ahn and S.J. Lee (2009). Evaluation of jet performance in drop-on-demand (dod) inkjet printing. *Korean J. Chem. Eng.* **26**(2), 339–348.
- Kawase, T., T. Shimoda, C. Newsome, H. Siringhaus and R. H. Friend (2003). Inkjet printing of polymer thin film transistors. *Thin Solid Films* **4389**, 279 – 287.
- Khalate, A.A., B. Bayon, X. Bombois, G. Scorletti and R. Babuška (2011). Drop-on-demand inkjet printhead performance improvement using robust feedforward control. In *IEEE Conference on Decision and Control and European Control Conference*, Orlando, USA, pp. 4183–4188.

- Khalate, A.A., X. Bombois, R. Babuška, G. Scorletti, S. Koekebakker, H. Wijshoff, W. de Zeeuw and R. Waarsing (2011). Performance improvement of a drop-on-demand inkjet printhead: a feedforward control based approach. In *27th International conference on Digital Printing Technologies (NIP-27)*, Minneapolis, USA, pp. 74–78.
- Khalate, A.A., X. Bombois, R. Babuška, H. Wijshoff and R. Waarsing (2010). Optimization-based feedforward control for a drop-on-demand inkjet printhead. In *American Control Conference*, Baltimore, USA, pp. 2182–2187.
- Khalate, A.A., X. Bombois, R. Babuška, H. Wijshoff and R. Waarsing (2011). Performance improvement of a drop-on-demand inkjet printhead using an optimization-based feedforward control method. *Control Engineering Practice* **19**(8), 771–781.
- Khalate, A.A., X. Bombois, G. Scorletti, R. Babuška, S. Koekebakker and W. de Zeeuw (2012). A waveform design method for a piezo inkjet printhead based on robust feedforward control. *IEEE Journal of Microelectromechanical Systems* **21**(6), 1365–1374.
- Khalate, A.A., X. Bombois, G. Scorletti, R. Babuška, R. Waarsing and W. de Zeeuw (2011). Robust feedforward control for a drop-on-demand inkjet printhead. In *IFAC World Congress*, Milan, Italy, pp. 5795–5800.
- Khalate, A.A., X. Bombois, R. Tóth and R. Babuška (2009). Optimal experimental design for LPV identification using a local approach. In *15th Symposium on System Identification*, Saint Malo, France, pp. 162–167.
- Khalate, A.A., X. Bombois, S. Ye, R. Babuška and S. Koekebakker (2012). Minimization of cross-talk in a piezo inkjet printhead based on system identification and feedforward control. *Journal of Micromechanics and Microengineering* **22**(11), 115035.
- Kima, B.H., S. Kimb, J.C. Lee, S.J. Shin and S.J. Kima (2012). Dynamic characteristics of a piezoelectric driven inkjet printhead fabricated using MEMS technology. *Sensors and Actuators A: Physical* **173**, 244–253.
- Koekebakker, S., M. Ezzeldin, A.A. Khalate, R. Babuška, X. Bombois, P.P.J. van den Bosch, G. Scorletti, S. Weiland, H. Wijshoff, R. Waarsing and W. Zeeuw (2013). Piezo printhead control: Jetting any drop at any time. In T. Basten, R. Hamberg, F. Reckers, and J. Verriet (Eds.), *Model-Based Design of Adaptive Embedded Systems*, Volume 22 of *Embedded Systems*, pp. 41–85. Springer New York. ISBN 978-1-4614-4820-4.
- Koo, H.S., M. Chen, P.C. Pan, L.T. Chou, F.M. Wu, S.J. Chang and T. Kawai (2006). Fabrication and chromatic characteristics of the greenish LCD colour-filter layer with nano-particle ink using inkjet printing technique. *Displays* **27**(3), 124–129.
- Korvink, J.G., P.J. Smith, D.Y. Shin, O. Brand, G.K. Fedder, C. Hierold and O. Tabata (Eds.) (2012). *Inkjet-based Micromanufacturing*, Volume 9. Wiley-VCH.

- Kose, I. E. and C.W. Scherer (2009). Robust l_2 -gain feedforward control of uncertain systems using dynamic iqcs. *International Journal of Robust and Nonlinear Control* **19**(11), 1224–1247.
- Krebs, F.C. (2009). Fabrication and processing of polymer solar cells: a review of printing and coating techniques. *Solar Energy Materials and Solar Cells* **93**(4), 394–412.
- Kwon, K.S. (2009a). Waveform design methods for piezo inkjet dispensers based on measured meniscus motion. *Journal of Microelectromechanical Systems* **18** (5), 1118–1125.
- Kwon, K.S. and W. Kim (2007). A waveform design method for high-speed inkjet printing based on self-sensing measurement. *Sensors and Actuators A: Physical* **140**(1), 75–.
- Kwon, K. S. (2009b). Methods for detecting air bubble in piezo inkjet dispensers. *Sensors and Actuators A: Physical* **153**(1), 50 – 56.
- Lee, H.H., K.S. Chou and K.C. Huang (2005). Inkjet printing of nanosized silver colloids. *Nanotechnology* **16**(10), 2436.
- Ljung, L. (1999). *System Identification - Theory for the User*. Prentice Hall, Upper Saddle River.
- Maciejowski, J.M. (2001). *Predictive Control with Constraints*. Pearson Education.
- McWilliam, I., M. Chong Kwan and D. Hall (2011). Inkjet printing for the production of protein microarrays. *Methods Mol Biol* **785**, 345–361.
- Megretski, A. and A. Rantzer (1997). System analysis via integral quadratic constraints. *IEEE Transactions on Automatic Control* **42**(6), 819–830.
- MicroFab Technologies Inc. (1999). Drive waveform effects on ink-jet device performance. Technical report, 99-03.
- Minemawari, H., T. Yamada, H. Matsui, J. Tsutsumi, S. Haas, R. Chiba, R. Kumai and T. Hasegawa (2011). Inkjet printing of single-crystal films. *Nature* **475**(7356), 364–367.
- M.Singh, H.M. Haverinen, P. Dhagat and G.E. Jabbour (2010). Inkjet printing process and its applications. *Advanced Materials* **22**(6), 673–685.
- Ohn, K., A. Ahlen and M. Sternad (1995). A probabilistic approach to multivariable robust filtering and open-loop control. *IEEE Transactions on Automatic Control* **40**(3), 405–418.
- Park, S.J., W. Sim, Y. Yoo and J. Joung (2006). Analysis of the micro droplet ejecting performance for industrial inkjet printing head. In *1st IEEE International Conference on Nano/Micro Engineered and Molecular Systems*, Zhuhai, China, pp. 1462–1465.

- Pekkanen, V., M. Mantysalo, K. Kaija, P. Mansikkamakib, E. Kunnari, K. Laine, J. Niittynen, S. Koskinen, E. Halonen and U.Caglar (2010). Utilizing inkjet printing to fabricate electrical interconnections in a system-in-package. *Micro-electronic Engineering* **87**(11), 2382 – 2390.
- Powell, M.J.D. (1978). A fast algorithm for nonlinearly constrained optimization calculations. In G. A. Watson (Ed.), *Numerical Analysis*, Lecture Notes in Mathematics, Vol. 630, pp. 144–157. Springer Verlag.
- Pshenichnyj, B.N. (1994). *The Linearization Method for Constrained Optimization*. Springer-Verlag.
- Rabbath, C.A. (1995). Sensitivity of the discrete- to continuous-time pole transformation at fast sampling rates. Master's thesis, McGill University, Canada.
- Sanchez, R.V., M.B. Madec and S.G. Yeates (2008). Inkjet printing of 3D metal-insulator-metal crossovers. *Reactive and Functional Polymers* **68**(6), 1052–1058.
- Scorletti, G. and V. Fromion (2006). Further results on the design of robust H_∞ feedforward controllers and filters. In *45th IEEE Conference on Decision & Control*, San Diego, USA, pp. 3560–3565.
- Scoutaris, N., M.R. Alexander, P.R. Gellert and C.J. Roberts (2011). Inkjet printing as a novel medicine formulation technique. *Journal of Controlled Release* **156**(2), 179–185.
- Shimoda, T. (2012). Ink-jet technology for fabrication processes of flat panel displays. *SID Symposium Digest of Technical Papers* **34**(1), 1178–1181.
- Skogestad, S. and I. Postlethwaite (2005). *Multivariable Feedback Control*. John Wiley and Sons Chichester.
- Starkey, P. (2011). EIPC seminar at SMT Nuremberg 2011. *Circuit World* **37**(3).
- Tóth, R. (2010). *Modeling and Identification of Linear Parameter-Varying Systems*. Springer.
- Tuan, H.D., P. Apkarian and T.Q. Nguyen (2001). Robust and reduced-order filtering: new LMI-based characterizations and methods. *IEEE Transactions on Signal Processing* **49**(12), 2975 –2984.
- Wei, J., C.Yue, G. Zhang, P.M. Sarro and J.F. Dijkman (2012). Monitoring of meniscus motion at nozzle orifice with capacitive sensor for inkjet applications. In *IEEE Sensors 2012*, Taipei, Taiwan, pp. 1–4.
- Wijshoff, H. (2008). *Structure and fluid-dynamics in piezo inkjet printheads*. Ph. D. thesis, University of Twente, The Netherlands.
- Wijshoff, H. (2010). The dynamics of the piezo inkjet printhead operation. *Physics Reports* **491**, 77–177.
- Williams, C. (2006). Ink-jet printers go beyond paper. *Physics World* **19**, 2429.

- Wu, B.M., S.W. Borland, R.A. Giordano, L.G. Cima, E.M. Sachs and M.J. Cima (1996). Solid free-form fabrication of drug delivery devices. *Journal of Controlled Release* **40**(1-2), 77–87.
- Xie, L., L. Lu, D. Zhang and H. Zhang (2004). Improved robust H_2 and H_∞ filtering for uncertain discrete-time systems. *Automatica* **40**(5), 873–880.
- Yang, L., A. Rida, R. Vyas and M.M. Tentzeris (2007). RFID tag and RF structures on a paper substrate using inkjet-printing technology. *IEEE Transactions on Microwave Theory and Techniques* **55**(12), 2894–2901.
- Zhou, K. and J.C. Doyle (1998). *Essentials of Robust Control*. Prentice-Hall, Englewood Cliffs, NJ.

Summary

Model-based Feedforward Control for Inkjet Printheads

Amol Ashok KHALATE

In recent years, inkjet technology has emerged as a promising manufacturing tool. This technology has gained its popularity mainly due to the facts that it can handle diverse materials and it is a non-contact and additive process. Moreover, the inkjet technology offers low operational costs, easy scalability, digital control and low material waste. Thus, apart from conventional document printing, the inkjet technology has been successfully applied as a micro-manufacturing tool in the areas of electronics, mechanical engineering, and life sciences. In this thesis, we investigate a piezo-based drop-on-demand (DoD) printhead which is commonly used for industrial and commercial applications due to its ability to handle diverse materials.

A typical drop-on-demand (DoD) inkjet printhead consists of several ink channels in parallel. Each ink channel is provided with a piezo-actuator which on the application of an actuation voltage pulse, generates pressure oscillations inside the ink channel. These pressure oscillations push the ink drop out of the nozzle. The print quality delivered by an inkjet printhead depends on the properties of the jetted drop, i.e., the drop velocity, the drop volume and the jetting direction. To meet the challenging performance requirements posed by new applications, these drop properties have to be tightly controlled.

The performance of the inkjet printhead is limited by two factors. The first one is the residual pressure oscillations. The actuation pulses are designed to provide an ink drop of a specified volume and velocity under the assumption that the ink channel is in a steady state. Once the ink drop is jetted the pressure oscillations inside the ink channel take several micro-seconds to decay. If the next ink drop is jetted before these residual pressure oscillations have decayed, the resulting drop properties will be different from the ones of the previous drop. The second limiting factor is the cross-talk. The drop properties through an ink channel are affected when the neighboring channels are actuated simultaneously. Generally, the drop consistency is improved by manual tuning of the piezo actuation pulse based on some physical insight or based on exhaustive experimental studies on the printhead. However, these ad-hoc procedures have proved to be insufficient in dealing with the above limitations.

In this thesis, a model-based control approach is proposed to improve the performance of a DoD inkjet printhead. It offers a systematic and efficient means to improve the attainable performance of a DoD inkjet printhead by reducing the effect of the residual oscillations and the cross-talk. Furthermore, the models that have been developed for this purpose can also give new insights into the operation of the printhead.

In order to achieve this goal, it is required to have a fairly accurate and simple model of an inkjet printhead. It is not easy to obtain a good physical model for an inkjet printhead due to insufficient knowledge of the complex interactions in the printhead. Therefore, in this thesis, we have used system identification, i.e. we use experimental measurements in order to develop a model. For this purpose, it is required that the piezo-actuator is also used as a sensor. Note that the crucial aspect in the model development is to obtain a model of the inkjet system close to its operating conditions. Therefore, we have collected measurements of the piezo sensor signal during the jetting of a series of drops at a given DoD frequency. For the printhead under investigation, we found that the dynamics of the ink channel are dependent on the DoD frequency. This phenomenon is caused by non-linearities in the droplet formation. Consequently, we have modeled the ink channel dynamics for every DoD frequency. In this thesis, it is shown that the set of local inkjet models obtained at different DoD frequencies can be encompassed by a polytopic uncertainty on the parameters of a nominal model. Using the same identification procedure, the cross-talk can also be modeled.

In order to improve the printhead performance the actuation pulse was re-designed. The new drive pulse is designed to provide good performance for all models in the area of uncertainty by means of robust feedforward control. The pulse also respects the pulse shape constraints posed by driving electronics (ASICs). Besides the robust actuation pulse, our approach also introduces an optimal delay between actuation of neighboring channels to reduce the cross-talk.

The current driving electronics limits the possibilities of reshaping the actuation pulse. Since it is expected that this limitation will be relaxed in the future, we have also developed procedure to design a robust pulse without pulse shape constraints. The performance improvement achieved with this unconstrained pulse has proved to be quite limited.

The proposed method is also useful for inkjet practitioners who do not have any insight in the inkjet dynamics. The efficacy of our approach is demonstrated by our experimental results. The proposed method was verified in practice by jetting a series of ink drops at various DoD frequencies and also by jetting a bitmap image. For the printhead under consideration, the drop-consistency is improved by almost four times with the proposed approach when compared to the conventional methods.

Samenvatting

Model-gebaseerd Feedforward Regeling voor Inkjet Printkoppen

Amol Ashok KHALATE

De laatste jaren heeft inkjettechnologie zich ontwikkeld tot een veelbelovende productie methode. Deze technologie heeft zijn populariteit vooral te danken aan het feit dat het diverse materialen kan verwerken en zijn contactloze additieve werkwijze. Bovendien heeft inkjettechnologie ook andere voordelen zoals lage operationele kosten, goede schaalbaarheid, digitale besturing, en weinig afval. Afgezien van het conventionele afdrukken van documenten, is de inkjettechnologie met succes toegepast als een microproductie instrument in elektronica, werktuigbouwkunde, en biowetenschappen. In dit proefschrift onderzoeken we een piëzo-gebaseerde *Drop-on-demand* (DoD) printkop die gewoonlijk wordt gebruikt voor industriële en commerciële toepassingen doordat het in staat is om diverse materialen te verwerken.

Een typische DoD inkjet printkop heeft meerdere parallel-geplaatste inkt kanalen. Elk kanaal is voorzien van een piëzo-actuator, die een spanningspuls omzet in drukschommelingen in het inktkanaal. Deze drukschommelingen duwen een inkt druppel uit het mondstuk. De printkwaliteit die een inkjet printkop levert is afhankelijk van de eigenschappen van de geschoten druppel, d.w.z. de snelheid van de druppel, het druppelvolumen en de schiet richting. Om aan de uitdagende prestatie-eisen te voldoen die gesteld worden door nieuwe toepassingen, moeten deze eigenschappen uiterst precies gereguleerd worden.

De prestatie van de inkjet printkoppen wordt beperkt door twee factoren. De eerste is de resterende drukschommelingen. De aandrijfpulsen worden ontworpen om een inkt druppel met een bepaald volume en snelheid te schieten in de veronderstelling dat het inktkanaal zich in evenwichtstoestand bevindt. Zodra de inkt druppel is geschoten, duurt het enkele microseconden vooraleer de drukschommelingen in het inktkanaal zijn uitgedoofd. Als de volgende inkt druppel geschoten wordt voordat deze resterende drukschommelingen uitgedoofd zijn, zullen de resulterende druppel eigenschappen verschillen van die van de eerdere druppel. De tweede beperkende factor is de zogenaamde *cross-talk*. De druppel eigenschappen worden via een inktkanaal beïnvloedt wanneer de naburige kanalen tegelijk worden gebruikt. In het algemeen wordt de druppel consistentie verbeterd door handmatige aanpassing van de piëzo-aandrijvingspuls. Deze aanpassing is louter gebaseerd op fysisch inzicht of op lange experimenten op de printkop. Echter, deze

ad-hoc procedures bleken ontoereikend te zijn in het omgaan met de bovenstaande beperkingen.

In dit proefschrift wordt een model-gebaseerde regeltechniek aanpak voorgesteld om de prestatie van een DoD inkjetprintkop te verbeteren. Het biedt een systematische en efficiënte manier om de prestatie te verbeteren door de effecten van de resterende drukschommelingen en de cross-talk te reduceren. Bovendien kunnen de modellen die voor dit doel ontwikkeld zijn ook inzicht geven in de werking van de printkop.

Om dit doel te bereiken, is een redelijk nauwkeurig maar eenvoudig model van een inkjet printkop vereist. Het is niet gemakkelijk om een goed fysisch model van een inkjet printkop te maken vanwege het gebrek aan kennis over diverse complexe interacties. Teneinde dit te realiseren hebben we in dit proefschrift systeemidentificatie gebruikt, d.w.z. we hebben experimentele metingen gebruikt om een model te ontwikkelen. Hiervoor is de piezo-actuator ook als sensor gebruikt. Merk op dat het belangrijke aspect in de model ontwikkeling is om het inkjet systeem dichtbij de werkomstandigheden accuraat te beschrijven. Daarom hebben we metingen van het piezo-sensorsignaal verzameld tijdens het schieten van een reeks druppels met een gegeven DoD frequentie. Voor de onderzochte printkop hebben we vastgesteld dat de dynamica van het inktkanaal afhankelijk is van de gekozen DoD frequentie. Dit fenomeen wordt veroorzaakt door niet-lineariteiten in de druppel vorming. Dientengevolge identificeerden we een model voor elke DoD frequentie. In dit proefschrift wordt aangetoond dat de verzameling van lokale inkjet modellen verkregen op verschillende DoD frequenties kan worden omsloten door een polytopische onzekerheid op de parameters. Gebruikmakend van bovenstaande identificatieprocedure kan de cross-talk dynamica ook worden gemodelleerd.

Om de prestatie van de printkop te verbeteren is de vorm van de aandrijvingspuls herontworpen. De nieuwe aandrijvingspuls is ontworpen om goede prestatie te leveren voor alle modellen in het onzekerheidsgebied (robuuste feedforward regeling) en respecteert de vorm-beperking van de aandrijvingselectronica. Naast deze robuuste aandrijvingspuls levert onze procedure ook een optimale vertraging die moet worden ingevoerd tussen de pulsen van naburige kanalen om de cross-talk te verminderen.

De huidige electronica beperkt de mogelijke vorm die de pulsen mogen nemen. Omdat de verwachting is dat deze beperking in de toekomst minder zal worden, hebben we ook een procedure ontwikkeld om een robuuste puls zonder vorm-beperking te ontwerpen. De prestatie verbetering die hiermee behaald is bleek in de praktijk echter beperkt.

De voorgestelde methode kan inkjet gebruiker inzicht geven in de inkjet dynamica. De werkbaarheid van onze aanpak is met een aantal experimentele resultaten geverifieerd. De voorgestelde methode is in de praktijk geverifieerd door middel van het uitstoten van een reeks inktdruppels met verschillende DoD frequenties en het printen van een afbeelding opgebouwd uit pixels. Voor de beschouwde printkop wordt de druppelconsistentie met bijna een factor vier verbeterd ten opzichte van de conventionele aanpak.

Curriculum Vitae



Amol Ashok Khalate was born on May 17, 1980 in Phaltan, India. In 1997, he started his study Instrumentation Engineering at the Government College of Engineering, Jalgaon (in North Maharashtra University, Jalgaon, India), where he graduated in June 2001. He perused his Master of Technology in Control System Engineering at Indian Institute of Technology, Kharagpur, India and graduated in June 2004. He worked as a flight control engineer for VSSC, Indian Space Research Organization, Trivandrum, India from August, 2004 to June, 2008. In July 2008, he started his Ph.D. project entitled: *‘Model-based Feedforward Control for Inkjet Printheads* within the Delft Center for Systems and Control (DCSC) under the supervision of Prof.dr. Robert Babuška and Dr.ir. Xavier Bombois. From July 2012, he is working for Océ Technologies B.V., Venlo, as a mechatronics designer.

